Safe Speed Assessment of DRDC Notional Destroyer in Ice (Phase 2 of Ice Capability Assessment)

Prepared for

Defence Research and Development Canada
Warship Performance Section
9 Grove Street
Halifax, NS, Canada, B2Y 3Z7
Attention: Dr. Malcolm Smith

Prepared by:

Dr. Claude Daley
Daley R&E
cdaley@mun.ca

Katherine Daley
Daley R&E
katherinehd@gmail.com

John Dolny
ABS Harsh Environment Technology Center
jdolny@eagle.org

31 March 2017
(Updated 18 April 2017)

Contents

Table of Figures

Table of Tables

Nomenclature

a	frame span, accelerations
A	nominal contact area
AM_x	added mass factor in x (similar for other degrees of freedom)
b_w	flange offset distance
B	beam
BL	ship baseline
C_B	block coefficient
C_M	midship coefficient
C_o	mass reduction coefficient
C_s	power function coefficient
C_{WP}	waterplane coefficient
C_W	width reduction factor
CG	centre of gravity
CL	ship centreline
D	frame overall height
E	Young’s modulus
E_{ice}	ice modulus of elasticity
E_t	tangent modulus
ex	process pressure-area model exponent
fa	shape parameter
F_{el}	elastic-plastic transition response force

F_{max}	maximum applied patch load
F_n	plastic response force, normal force
F_o	initial plastic capacity
FP	forward perpendicular
fr. no.	frame number
f_x	shape parameter
F_{y_f}	yield strength (framing material)
F_{y_p}	yield strength (plating material)
F_x	force in surge (similar for other degrees of freedom)
GPa	gigapascals
h	patch load height
h_{ice}	ice thickness
h_w	web height
H	height (depth)
IE_i	ice indentation energy
IE_s	structural indentation energy
j	frame attachment parameter
KE_e	effective kinetic energy
k_{el}	elastic response constant
kg	kilograms
k_p	elasto-plastic structural capacity parameters
k_s	power function coefficient
kn	knots
kN	kilonewtons
L_{OA}	length overall
L_{BP}	length between perpendiculars
L_{eice}	ice effective length
l,m,n	direction cosines
m	metres
M	displacement
M_{ship}	mass of ship
M_e	equivalent mass
$M_{e\ ship}$	equivalent mass of ship
M_{sx}	mass of ship (including added mass) in x direction
$M_{sy\ etc}$	mass of ship (including added mass) in y, z directions
I_{sx}	mass moment of inertia of ship (including added mass) in x rotation
$I_{sy\ etc}$	mass moment of inertia of ship (including added mass) in y, z rotations
MN	meganewtons
MPa	megapascals
Q	line load
P_{av}	average pressure in nominal contact area
P_o	average pressure in a 1 m^2 contact area
P_{o_eff}	effective average pressure in a 1 m^2 contact area
rx	mass radius of gyration in x (similar for y,z)
RPM	rotations per minute
S	frame spacing
sf	ice flexural strength
t_f	flange thickness
t_p	plate thickness
t_w	web thickness
T	draft

V	vessel speed, speed in individual degrees of freedom
W	frame flange width
w	patch load width
wf	width of flange
Wnom	nominal patch load width
Xcen	load location
x_{cg}	x distance to center of gravity
x_{fp}	location of station from forward perpendicular along x-axis
$x_{station}$	location of station along the x-axis
y	vessel midline position (distance from ice edge)
Y_{cen}	load location
y_{cg}	y distance to center of gravity
Z_{cen}	load location
z_{cg}	y distance to center of gravity
z_{keel}	location of station above keel along z-axis
zs	allowable permanent deflection of hull
α	waterline angle
β	frame angle
β'	normal frame angle
λ,μ,ν	x,y,z moment arms
ζ_c	ice crushing indentation
ζ_n	normal indentation
$\ddot{\zeta}$	normal acceleration
ζ_s	structural indentation
θ	wedge offset angle
ρ_{ice}	ice density
σ_f	ice flexural strength (same as sf)
σ_y	yield strength
σ_{y_ice}	ice yield strength
υ_{ice}	ice Poisson’s ratio
φ	nominal ice wedge angle
φ_{eff}	effective ice wedge angle
φ_w	web angle
ASPPR	Canadian Arctic Shipping Pollution Prevention Regulations
DDePS	Direct Design for Polar Ships
DOE	Design of Experiments
DRDC	Defence Research and Development Canada
FEA	Finite Element Analysis
FN	Frame Number
FO	Frame Orientation
IACS	International Association of Classification Societies
IC	Ice Class
LR	Lloyd’s Register
ONR	U.S. Office of Naval Research
ND	Notional Destroyer
RSM	Response Surface Methodology
SN	Ship Name
ST	Ship Type
$STePS^2$	Sustainable Technology for Polar Ships and Structures

Acknowledgements

This study has been funded by Defence Research and Development Canada, Warship Performance Section. Their support is gratefully acknowledged. Dr. Malcolm Smith and Dr. John MacKay are thanked for his interest and support. The work is part of a Canada-US joint interest in arctic vessel operations.

A parallel study was recently completed for the US Office of Naval Research (ONR), in which ABS lead the investigation. This study has made use of many of the same approaches and software that were employed for the ONR study.

1. Introduction

DRDC has a continuing interest in understanding the structural capability of its vessels when deployed in high latitude environments with potential for ice impact loading on the hull structure in the marginal ice zone. This project is the second phase of an examination of a concept vessel called the Notional Destroyer, which has characteristics similar to many naval patrol/frigate/destroyer class vessels with a hull structure that is not strengthened for ice impact. This report expands on the work conducted in Phase 1 (Daley 2015) and includes new approaches for the direct analysis of structural capability under ice loads. In this report, new bow structural panels and stem structure are evaluated. These new analysis approaches have been tailored for application to non-ice strengthened vessels such as naval vessels.

The objectives of this project are to continue exercise the state-of-the-art of available technologies to estimate operational capabilities and limitations for non-ice strengthened and light ice-strengthened Canadian Navy assets operating in ice conditions. Related work supported by the US Navy and US Coast Guard has been used.

This report includes the use of a new version of the software assessment tool called "Direct Design for Polar Ships" (DDePS), which is now called **DDePS_2a_Safe_Check** (latest version v3.5). This updated software tool allows a user to explore damage estimates and develop guidance for speed limitations based on deterministic impact scenarios for a specific ship.

This report also includes the use of a novel ship-ice simulation program called GEM. GEM is capable of rapidly modelling the loads and vessel behavior for ships operation in open pack ice.

2. Review of Notional Destroyer Bow Structure

General Vessel Description

The Notional Destroyer is a concept warship which is about 150 m in length and weighs from 7700 tonnes to 9100 tonnes, depending on age and ice accretion. The following material is extracted from Notional Destroyer Particulars and Summary (DRDC 2015). A sketch of the vessel layout is given in Figure 1. Figure 2 shows the lines of the vessel. The operating waterlines are shown for reference. The main particulars are given in Table 1.

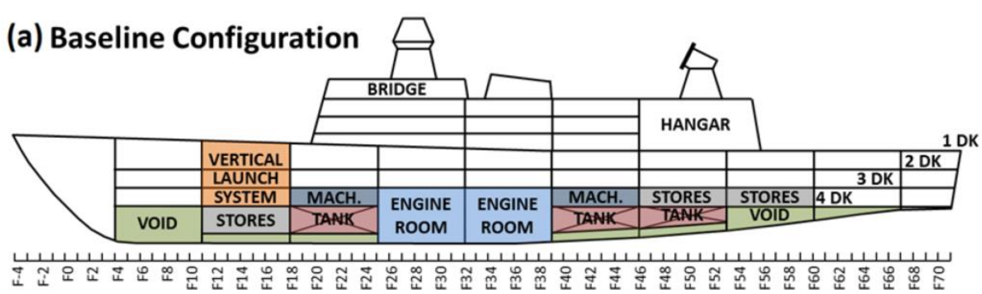

Figure 1: Notional Destroyer – Concept of General Layout

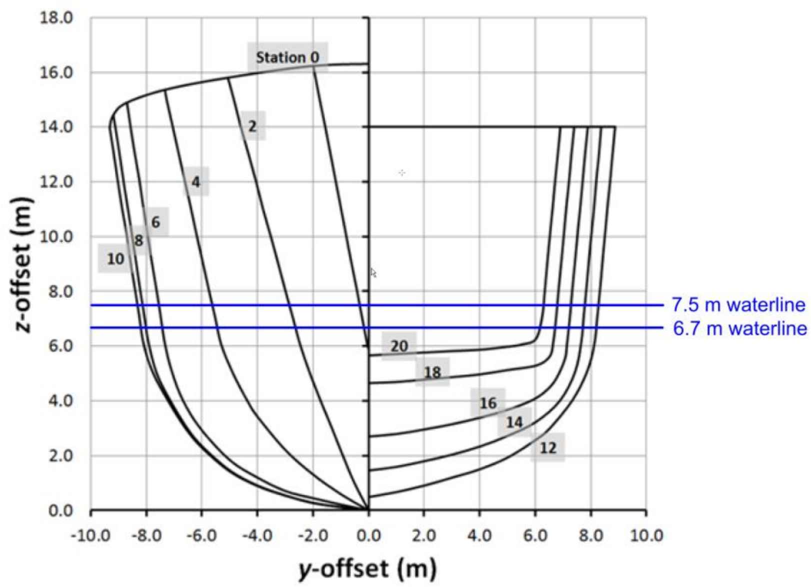

Figure 2: Notional Destroyer – Body Lines

Table 1: Notional Destroyer – Main Particulars

Particular	***Beginning of Life (no ice accretion)***	***End of Life (with max ice accretion)***
Length overall	151.4 m	
Overall depth	16.5 m	
Amidships depth	14.0 m	
Maximum breadth	18.7 m	
Displacement	7673 t	9095 t
Length along waterline	142.8 m	143.5 m
Length between perpendiculars	137.8 m	138.5 m
Amidships location [a]	68.9 m	69.2 m
Longitudinal center of gravity [a]	72.0 m	73.8 m
Waterline breadth	16.8 m	17.0 m
Draft	6.7 m	7.5 m
Block Coefficient	0.48	0.51

[a.] *Distance aft from forward perpendicular (FP). The FP is 0.80 m and 1.48 m forward of frame 0 (F0 at x=0) for the beginning and end of life, respectively.*

Hull Form Parameters

In order to conduct an ice impact assessment, the 3D angles and coordinates of impact locations must be known. The body lines from Figure 2 were imported into Rhinoceros (2010) to create a full 3D representation of the hull (Figure 3). The angles at various stations (to be used as impact locations) were extracted (Figure 4) and are listed in Table 2 for the 7.5 m draft (end of life) and in Table 3 for the 6.7 m draft (beginning of life).

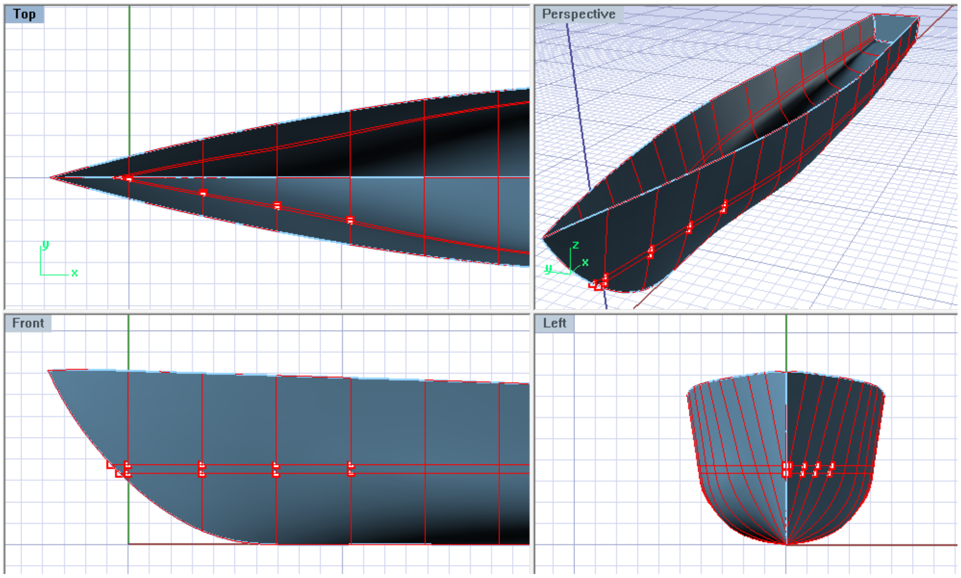

Figure 3: Notional Destroyer – Rhinoceros 3D Model

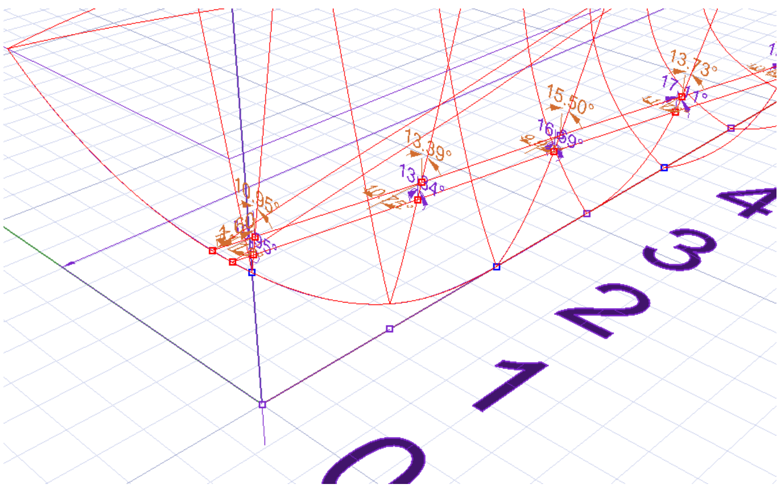

Figure 4: Extraction of hull angles from Rhinoceros 3D Model

Table 2: Coordinates and angles for 7.5 m waterline

station	$x_{station}$	x_{fp}	z_{keel}	x_{cg}	y_{cg}	z_{cg}	α	β	***fr.no.***[a]
0	0	1.6	7.5	72.2	0.3	0	11.1	11.0	0
1[b]	6.9	8.5	7.5	65.3	1.7	0	10.8	13.4	4
2	13.9	15.5	7.5	58.3	2.9	0	9.9	15.5	7
3	20.8	22.4	7.5	51.4	4.3	0	11.8	13.7	11
4	27.7	29.3	7.5	44.5	5.7	0	10.8	10.5	14
5	34.7	36.3	7.5	37.5	6.8	0	8.4	9.8	18
6	41.6	43.2	7.5	30.6	7.5	0	5.2	7.9	21
7	48.5	50.1	7.5	23.7	8.0	0	2.4	7.8	25
8	55.5	57.1	7.5	16.7	8.2	0	1.3	8.2	28
9	62.4	64.0	7.5	9.8	8.3	0	0.9	8.5	32
10	69.4	71.0	7.5	2.8	8.3	0	0.5	8.5	36

[a.] approximate frame numbers [b.] 4 locations for ice impact analysis are highlighted

Table 3: Coordinates and angles for 6.7 m waterline

station	$x_{station}$	x_{fp}	z_{keel}	x_{cg}	y_{cg}	z_{cg}	α	β	fr.no.[a]
0	0	0.8	6.7	71.2	0.2	0	10.7	11.0	0
1	6.9	7.7	6.7	64.3	1.5	0	10.2	13.3	4
2	13.9	14.7	6.7	57.3	2.6	0	9.9	16.7	7
3	20.8	21.6	6.7	50.4	4	0	12.1	17.1	11
4	27.7	28.5	6.7	43.5	5.5	0	10.1	13.3	14
5	34.7	35.5	6.7	36.5	6.7	0	8.3	9.8	18
6	41.6	42.4	6.7	29.6	7.5	0	5.0	7.9	21
7	48.5	49.3	6.7	22.7	7.9	0	2.3	7.9	25
8	55.5	56.3	6.7	15.7	8	0	1.0	8.6	28
9	62.4	63.2	6.7	8.8	8.1	0	0.8	9.5	32
10	69.4	70.2	6.7	1.8	8.2	0	0.5	9.5	36

[a.] *approximate frame numbers*

Midship Structural Information

The structure of the Notional Destroyer is representative of a warship, and is intentionally very light in comparison to an ice class ship. The information given below describes the structural characteristics of the outer hull structure, which is the structure that would be involved in an ice impact. Ice impact loads are highly localized, and so the structure of the outer hull determines the ice capacity in an impact. There are no significant global strength issues for any conceivable ice interaction for this type of vessel. The vessel's global strength would only be in danger if it were to ram a massive ice feature. Such operations would cause also extensive local damage and are thus not considered. The material parameters are listed in Table 4. The structural layout parameters are listed in Table 5. Additional framing parameters are shown in Figure 5 and Table 6 (taken from DRDC 2015). Figure 5 shows the midship cross section with plating and framing scantlings given.

Table 4: Notional Destroyer – Material Properties

Parameter	Value
Young's modulus [a]	207 GPa
Poisson's ratio [a]	0.3
Yield strength [a]	355 MPa
Density [a]	7850 kg/m^3
Post Yield behavior [b]	Bi-linear kinematic hardening
Post Yield modulus [b]	1.5 GPa

[a.] *these values were provided by DRDC*
[b.] *assumed by author*

Table 5: Notional Destroyer – Structural Arrangement Particulars (Midships and Bow)

Structural Parameter	***Value***
Web Frame spacing [a]	2.0 m
Hull longitudinal stiffener spacing [a]	550 mm
Vertical spacing between decks [a]	2.75 m
Deck longitudinal stiffener spacing [a]	575 mm
Vertical stiffener spacing on watertight bulkheads [a]	575 mm
Transverse offset of longitudinal bulkheads from centerline [a]	3.45 m
Vertical stiffener spacing on longitudinal bulkheads and girders [a]	575 mm
Brackets connecting longitudinal hull frames and web frames [b]	none

[a.] *these values were provided by DRDC*
[b.] *assumed by author*

Table 6: Notional Destroyer – Transverse Framing Particulars (Midships)

Primary Member [a]	***Location***	***Typical Scantling***	***Deep Scantling***
Transverse web frame	Between Nos. 1 and 2 decks	191x7W 40x9F	N/A
Transverse web frame	Between Nos. 2 and 3 decks	210x7W 45x10F	N/A
Transverse web frame	Between Nos. 3 and 4 decks	230x7W 50x10F	560x10W 120x25F
Transverse web frame	Between Nos. 4 and inner bottom	273x7W 60x12F	608x11W 130x27F
Transverse web frame	Between inner bottom and keel	364x8W 80x16F	651x11W 140x29F
Deck beam	No. 1 deck	220x7W 50x10F	N/A
Deck beam	Internal decks	225x8W 120x15F	N/A
Plate floor	Engine rooms	1355x7W 165x14F	N/A
Plate floor	Beneath inner bottom in stores compartments and tanks	10 mm web	N/A

[a.] *all values were provided by DRDC*

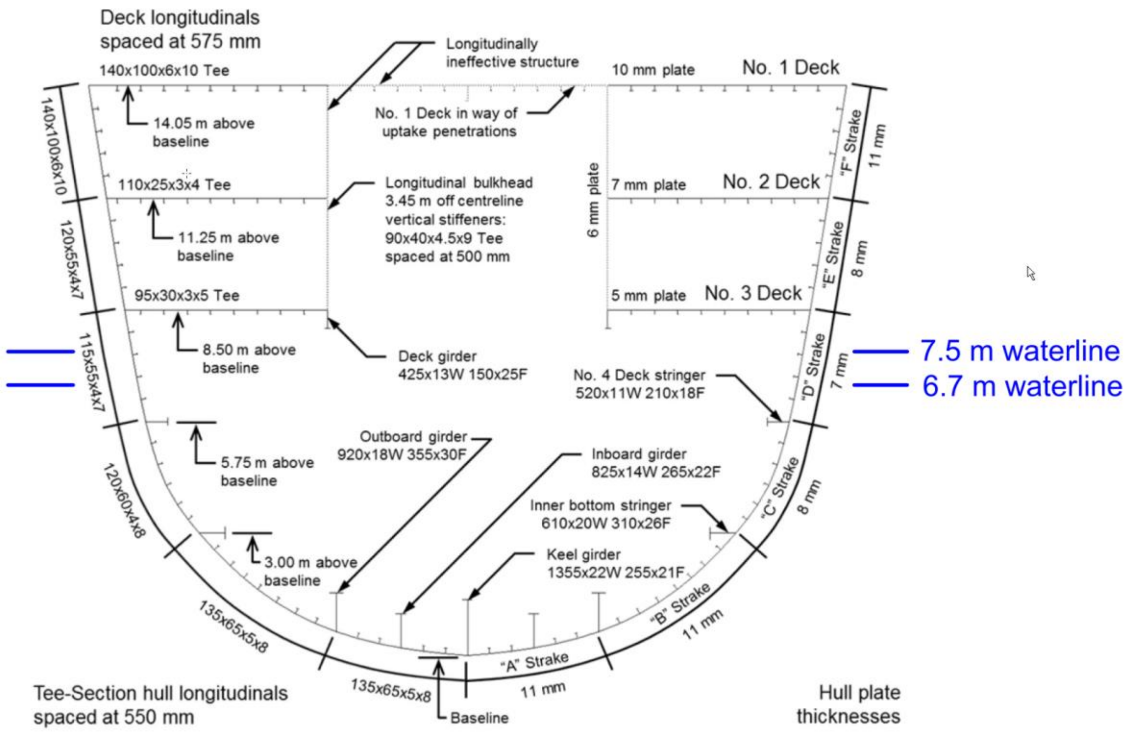

Figure 5: Notional Destroyer – Midship Structure

Bow Structural Information

A more recent report provided by DRDC (Lloyds Register 2016) provides the notional structure for the bow region of the Notional Destroyer. This information has been used here to develop LS-Dyna structural models for the bow. Figure 6 shows the general structural layout of the decks and bulkheads in the bow. Local framing is omitted for clarity. From the Rhino model in Figure 6, individual panel models were developed. Table 7 lists the plating, longitudinal framing and transverse framing scantlings on the hull in the bow region.

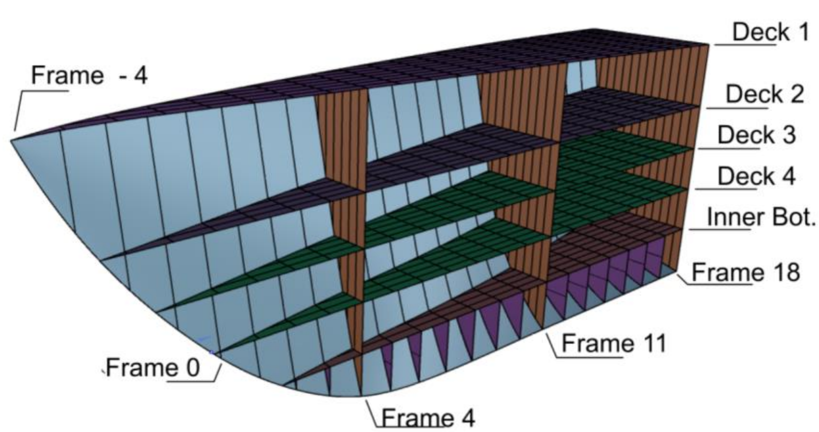

Figure 6: Notional Destroyer – Bow Structure (Longitudinal and Transverse framing omitted)

Table 7 Notional Destroyer –Framing Particulars (Bow Forward between Decks 3,4)

Member [a]	***Location***	***Scantling***
Transverse web frame	Between Frames 11 and 18	200x10W 120x8F
Longitudinal frame	Between Frames 11 and 18	120x5W 60x6F
Shell Plating	Between Frames 11 and 18	8.5 mm
Transverse web frame	Between Frames 4 and 11	220x10W 140x8F
Longitudinal frame	Between Frames 4 and 11	130x7W 60x12F
Shell Plating	Between Frames 4 and 11	9.5 mm
Transverse web frame	Between Frames -4 and 4	250x13W 140x12F
Longitudinal frame	Between Frames -4 and 4	140x6W 100x10F
Shell Plating	Between Frames -4 and 4	10.5 mm
Stem Bar frame	At Stem	67x36W
Longitudinal frame	Coming to Stem	140x6W 100x10F
Shell Plating	Attached to Stem	10.5 mm

[a.] all values were obtained from the LR report provided by DRDC

3. LS-DYNA Models of the Bow Structure

Throughout this report, we are employing the LS-DYNA finite element program to model both ice loads and structural response. LS-DYNA is an explicit-dynamic commercial finite element analysis code capable of dealing with complex contact, nonlinear, transient, and dynamic problems. It can handle many simulation environments including, FEM, iCFD, ALE, SPH, EFG, X-FEM, DEM and others.

Ice loads generally cause only localized damage. Consequently, models of elastoplastic response can be quite localized. For this project, four regions of the bow have been evaluated. The regions are shown in Figure 7. Figure 8 compares the frame dimension notation from DRDC and Lloyd's Register, DDePS, and LS-DYNA. Figures 9, 10, and 11 shows details of the LS-DYNA representative panel models for frames 0 – 3, frames 7 – 10, and frames 14 – 17, respectively.

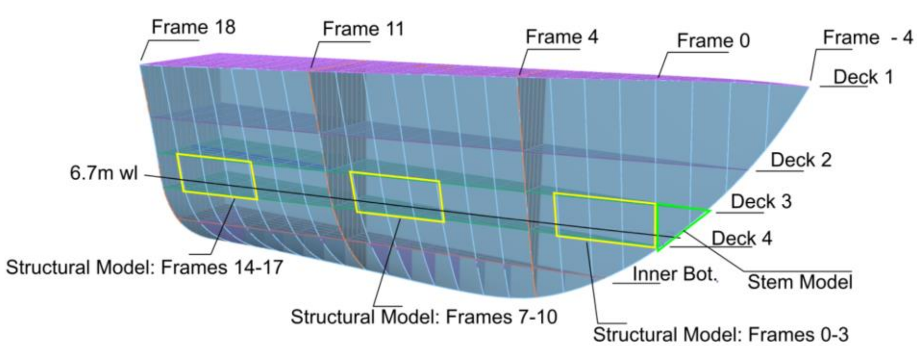

Figure 7: Notional Destroyer Bow with modeling areas shown

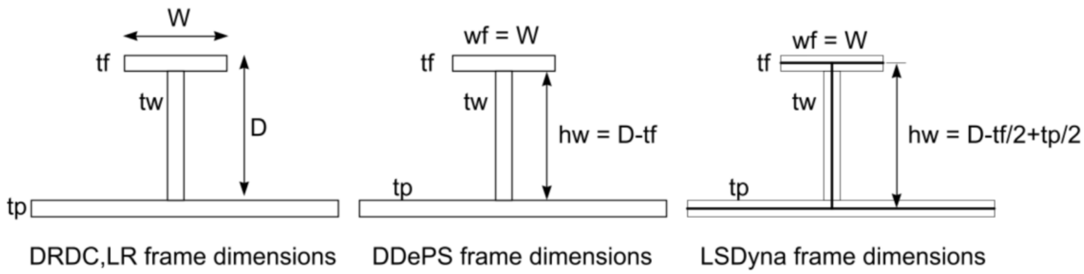

Figure 8: Frame dimension definitions

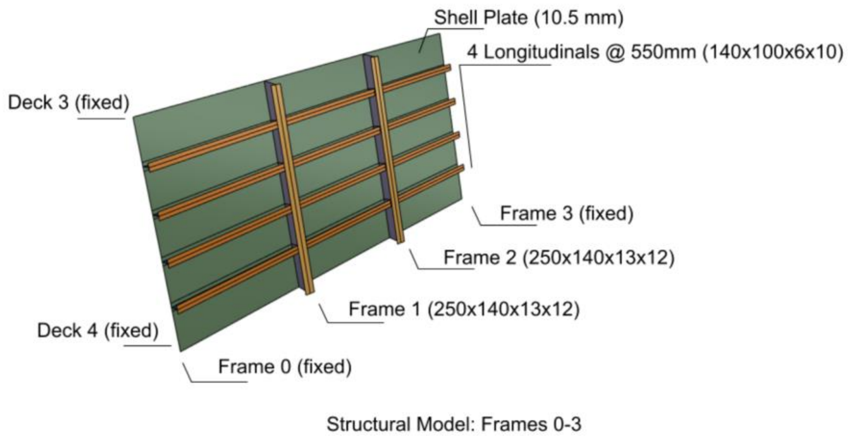

Figure 9: Frame 0-3 panel model (NDP1_03)

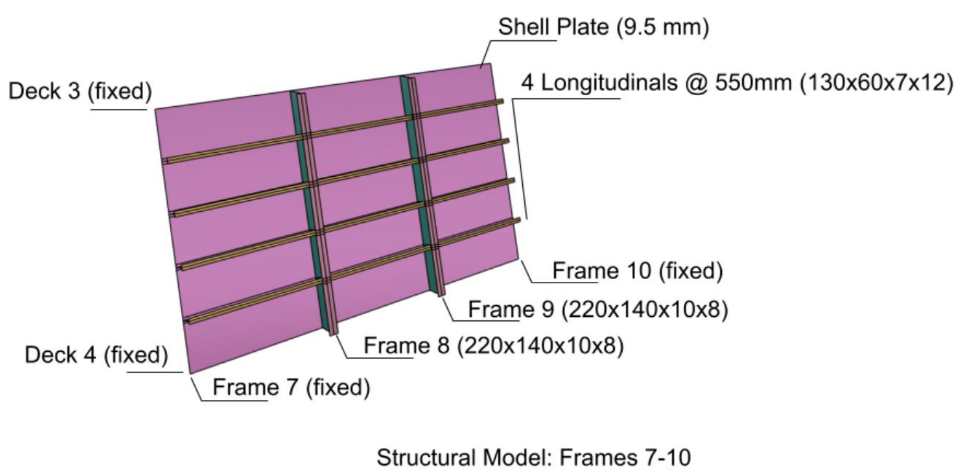

Figure 10: Frame 7-10 panel model (NDP1_710)

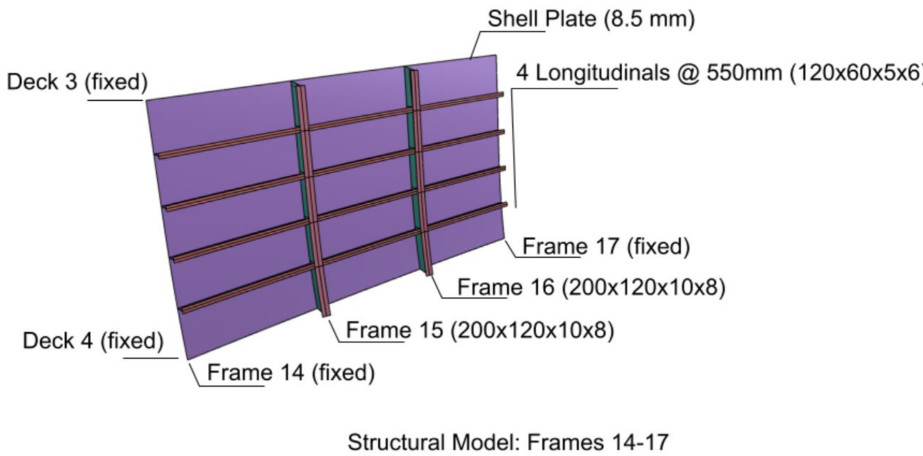

Figure 11: Frame 14-17 panel model (NDP1_1417)

Patch Load Analysis

To characterize the response of each representative panel and different structural components, a series of patch loads were applied to the models via quasi-static nonlinear finite element simulations. Three load patches of different sizes and aspect ratios were applied at several locations on each panel. Table 1 lists all the load cases considered. Figure 12 shows the patch loads applied to the forward-most panel – NDP1_03 (runs D_001 through D_006). Loads are applied at the mid-span of the longitudinal frame (green member) and directly on a transverse web frame (orange member).

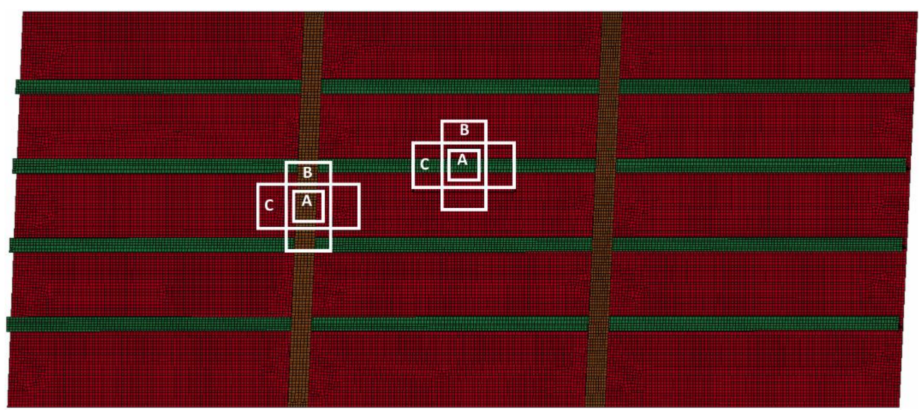

Figure 12: Patch load cases on longitudinal (green) and web frame (orange) – e.g. NDP1_03

Table 8: Patch load cases for DRDC Notional Destroyer

Run #	***F_{max} (MN)***	***w (m)***	***h (m)***	***structure_k_file***	***description***
D_001	1.0	0.2	0.2	NDP1_03_rot.k	centered_load_on_longl_A
D_002	1.0	0.3	0.6	NDP1_03_rot.k	centered_load_on_longl_B
D_003	1.0	0.7	0.3	NDP1_03_rot.k	centered_load_on_longl_C
D_004	1.0	0.2	0.2	NDP1_03_rot.k	centered_load_on_wf_A
D_005	1.0	0.3	0.6	NDP1_03_rot.k	centered_load_on_wf_B
D_006	1.0	0.7	0.3	NDP1_03_rot.k	centered_load_on_wf_C
D_011	1.0	0.2	0.2	NDP1_710_rot.k	centered_load_on_longl_A
D_012	1.0	0.3	0.6	NDP1_710_rot.k	centered_load_on_longl_B
D_013	1.0	0.7	0.3	NDP1_710_rot.k	centered_load_on_longl_C
D_014	1.0	0.2	0.2	NDP1_710_rot.k	centered_load_on_wf_A
D_015	1.0	0.3	0.6	NDP1_710_rot.k	centered_load_on_wf_B
D_016	1.0	0.7	0.3	NDP1_710_rot.k	centered_load_on_wf_C
D_021	1.0	0.2	0.2	NDP1_1417_rot.k	centered_load_on_longl_A
D_022	1.0	0.3	0.6	NDP1_1417_rot.k	centered_load_on_longl_B
D_023	1.0	0.7	0.3	NDP1_1417_rot.k	centered_load_on_longl_C
D_024	1.0	0.2	0.2	NDP1_1417_rot.k	centered_load_on_wf_A
D_025	1.0	0.3	0.6	NDP1_1417_rot.k	centered_load_on_wf_B
D_026	1.0	0.7	0.3	NDP1_1417_rot.k	centered_load_on_wf_C

Figure 13 presents the results of the load cases shown in Figure 12 for NDP1_03. This is a plot of applied force (y-axis) versus structural deformation (x-axis) measured at the intersection of the plate and web directly under the center of the load patch. For the longitudinal frame load cases, the Polar Class Unified Requirements (IACS 2011) nominal frame limits are also identified. These limit states were described in Section 6 of the Phase 1 Report (Daley 2015). While the frame response varies for each case, the limit states consistently predict the onset of large deformations and a transition to loss of stiffness. At these load levels the observable permanent deformation would be quite small but plasticity is present.

Example von-Mises stress distribution fringe plots are shown for case D_001 (i.e. smallest load patch applied to the longitudinal frame) in Figure 14. The left-side figure approximately represents the predicted plastic limit state. Areas highlighted in red indicate where the stress has exceeded the material yield point (355 MPa). The right-side figure shows the response in an overload state.

The web frame load cases are also shown in Figure 13. In all cases the response remains elastic at the corresponding frame limit state (~0.2 to 0.3 MN). In case D_004 (i.e. small concentration load patch on the web frame), the web frame exhibits a rapid loss in capacity at about 0.95 MN. However, the longitudinal frames would reach their limit state at a much lower load level, so it is not necessary to define a specific limit for these large members.

The response of the other panels (NDP1_710 and NDP1_1417) are shown in Figure 15. These plots also confirm an accurate prediction of the longitudinal frame plastic limit states prior to any major loss of stiffness. Furthermore, the FE results reflect the fact that the scantlings of these of panels are lighter than NDP1_03.

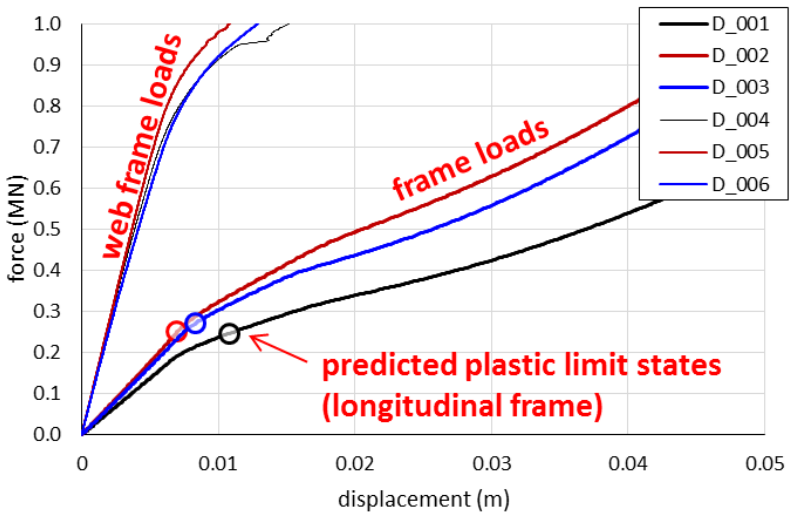

Figure 13: Response of structural panel to various load cases – e.g. NDP1_03

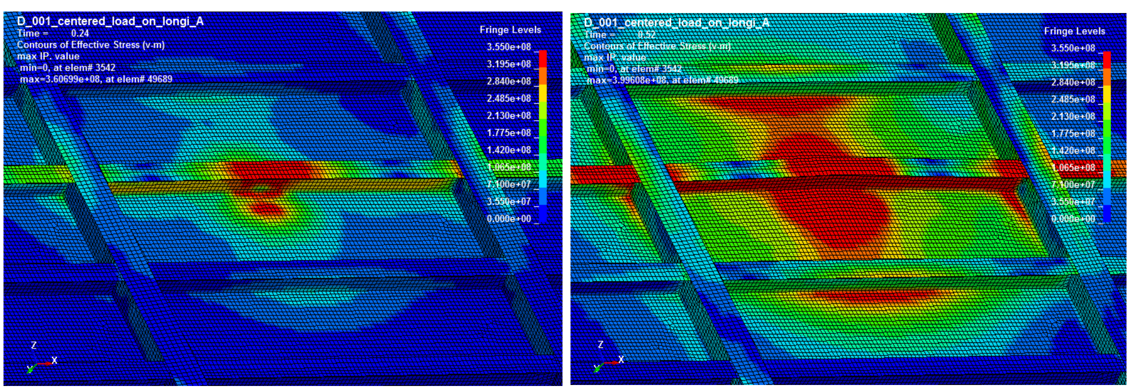

Figure 14: von-Mises stress distribution at the frame plastic limit state (left) and in overload condition (right) – e.g. run D_001

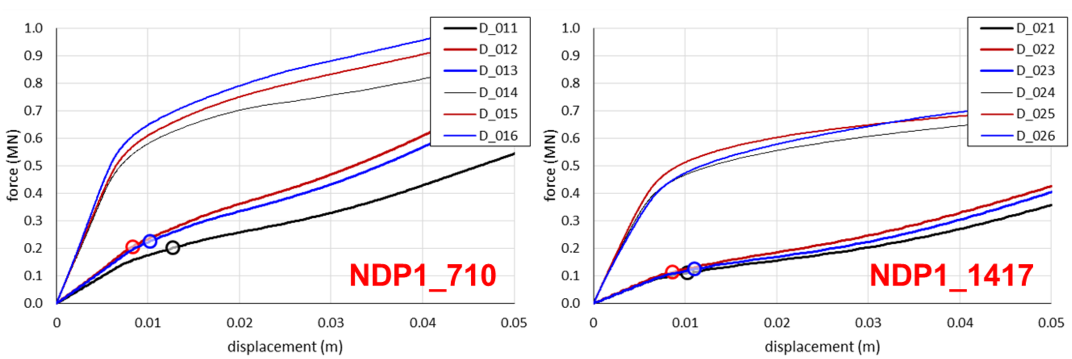

Figure 15: Response of structural panels to various load cases – e.g. NDP1_710 and NDP1_1417

4. Initial Safe Speed Analysis - DDePS

The Phase 1 Report (Daley 2015) presented a safe speed analysis of the Notional Destroyer assuming nominal midbody scantlings in the bow area. As an initial check, the ship is re-analyzed here taking into account the bow scantlings provided by DRDC (Lloyds Register 2016) and described above.

Overview of DDePS Model and Equations

Direct **De**sign for **P**olar **S**hips (DDePS) is a Microsoft Excel based spreadsheet tool capable of modeling a large set interaction scenarios between a ship and ice. The impact models, described in several papers and technical reports (Daley, 1999, 2000, 2002, Kendrick & Daley, 2006a, 2006b, 2009, 2011, Daley & Liu, 2009, Dolny et al. 2013) are based on the same overall methodology found in the IACS Polar Class Unified Requirements (IACS 2011) but consider a wide range of scenarios, including infinite and finite ice floes.

The collisions are solved using an analysis of energy. From an external point of view, the interaction between the ship and ice floe is treated as a rigid body interaction in 3-dimensional space. In most impact cases, the collision is assumed to occur quickly, as if the ice-hull contact is fixed at a single point. From the internal dynamic point of the view, the ice crushing is modeled as a 'process' pressure-area model. The momentary ship-ice impact force can be analytically calculated in terms of energy and momentum balance.

For the purposes of this project, the 2a (glancing impact) scenario and the 1a (head-on impact) scenario are used. An enhanced version of DDePS has been recently developed (ABS 2017, ABS 2016, Dolny 2017) and is used here. It builds upon the original DDePS Case 2a (glancing impact with a wedge edge) by incorporating several new technical elements and user features, and combines various structural limit checks.

Case 2a Interaction Scenario

For the purposes of evaluating technical safe limit speeds for ships in ice, DDePS Case 2a (glancing collision on the bow shoulder) is the core model. A simplified version of this interaction scenario, a glancing collision on the edge of a thick level ice sheet, was adopted for the IACS Polar Class Unified Requirements design ice load model (Daley, 2000). Figure 16 is a sketch of the 2a scenario.

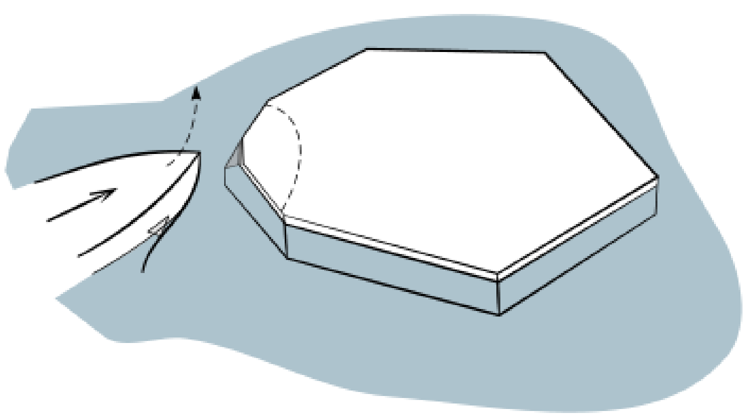

Figure 16: Safe Speed Collision Scenario 2a

The total force during the impact event is limited by one of two limit conditions. When the ship impacts an ice feature, the force increases as the hull penetrates. This penetration will cease if either the ship runs out of energy (i.e. the normal speed becomes zero) or the downward component of the force causes the ice to fail in flexure. The maximum structural impact force is determined either by a 'momentum limit' or by a 'flexural failure limit'. Therefore, two models are required to determine the impact force: a crushing impact force model and a flexural force limit model.

Case 1a Interaction Scenario

A second scenario, DDePS Case 1a (head-on collision on the bow stem) is the second model used for this safe-speed evaluation. This model derives from the design scenario used in the Canadian ASPPR (Arctic Shipping Pollution Prevention Regulations) ice class regulations. The interaction geometry for this scenario is different from the 2a scenario, in that the vessel and ice respond differently and thus the interaction forces are different in both magnitude and form (sensitive to different parameters). Figure 17 is a sketch of the 1a scenario.

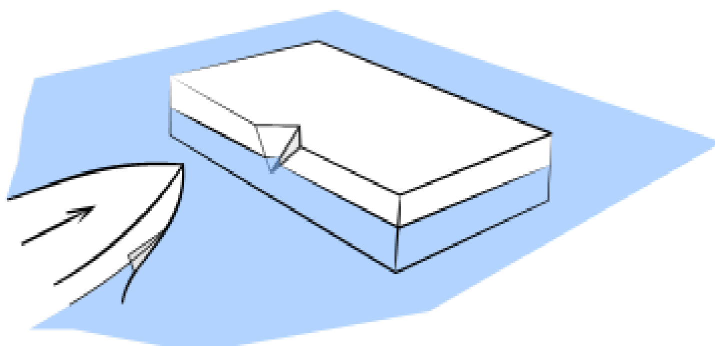

Figure 17: Safe Speed Collision Scenario 1a

Ice Crushing Force Derivation

Both the 1a and 2a scenarios are modeled as impacts, solvable by considering the conversion of kinetic energy to ice crushing energy. The solution of the energy equations requires that force is described as a function of indentation. By using an ice 'process' pressure-area relationship, it is possible to derive a force-indentation relationship. This assumption means that ice force will depend only on indentation, and the maximum force occurs at the time of maximum penetration. The collision geometry is the ice/structure overlap geometry. The average pressure P_{av} in the nominal contact area A is related to the nominal contact area as;

$$P_{av} = P_o A^{ex} \tag{1}$$

P_o is the average pressure when the contact area is 1m^2 and ex is a constant (typically ex = -0.1). The above equation is a 'process' pressure area model (in contrast to a 'spatial' pressure area model). The 'process' pressure area model describes the development of the average contact pressure (and its nominal contact area) throughout the ice penetration process. A 'spatial' pressure area model describes the spatial variation of pressure in the contact area at a moment in time.

The ice force is related to the nominal contact area. The relationship between the normal indentation and normal contact area can be found for each specific contact situation. For the case of a general wedge edge ice geometry, as shown in Figure 18, the contact area *A* can be expressed as;

$$A = \zeta_n^2 \left(\frac{\tan(\phi/2 - \theta) + \tan(\phi/2 + \theta)}{2 \sin(\beta') \cos^2(\beta')} \right) \quad (2)$$

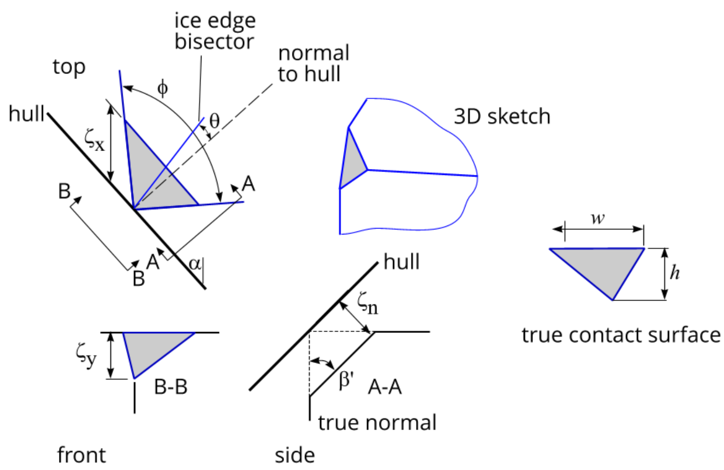

Figure 18: General wedge edge interaction geometry

For simplicity if we assume the wedge angle is normal to the hull, i.e. $\theta = 0$, areas can be expressed as;

$$A = \zeta_n^2 \left(\frac{\tan(\phi/2)}{\sin \beta' \cos^2 \beta'} \right) \quad (3)$$

The total normal force can then be expressed as;

$$F_n = P_{av} A = P_o A^{1+ex} \quad (4)$$

Combining equations *(3)* and *(4)*, the impact force can be stated as;

$$F_n = P_o \zeta_n^{2+2ex} \left(\frac{\tan(\phi/2)}{\sin \beta' \cos^2 \beta'} \right)^{1+ex} \quad (5)$$

After grouping shape terms;

$$F_n = P_o \ fa \ \ {\zeta_n}^{fx-1} \quad (6)$$

Where the shape parameters *fx* and *fa* are as follows;

$$fx = (3 + 2\,ex) \tag{7}$$

$$fa = \left(\frac{\tan(\phi/2)}{\sin(\beta')\cos^2(\beta')}\right)^{1+ex} \tag{8}$$

The ice indentation energy IE_i can be obtained by integrating the force over the depth of normal penetration;

$$IE_i = \int_0^{\zeta_n} F_n d\zeta_n = \frac{P_o}{3 + 2ex}\left(\frac{\tan(\phi/2)}{\sin\beta' \cos^2\beta'}\right)^{1+ex} \zeta_n^{3+2ex} \tag{9}$$

Finally, the indentation energy IE_i can be stated as;

$$IE_i = \frac{P_o}{fx} fa\, {\zeta_n}^{fx} \tag{10}$$

By equating the ice indentation energy to the effective kinetic energy KE_e, the normal penetration of the ice ζ_n can be expressed as;

$$\zeta_n = \left(\frac{KE_e \cdot fx}{P_o \cdot fa}\right)^{1/fx} \tag{11}$$

With the indentation determined, the force, contact size and pressures are readily found. The above equations describe the forces in the 2a case. A similar approach is taken for the 1a case (see DDePS references).

DDePS Evaluation of Notional Destroyer

Table 9 shows the DDePS input parameters for the ship. As described earlier the bow scantlings get stronger towards the stem of the vessel. The representative panel for each impact location is shown as FEA Grillage in the bottom row of the table

Table 9: DDePS input deck for the DRDC Notional Destroyer

ship name	--	SN	DRDC_ND	
ship type	--	ST	Destroyer	
ice class	--	IC	ow	
length overall	m	Loa	151.4	
length between perpendiculars	m	Lbp	138.5	
beam	m	B	17.00	
draft	m	T	7.50	
height (depth)	m	H	14.00	
block coef.	--	CB	0.510	
waterplane coef.	--	Cwp	0.788	
midship coef.		Cm	0.798	
displacement	tons	M	9231.00	

Hull Data			**1**	**2**	**3**	**4**	**5**
region	--	HA	Bow	Bow	Bow	Bow	Bow
frame number	--	FN	FR 4	FR 7	FR 11	FR 14	FR 18
longitudinal distance from CG	m	x	65.30	58.30	51.40	37.50	30.60
transverse distance from CG	m	y	1.70	2.90	4.30	6.80	7.50
vertical distance from CG	m	z	0.00	0.00	0.00	0.00	0.00
waterline angle	deg	α	10.75	9.92	11.80	8.40	5.20
frame angle	deg	β	13.40	15.50	13.70	9.80	7.90
Offered Ice Frame Data			**1**	**1**	**1**	**1**	**1**
frame orientation angle (to waterline)	deg	OA	0°	0°	0°	0°	0°
frame orientation type	--	FO	Longitudinal	Longitudinal	Longitudinal	Longitudinal	Longitudinal
frame attachment parameter, for trans	--	j	2	2	2	2	2
yield strength - framing material	MPa	Fy_f	355	355	355	355	355
yield strength - plating material	MPa	Fy_p	355	355	355	355	355
main frame span (=web frame spacing	mm	a	2000	2000	2000	2000	2000
main frame spacing	mm	s	550	550	550	550	550
plate thickness (gross offered)	mm	tp_ofrd	10.5	9.5	9.5	8.5	8.5
offered frame	--	ofrd_frm	Built Section	Built Section	Built Section	Built Section	Built Section
web angle	deg	fiw	90	90	90	90	90
web height (for built sections only)	mm	hw	130	118	118	114	114
web thickness (gross) (for built sectio	mm	tw_gr	6	7	7	5	5
flange width (for built sections only)	mm	wf	100	60	60	60	60
flange thickness (gross) (for built sect	mm	tf_gr	10	12	12	6	6
flange offset distance (for built sectior	mm	bw	0	0	0	0	0
fea grillage	--		NDP1_03	NDP1_710	NDP1_710	NDP1_1417	NDP1_1417

DDePS is used to compute ice load parameters (such as force, pressure, area, line load, etc.) for various combinations of impact scenarios (such as speed, impact location, ice thickness or floe size, strength parameters, etc.). A sketch of the assumed impact scenario is provided in Figure 19. The ice floe is assumed to be oriented normal to the point of contact. For the purposes of computing the mass and moments of inertia, the floe is idealized as a square with uniform thickness. The wedge shape at the impact point is simply used for the contact model.

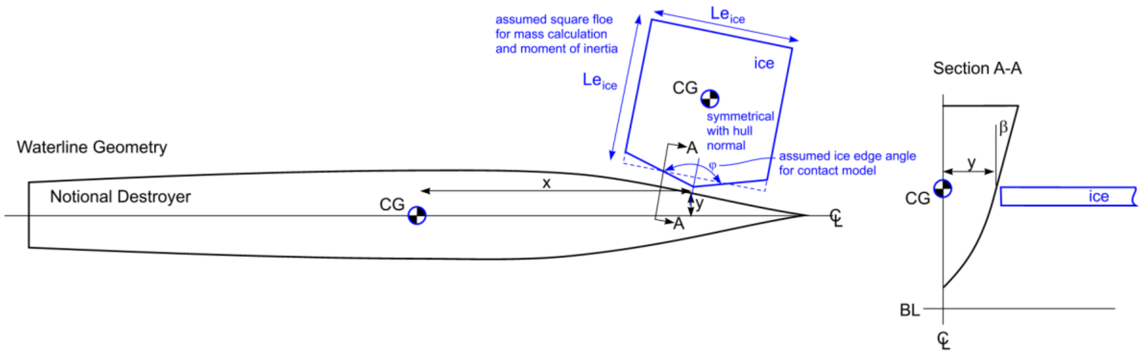

Figure 19: Impact scenario for safe speed assessment

Technical limit speeds are established in (Daley 2015) using the direct line load criteria method, which is when the loading term just equals the structural capacity for the frame for a given interaction scenario. Line load (*Q*) is used as the basis for comparison and establishing the technical safe speed limits. Line load is the closest parameter that relates to the load encountered by a single frame. The limit state is the initial formation of a 3-hinge plastic mechanism of a side shell longitudinal under a patch load. This was shown (e.g. Daley and Hermanski 2009) to produce plasticity in the frame but without any observable permanent dent size.

Figure 20 and 21 shows sample outputs from DDePS (in this case total force versus forward ship speed). Both plots are for 20 m floes of various thicknesses (10 – 50cm). Figure 20 is for Frame 11 (NDP1_710) and Figure 21 is for Frame 14 (NDP1_1417). Recall the approximate load levels of the longitudinal frame plastic limit states at these locations are approximately 0.1 – 0.2 MN (see Figure 15).

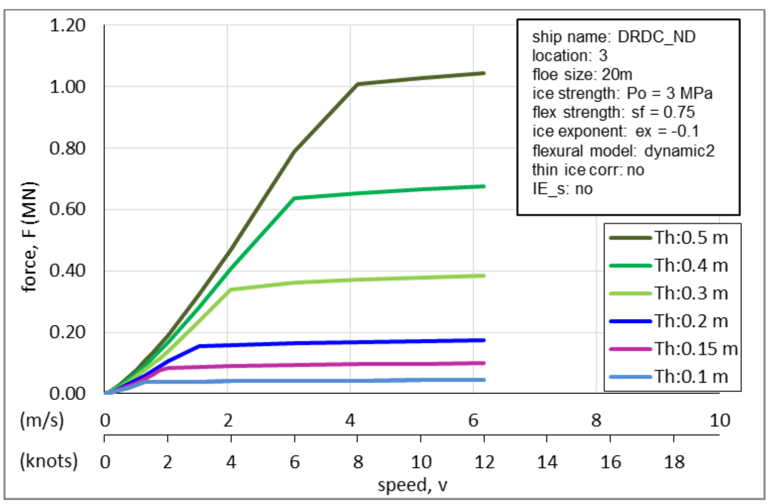

Figure 20: Sample DDePS outputs – force versus speed at location 3

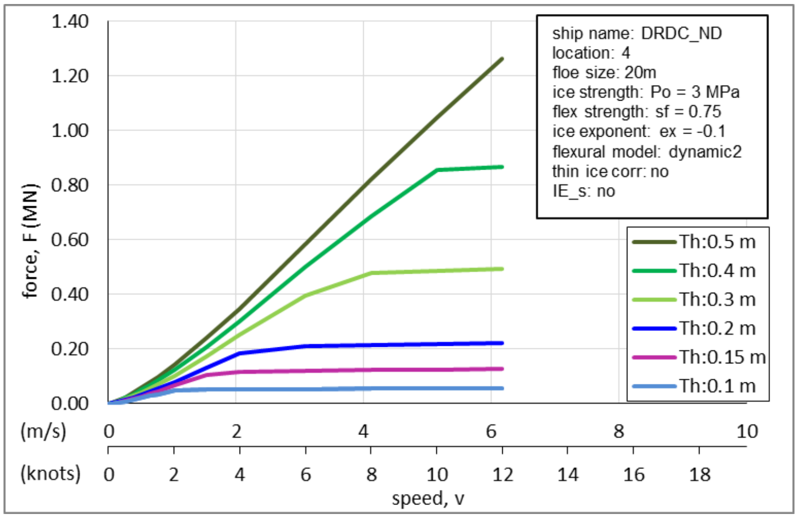

Figure 21: Sample DDePS outputs – force versus speed at location 4

Figure 22 presents the technical safe speed results for the Notional Destroyer assuming the following parameters. In each plot, there are five curves representing different limits for different frame locations.

- Ice crushing strength, P_o = 3 MPa (*ex* = -0.1)
- Ice flexural strength, σ_f = 0.75 MPa
- Floe size: 5 m – 200 m
- Thickness: 30 cm, 50 cm, 1 m
- Speed: 0 knot – 14 knots

The plots in Figure 22 indicate that impacts at location 4 (Frame 14, purple line) represent the limiting condition for this ship. This is due to the relatively weaker scantlings in this area of the bow combined with the impact location with respect to the ship's CG and the hull angles (α and β).

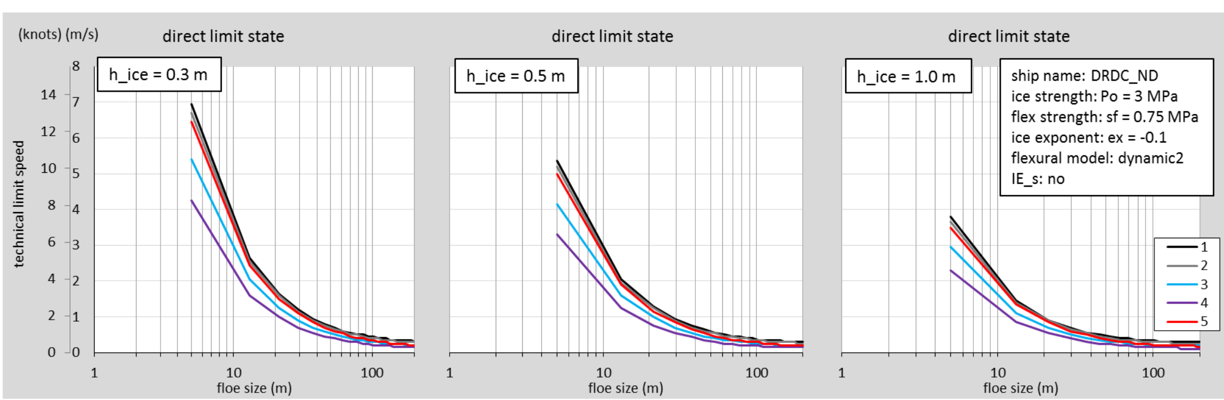

Figure 22: Direct technical safe speeds versus floe size for various thicknesses,30 cm, 50 cm, and 1.0 m

Figure 23 is a summary plot of all the technical safe speed curves shown above. For each impact scenario (combination of floe size and thickness), the minimum limit speed was taken of all the impact locations. The results confirm the outcomes of the Phase 1 Report (Daley 2015) that the ice capability of Notional Destroyer is severely limited. By using the actual bow scantlings as opposed to nominal midbody scantlings, there is a slight increase in capability but operations could only take place in extremely light conditions. Even when the ice is thin (less than 20 cm) and floe sizes are relatively small (less than 20m), speeds would be limited to about 2-3 knots. Operations in brash ice (generally considered less than 5m floe size) could be sustained if speeds are kept under 5 knots.

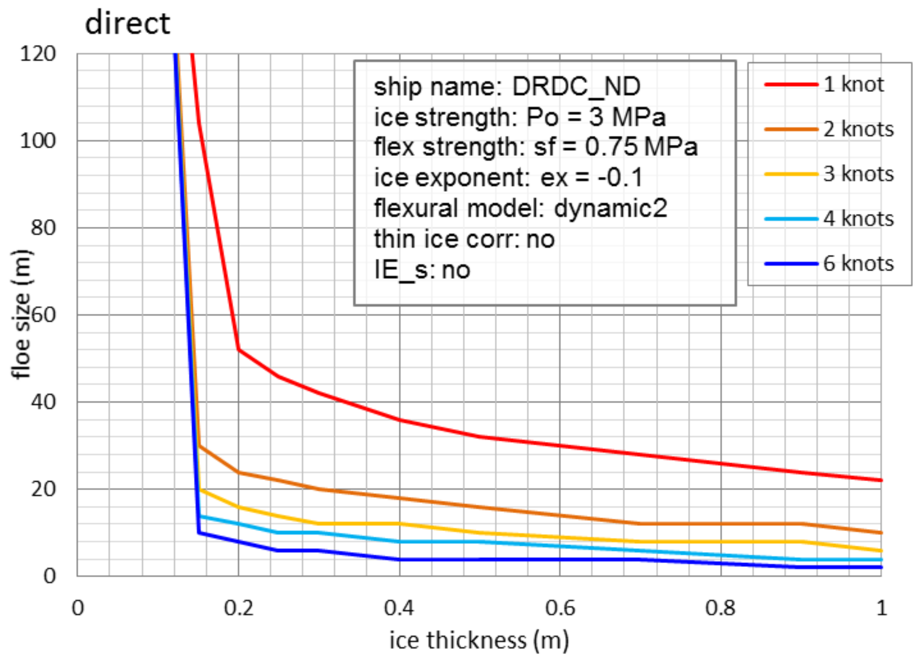

Figure 23: Summary plot of safe speed curves – direct limit state

5. Ice Crushing Forces Considering Deformable Structures

This section describes an update to the DDePS ice load model to account for energy absorption due to structural deformation during a ship-ice interaction event and its influence on load magnitudes and subsequent ice capability assessments. This approach was originally developed and applied in reports by ABS (2015) and Daley (2015). It was later updated and applied in several case studies by Dolny (2017) and ABS (2017, 2016). This section describes a methodology that is largely taken from those reports.

During a ship-ice interaction event, energy may be absorbed by deforming the structure elastically and plastically in addition to the energy expended into crushing the ice. Most standard models of ship-ice interaction (e.g. the ice load model described in Daley (2015) and applied in the direct safe speed assessment presented above assume the ship to be a perfectly rigid body. This assumption is in general valid for stiff structures (i.e. high ice class ships). However, for non-ice classed (or even light-ice classed) ships, a substantial portion of the effective kinetic energy KE_e can be expended into deforming the relatively compliant structure. This concept is generalized by the following energy balance equation where IE_i and IE_s are the ice and structural indentation energies respectively.

$$KE_e = IE_i + IE_s \quad (12)$$

For complex structural arrangements, no analytical equation exists to represent the combined structural and ice indentation processes. Daley & Kim (2010) approached this problem numerically by simplifying the ice load to a point load (highly localized force) and the plastic response of the structure was represented by a linear deformation function;

$$F_n = k_p \zeta_n + F_o \quad (13)$$

The concept, sketched in Figure 24, was implemented into a spreadsheet tool as a practical way to evaluate ice loads with the consideration of the ship's plastic deformation. Daley and Kim applied a 'design of experiments' (DOE) method to develop regressions models for the k_p and F_o terms. The models are functions of a range of input variables which represent the structural parameters of a stiffened panel (frame spacing, span, dimensions, plate thickness, etc.). This is a very useful model that can easily be implemented into a spreadsheet tool. However for large collisions that involve extensive damage and larger ice contact areas, the assumption of a point load is no longer valid.

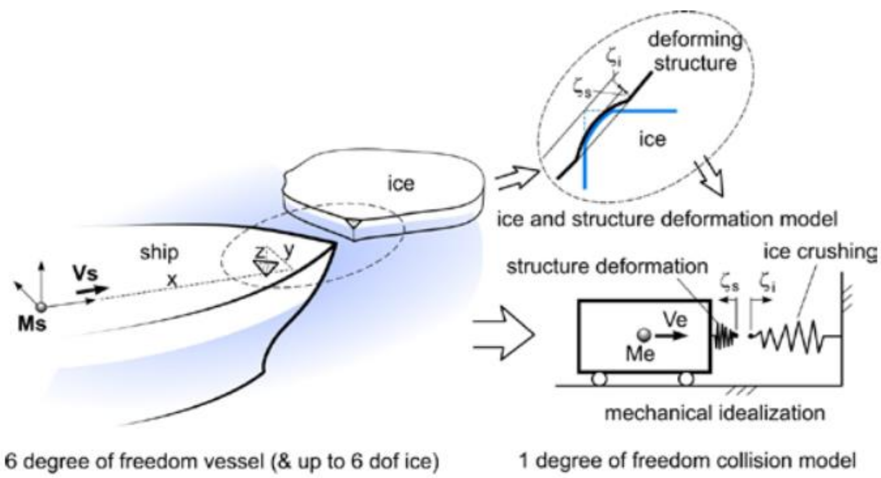

Figure 24: Concept sketch for compliant ship-ice collision model (from Daley & Kim, 2010)

In order to appropriately quantify the structural indentation energy, a more sophisticated approach has been developed which takes into account a more realistic developing load patch. Consider the idealized sketch in Figure 25. For a rigid structure indenting an ice edge, the ice edge crushes and the load patch develops as a growing triangular area (top). When the structure is deformable, local plastic and elastic deformations develop in the structure along with ice crushing. The changing structural shape alters the load distribution (i.e. patch shape) and the force development. This process can be expressed as a power function where total contact force F_n is related to 'total' normal indentation ζ_n of the structure from its initial contact point;

$$F_n = C_s \zeta_n^{k_s} \quad (14)$$

The total normal indentation is simply the sum of the structural deformation and ice crushing indentation ($\zeta_n = \zeta_s + \zeta_c$). The specific power function coefficients, C_s and k_s, must be obtained from a numerical simulation analysis of a ship grillage impacting an ice edge. This section describes the setup and calibration of a numerical ice model and ship specific ice-structure interaction analyses using the representative structural panels of the Notional Destroyer.

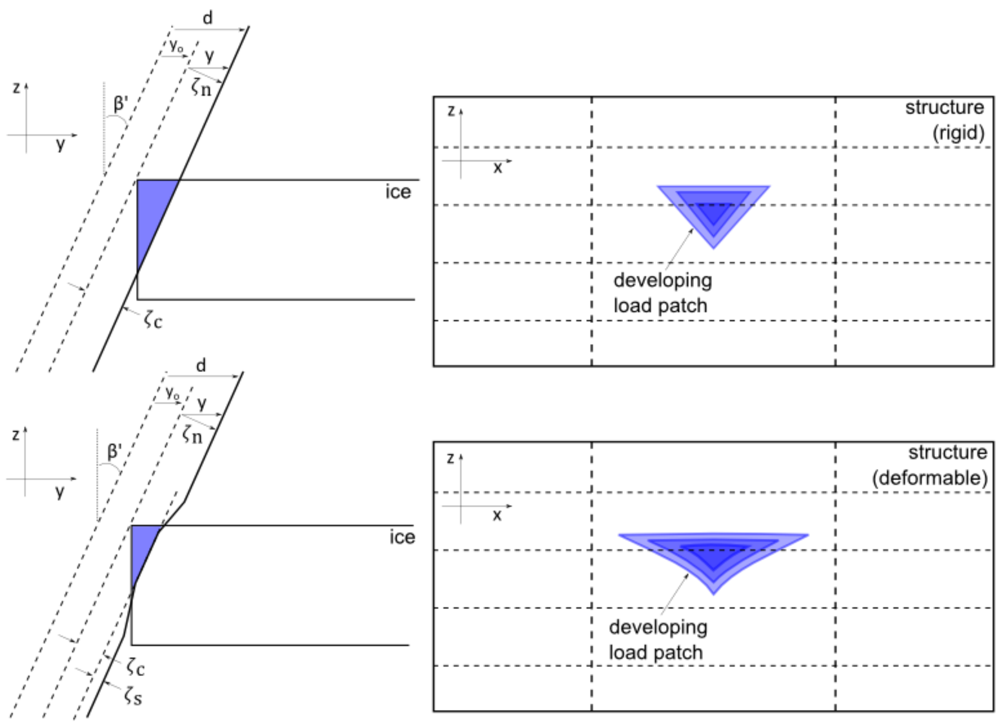

Figure 25: Sketch of interaction model for rigid (top) and deformable (bottom) structures

The sum of ice and structural indentation energies can be obtained by integrating the total force over the depth of 'total' normal indentation;

$$IE_i + IE_s = \int_0^{\zeta_n} F_n d\zeta_n \quad (15)$$

By equating the sum of the ice and structural indentation energies to the effective kinetic energy of a collision and integrating the force, one arrives at;

$$KE_e = \int_0^{\zeta_n} F_n d\zeta_n = \frac{C_s \zeta_n^{k_s+1}}{k_s + 1} \quad (16)$$

The 'total' normal indentation ζ_n can be solved for and expressed as equation *(17)*. It can then be used to solve for the normal force by referring back to equation *(14)*;

$$\zeta_n = \left(\frac{KE_e(k_s + 1)}{C_s}\right)^{\frac{1}{k_s+1}} \quad (17)$$

In order to resolve the structural indentation ζ_s portion of the total indentation, the results of numerical simulations are used to find a relationship with normal force. Later it is demonstrated that the force versus structural indentation response can be simplified into two linearized portions, elastic and plastic;

$$\zeta_s = f(F_n) \tag{18}$$

Once the structural indentation is known, the ice indentation portion ζ_i is then simply the difference and is used to determine the size of the load patch.

$$\zeta_i = \zeta_n - \zeta_s \tag{19}$$

Numerical Simulations

Equations *(14)* and *(19)* describe power functions that are derived from the results of numerical simulations between ship structural grillage models interacting with a deformable ice material. The general purpose commercial finite element analysis code LS-DYNA was used to calibrate and conduct a series of simulation experiments.

Several researchers have attempted to model ice crushing behavior numerically and recently LS-DYNA has been applied to an increasing number of ice problems. Gagnon & Derradji-Aouat (2006) first calibrated and applied LS-DYNA's *MAT_CRUSHABLE_FOAM (MAT_063)* material model to match ice impact parameters (peak force, impact duration, and pressure distribution) obtained from field trials of the Canadian Coast Guard Icebreaker TERRY FOX. Zong (2012) later applied the same 'crushable foam' ice model to simulate bow glancing collisions and calibrated the constitutive material parameters to produce process-pressure area relationships that match different IACS Polar Class P-A curves. Liu et. al (2012) modeled ice with an elasto-plastic material card which considers kinematic hardening *MAT_PLASTIC_KINEMATIC (MAT_003)* and compared peak impact forces and time histories against the Popov + P/A analytical model that is implemented in the IACS Polar Rules and described in Daley (2015). Reasonable agreement was shown between the numerical and analytical models. Additional studies by ABS (2015) and Dolny (2017) also utilized numerical material models for ice in LS-DYNA following the same methodology described in this section.

Each of these researchers recognize that the numerical treatment of ice as an elasto-plastic continuum material in a finite element form introduces significant simplifications and ignores many of the complex ice failure mechanisms such as spalling, splitting, high internal spatial pressure zones, etc. Furthermore, results can be quite sensitive to factors such as contact geometries, contact algorithms, numerical parameters, and mesh size. Nevertheless, it is possible to carefully employ these methods to achieve certain desired results.

Figure 26 illustrates the use of LS- DYNA analyses to obtain the coefficients C_s and k for a sample structural arrangement. The blue curve represents the force versus indentation results from an LS-DYNA simulation considering a rigid plate crushing a 70 cm ice edge (123° wedge angle). For a properly calibrated ice model, this curve will agree with the analytical model (dotted blue line) for the assumed pressure-area parameters. The red curves represent the force versus total normal indentation (ice and structure) considering a deformable structure crushing the same ice model. A power function in the form of equation *(14)* can be fit to this curve as shown by the dotted red line.

The areas under either of these curves represents energy. Thus for any given available effective kinetic energy of a ship-ice collision scenario (arbitrarily highlighted in this plot), the maximum force can be determined. For this particular example of a weak non-ice strengthened structure, the force is reduced significantly (about 30% lower) if the structural indentation energy is considered in the crushing process.

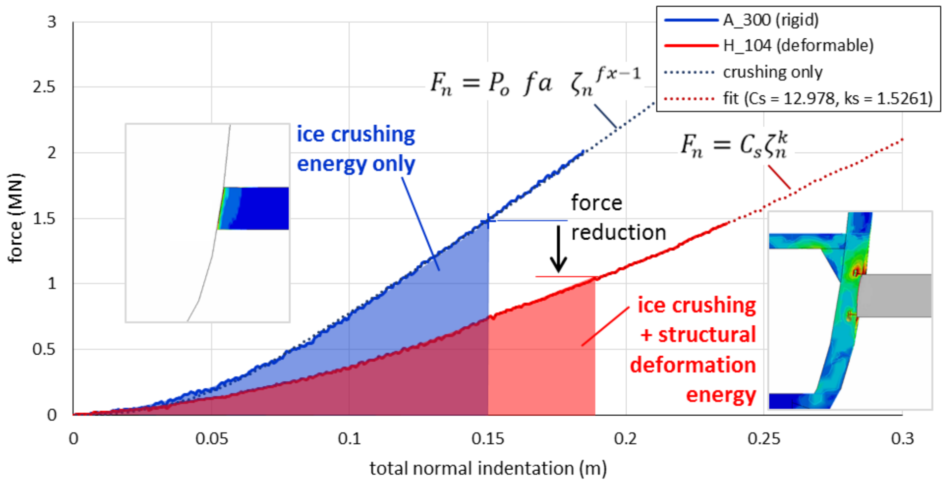

Figure 26: LS-DYNA analysis results for rigid and deformable structures crushing an ice edge

Calibration of the Numerical Ice Model

In order to carry out numerical simulations of a compliant structure interacting with a deformable ice model, the ice material model must first be developed and calibrated. Ice loads on ships depend on many factors and ice failure mechanisms. Ice-structure interaction is a complex phenomenon with many interrelated variables and significant uncertainty. Loads can be governed by local ice crushing, flexural bending, radial or circumferential cracking, friction, ice clearing, and even the dynamic response of the impacting structure; among many additional factors. The selection of an appropriate ice load model and calibration of its parameters to achieve desired strength characteristics is therefore a challenge. The calibration effort described in this section is focused on the crushing process of the ice. The ultimate objective is to produce proper load levels (i.e. forces and contact areas) and pressure distributions that reasonably agree with empirical data.

First, we'll consider some available data. Figure 27 shows pressures measured in a lab setting during the STePS[2] project (Bruneau, Colbourne, et al., 2013; Bruneau, Dillenburg, & Ritter, 2013). Ice cones of various dimensions were grown in the lab and crushed against rigid indenters. Forces and contact areas were measured using a variety of techniques and pressures were determined. Contact pressures were measured in the 10 MPa range over areas up to 0.1 to 0.2 m^2. Ice pressures measured in the field show pressures on the order of a few MPa at about 0.5 to 1m^2. Design local pressures in the IACS polar rules range from a few megapascals up to 6 MPa for the highest ice class and are typically applied over several square meters.

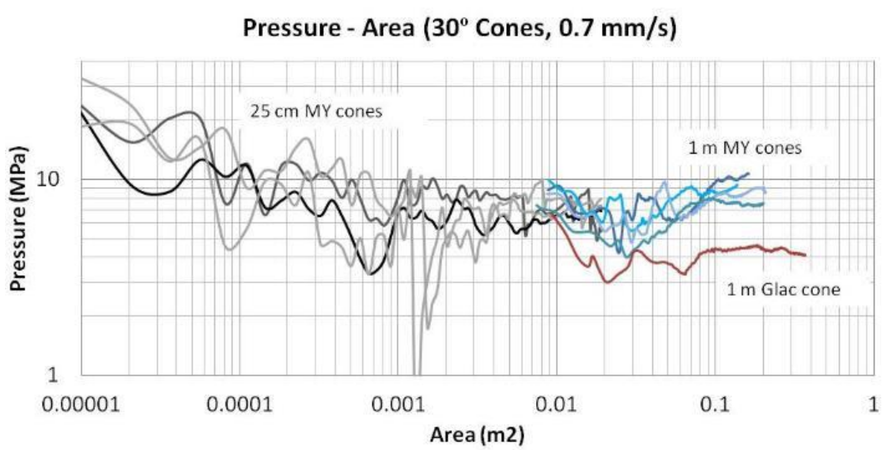

Figure 27: Measured pressures in STePS2 lab tests (Bruneau, Colbourne, et al., 2013)

To develop an ice material model in LS-DYNA, a design of experiments (DOE) response surface methodology (RSM) approach was employed to systematically investigate the influence of elasto-plastic material parameters and geometric attributes on load magnitudes and pressure distributions during an ice-structure interaction process. Within the DOE umbrella of experimental design philosophies, the RSM employs mathematical and statistical methods to analyze the influence of various factors on a particular response (Montgomery, 2008). For complex and often highly nonlinear computer experiments, the RSM offers an attractive option to develop representative metamodels of the simulation results.

A sketch of the problem is provided in Figure 28 where a rigid shell intender is used to crush a deformable ice model. The variable factors and their levels, fixed factors and responses are presented in Table 10 and an example constitutive model for the ice (elasto-plastic stress-strain curve) is plotted in Figure 29. Initially, the only variable factors for the ice model was the material yield strength σ_y and the ice thickness h_{ice}. This was a deliberate decision intended to simplify the analysis. The objective of this exercise was to develop regressions for parameters of an elasto-plastic material model (a proxy for ice) that will produce target process-pressure area curves, which are empirically defined for a given set of geometric conditions. The result is a 'constructed' model, however it is well recognized that the elasto-plastic numerical treatment of ice crushing is highly idealized and does not capture many of the complex ice failure mechanisms that occur in reality.

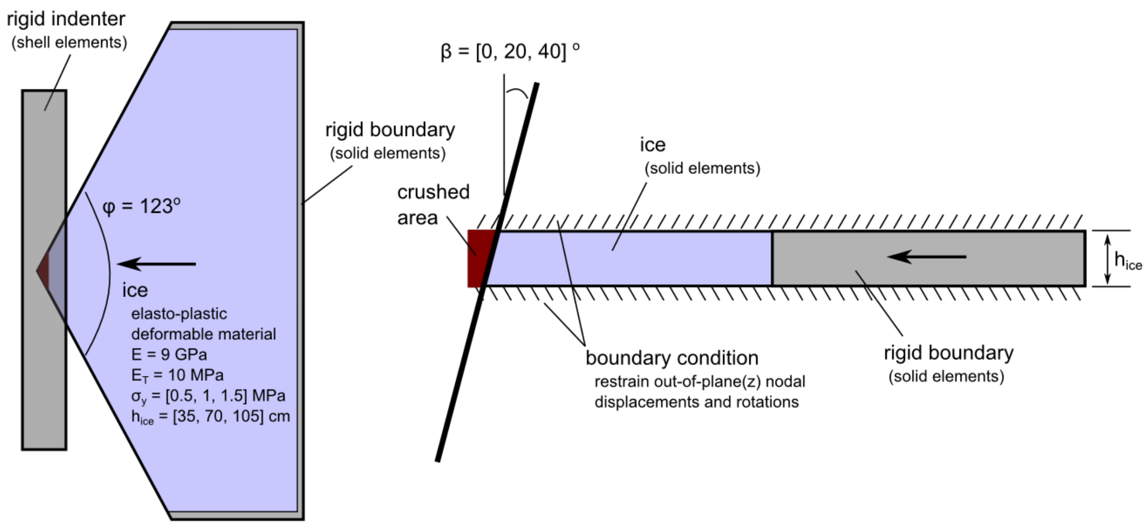

Figure 28: Sketch of DOE problem for ice calibration

Table 10: Factors and responses for ice calibration exercise

Factors	***Description***	***Symbol***	***Units***	***Low***	***Medium***	***High***
A	*material yield strength*	σ_y	*MPa*	0.5	1	1.5
B	*ice thickness*	h_{ice}	*m*	0.35	0.7	1.05
C	*frame angle*	β	°	0	20	40
fixed	*ice wedge angle*	Φ	°		123	
fixed	*ice density*	ρ_{ice}	kg/m^3		900	
fixed	*ice modulus of elasticity*	E_{ice}	*GPa*		9.0	
fixed	*ice Poisson's ratio*	ν_{ice}	--		0.3	
fixed	*ice tangent modulus*	E_t	*MPa*		10.0	
Responses	***Description***	***Symbol***	***Units***			
R1	*nominal pressure at 1m²*	P_o	*MPa*			
R2	*process P-A exponent*	*ex*	--			

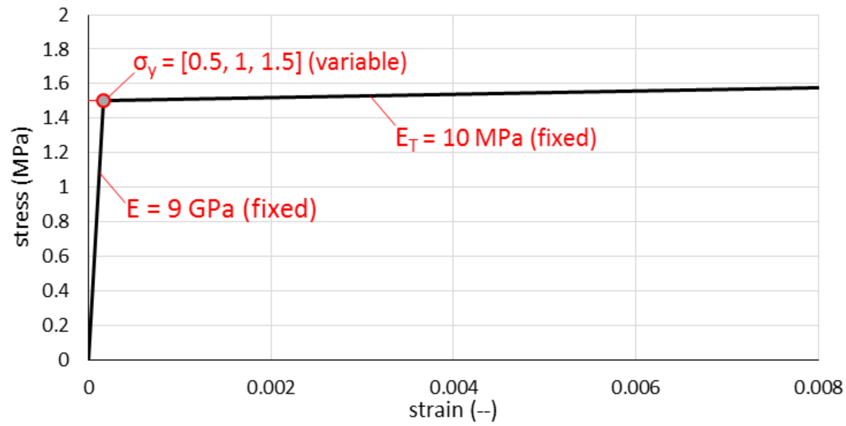

Figure 29: Stress-strain curve for elasto-plastic numerical ice material

The rigid indenter is a plate modeled with shell elements and rotated to variable beta β angles (0-40°). The ice is a 123° wedge, with variable thickness (35 to 105 cm), modeled with solid elements and bounded on the back edges with a rigid support (also solid elements). Boundary conditions are imposed on the top and bottom of the ice edge to restrain out-of-plane displacements and rotations. The purpose of this restraint is to isolate the crushing problem and remove bending and bulging effects from the simulations. This is later shown to effectively concentrate contact pressures within the contact area.

In DDePS the nominal wedge angle φ is assumed to be 150°. However, considering the patch size reduction to account for ice pressure concentration (i.e. $w = 0.7 \cdot W_{nom}$), the effective pressure acting on the structure is actually increased and applied over a smaller contact area. It can be shown, by rearranging the equations for the patch size reduction, that an effective pressure-area model with *ex* = -0.1 and a new parameter P_{o_eff} can be derived as equation *(20)*. Furthermore, a reduced ice wedge angle can be determined following equation *(21)* to match the effective contact area. For a 150° nominal wedge angle, the equivalent effective wedge is 123° and therefore used in these ice calibration simulations.

$$P_{o\_eff} = \frac{P_o}{{C_w}^{2+2ex}} \tag{20}$$

$$\phi_{\text{eff}} = 2\tan^{-1}\left(C_w^2 \tan\left(\frac{\phi}{2}\right)\right) \tag{21}$$

This is illustrated by Figure 30 for a nominal pressure-area model of P_o = 3 MPa, *ex* = -0.1 and a wedge angle φ= 150° (black curve). Considering the patch area reduction (while maintaining constant force), the effective P-A acting on the structure is shown in Figure 30 by the red curve. Following equation *(20)* and a reduced wedge angle according to equation *(21)*, an equivalent effective P-A relationship can be derived as P_{o_eff} = 5.7 MPa, *ex* = -0.1. The plot shows exact agreement with the effective P-A curve.

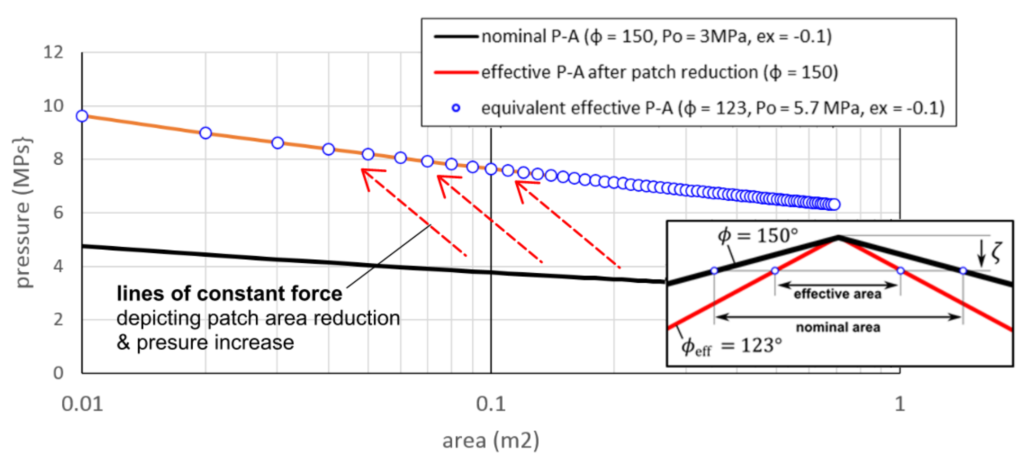

Figure 30: Diagram of patch size reduction and effective P-A relationship

Figure 31 is a snapshot of the simulation setup for an example ice calibration simulation (referred to as A_104). The solid elements for the ice are refined in the area of contact to a fine mesh (3 to 7 cm edge length in the crushing zone). This mesh size was selected based on the similar approximate mesh size of the structural models which are explained in the case studies. A 3.5 cm mesh size was selected for the rigid plate. The final size of the ice model and mesh size selections were the result of a mesh convergence analysis and represent a balance between computational cost and numerical accuracy.

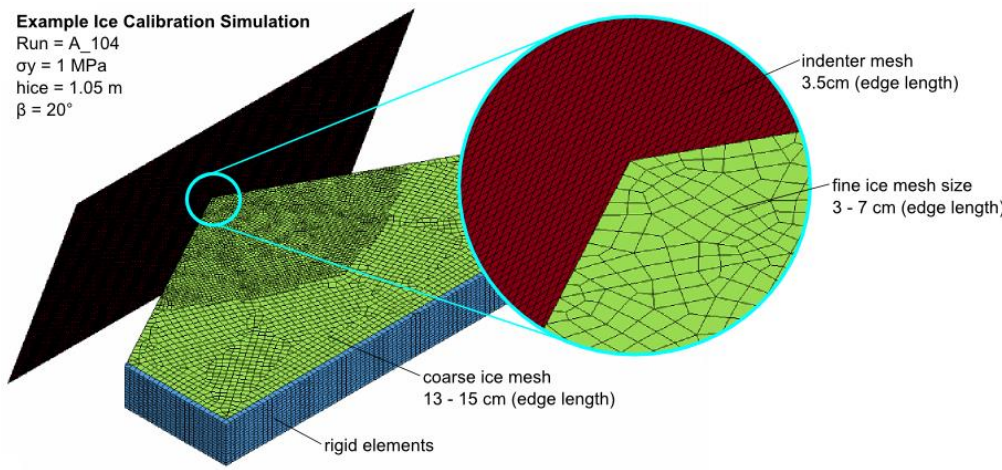

Figure 31: Numerical simulation setup for ice calibration simulation A_104

Figure 32 through Figure 37 present detailed results from two selected ice calibration simulation cases (A_104 and A_101 respectively). Plots are provided of the pressure distributions at 3 instances, force-time histories, area-time histories (nominal and measured), and the pressure-area results (nominal process, curve fit and measured process).

The nominal area, highlighted on the pressure distributions (white outline) and plotted on the area time histories (black), is computed as a function of the overlap geometry and indentation depth. This nominal area is used with the contact force to determine the nominal pressure-area relationship (black dots in Figures 34 and 37). For each simulation, the 'computed' pressure area terms (P_o and *ex*) are determined by fitting a power function curve (blue) to the nominal process pressure-area data.

LS-DYNA's 'interface pressure' functionality was also used to obtain a measured contact area at each time step. The measured area is determined by the number of shell elements that are activated with a contact pressure at each time step. In almost all cases, this the measured area is larger than the nominal area. This is a result of the mesh size and contact model employed in LS-DYNA. While it is not used as part of the calibration, it highlights concentrations of peak pressures inside the contact area, which are a desirable effect.

Nominal and measured pressures are both useful, but distinct quantities. Nominal pressures are used in analytical impact calculations (such as in DDePS or GEM). Nominal pressures are extracted from the LS-Dyna results for verification that the LS-Dyna and DDePS values are comparable. The measured pressures are based on actual contact areas and will influence the local structural response in LS-Dyna. These are extracted for general reference, since there is no specific target for the pressures. At this point, the local pressures are not unreasonable.

The simulations are focused on achieving the right collision force with the right general contact patch size. These goals can be achieved by getting the nominal values right. Also getting the specific local pattern of contact pressures correct would be ideal, but is beyond current aims.

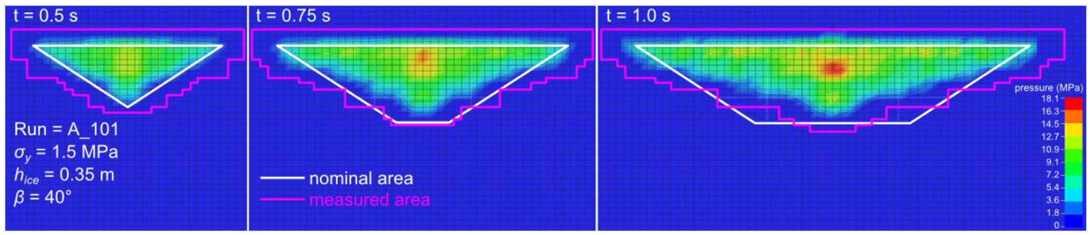

Figure 32: Interface pressures - ice calibration experiment A_101

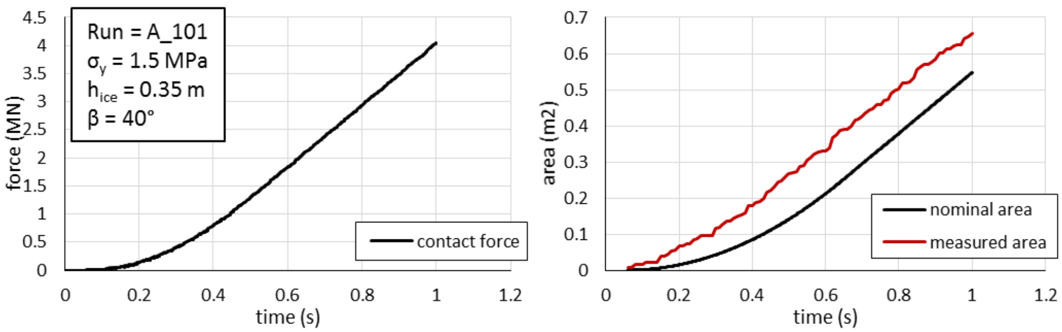

Figure 33: Time histories of force and contact area - ice calibration experiment A_101

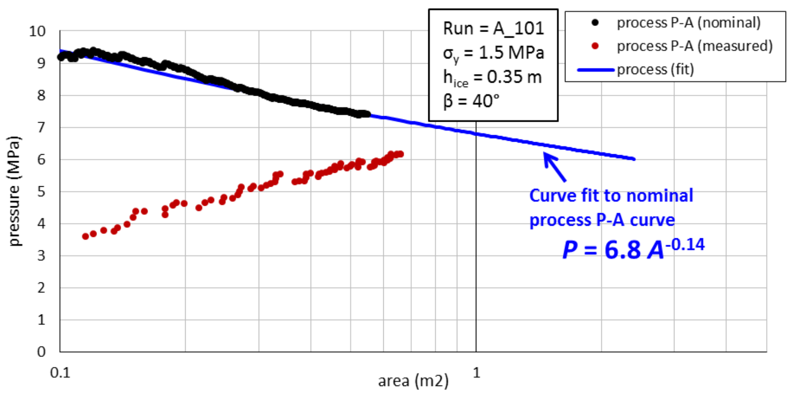

Figure 34: Process-pressure area curves - ice calibration experiment A_101

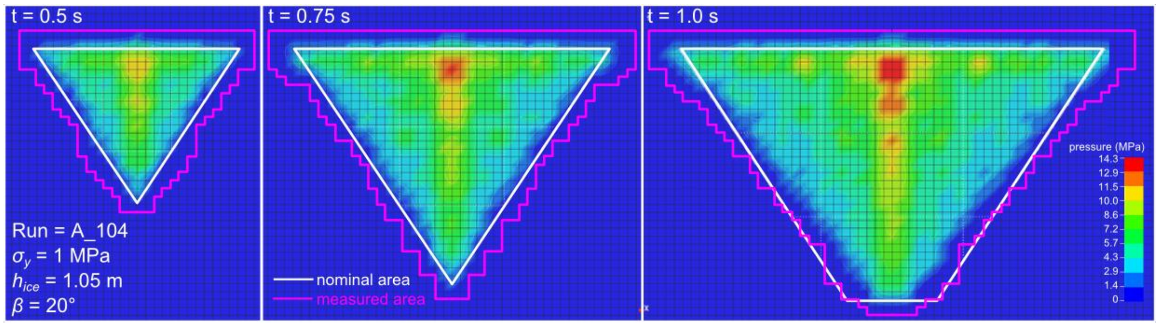

Figure 35: Interface pressures - ice calibration experiment A_104

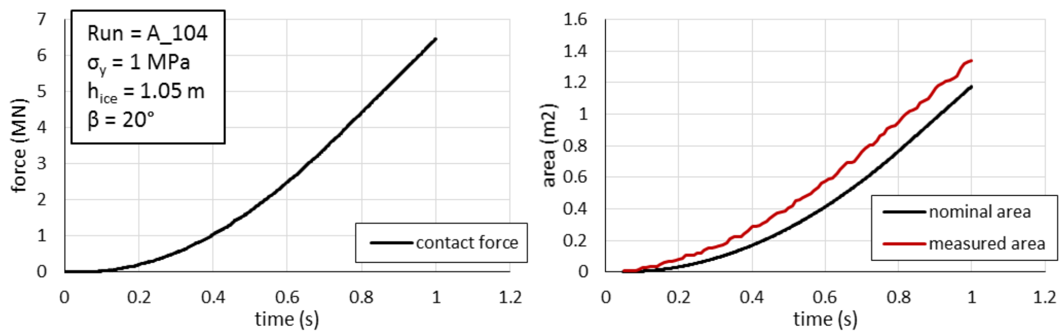

Figure 36: Time histories of force and contact area - ice calibration experiment A_104

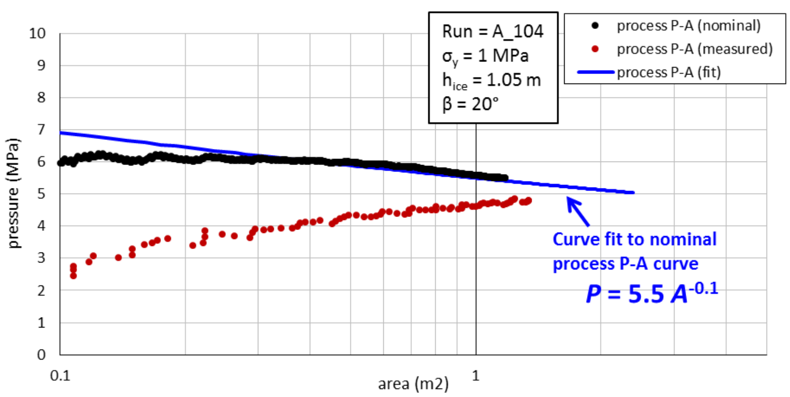

Figure 37: Process-pressure area curves - ice calibration experiment A_104

A summary of the initial ice calibration runs and their results are provided in Table 11. For the numerical experiments described in this section, randomization is not necessary because there is no standard error in computational models. Thus, the results are sorted here in standard order. 15 initial simulations were conducted and analyzed. For each run, the P-A terms (i.e. response parameters P_o and *ex*) were obtained by fitting a curve to the nominal pressure-area relationship. These are listed in the table as "computed" responses. The range of P_o was 3.3 to 9.2 MPa and the range of *ex* was -0.2 to 0. These response levels suitably cover most target P-A model that are of interest for this study.

Table 11: Numerical ice calibration experiments and results – initial runs

Initial Runs							
run	***σ_y (MPa)***	***h_{ice} (m)***	***β (°)***	***computed ****		***predicted *****	
				P_o (MPa)	***ex***	***P_o (MPa)***	***ex***
A_101	1.5	0.35	40	6.8	-0.14	6.9	-0.1
A_102	0.5	0.7	20	3.5	-0.1	3.8	-0.1
A_103	0.5	1.05	0	3.3	0.0	3.1	0.0
A_104	1	1.05	20	5.5	-0.1	6.0	0.0
A_105	1.5	0.7	20	6.9	-0.09	7.2	-0.1
A_106	1	0.7	40	6.7	-0.07	6.1	-0.1
A_107	0.5	0.35	40	3.3	-0.2	3.3	-0.2
A_108	1	0.35	20	4.9	-0.05	5.0	-0.1
A_109	1.5	0.35	0	6.5	0.0	6.4	0.0
A_110	1.5	1.05	40	9.2	0.0	9.1	0.0
A_111	0.5	1.05	40	5.3	0.0	5.3	0.0
A_112	1	0.7	0	5.0	0.0	4.8	0.0
A_113	0.5	0.35	0	3.4	0.0	3.4	0.0
A_114	1.5	1.05	0	6.5	0.0	6.4	0.0
A_115	1	0.7	20	5.2	-0.1	5.5	-0.1

* computed values are from curve fits to LS-DYNA results (e.g. Figure 37)

** predicted is as computed from equations (22) and (23)

Stat-Ease, Inc.'s software package, Design Expert® Version 8.0.6, was used to determine the treatment combinations and analyze the results. Once the initial simulations were completed and the results were populated, regression calculations were conducted to check all polynomial models for each response. The effects for all model terms were calculated and statistical methods were used to compare each possible model (Stat-Ease, 2010). For both response parameters, two-factor interaction models were suggested and selected to develop metamodels. The metamodels for P_o and ex are shown in equations *(22)* and *(23)* respectively.

$$P_o$$

$$P_o = 2.06 + 2.90\sigma_y - 0.56h_{ice} - 0.04\beta + 0.36\sigma_y h_{ice} + 0.01\sigma_y\beta + 0.08h_{ice}\beta \qquad (22)$$

$$ex = -0.02 + 0.03\sigma_y + 0.004h_{ice} - 0.007\beta - 0.04\sigma_y h_{ice} + 0.0007\sigma_y\beta + 0.006h_{ice}\beta \qquad (23)$$

In order to further verify the metamodels, an additional 12 simulations were run as verification experiments. These are necessary to test the metamodels for treatment combinations that were not tested in the original experiments. The three variable factors were selected randomly for each verification run. Their results are presented in Table 12 and comparisons are made in Figure 38 between the metamodel predictions and the direct numerical simulation results. P_o is predictable for a range of strength levels (3 to 9 MPa) and while not perfectly aligned with unity, the metamodel results corroborate quite reasonably with the direct simulation results with some minimum acceptable variance. The exponent *ex* is less predictable but the values are within a reasonable range (-0.25 to 0).

Table 12: Numerical ice calibration experiments and results – verification runs

Verification Runs							
run	***σ_y (MPa)***	***h_{ice} (m)***	***β (°)***	***computed***		***predicted***	
				P_o (MPa)	***ex***	***Po (MPa)***	***ex***
A_201	0.5	0.35	50	3.6	-0.25	3.3	-0.2
A_202	0.625	0.7	10	3.8	0.0	3.9	0.0
A_203	1.25	0.7	30	6.65	-0.08	6.7	-0.1
A_204	0.5	0.35	0	3.4	0.0	3.4	0.0
A_205	1.5	1.05	30	8.35	-0.03	8.4	0.0
A_206	1.5	0.35	10	6.5	-0.04	6.5	0.0
A_207	1.375	0.7	10	6.25	-0.03	6.4	0.0
A_208	0.875	0.35	20	4.5	-0.06	4.6	-0.1
A_209	1.5	1.05	40	9.3	-0.01	9.1	0.0
A_210	0.625	1.05	0	3.7	0.0	3.5	0.0
A_211	1.275	0.21	10	5.7	-0.04	5.7	0.0
A_212	1.2911	0.14	10	5.6	-0.04	5.7	0.0

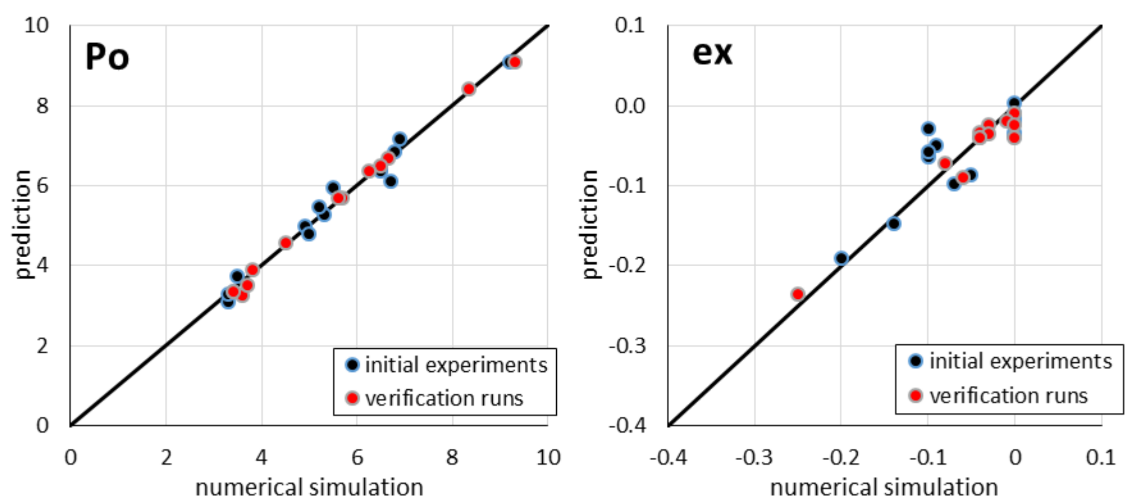

Figure 38: Regression predictions versus numerical simulation results for P_o and *ex*

Given an ice thickness h_{ice}, frame angle β, and target effective nominal pressure term P_o, equation *(33)* can be rearranged to find an appropriate ice yield strength σ_y for the numerical model;

$$\sigma_y = \frac{P_o - 2.06 + 0.56h_{ice} + 0.04\beta - 0.08h_{ice}\beta}{2.90 + 0.36h_{ice} + 0.01\beta} \qquad (24)$$

Extended Calibration Runs and Linear Regression

An additional set of calibration runs were carried out to investigate the effect of the ice wedge angle φ on the process pressure-area development produced in the numerical model. By considering this additional parameter, more general predictive metamodels can be developed for P_o and *ex* for application to different interaction scenarios. Figure 35 is a sketch of the additional wedge angles considered – 90°, 120°, and 150°. A total of 54 additional simulations were run and processed in the same manner as the previous section. The table in Appendix 1 lists the detailed parameters and results (i.e. computed P_o and *ex* terms) from these simulations. Ice thickness (h_{ice}) and indenter frame angles (β) were varied as listed in Table 10.

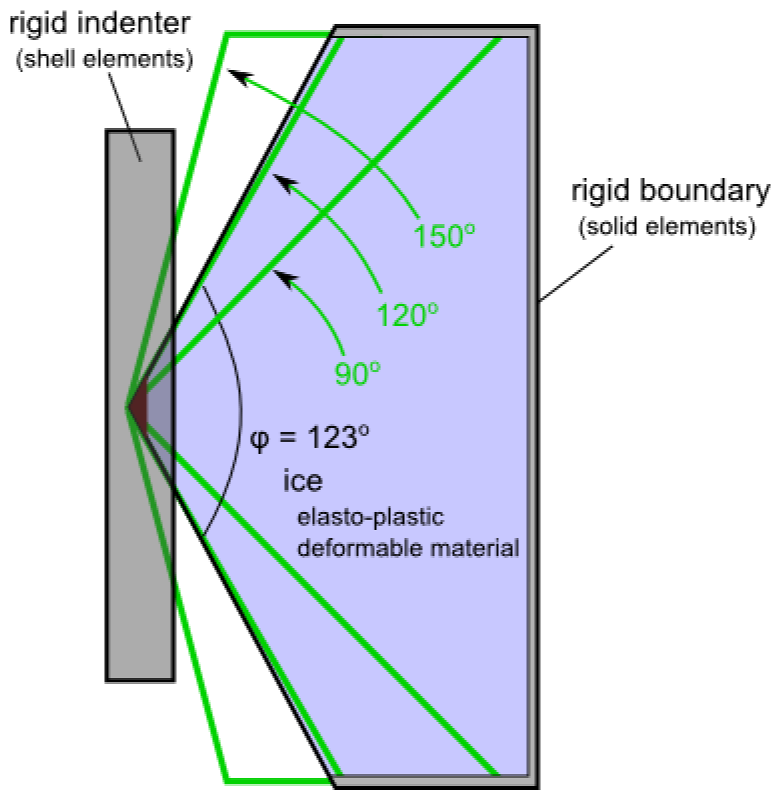

Figure 39: Extended ice calibration runs to consider ice wedge angle (φ)

These results were also analyzed using Design Expert® Version 8.0.6 to compare various response metamodels. Using the extended runs together with the initial calibration runs presented earlier, linear single-factor regressions were found to give reasonable predictions for P_o and *ex*. Equations *(25)* and *(26)* are the updated metamodels derived from the extended data set to include wedge angle. Figure 40 compares the numerical simulation results with the metamodel predictions. It is shown that Po is predictable for a range of strength levels (3 to 9 MPa) and the metamodel results corroborate quite reasonably with the direct simulation results with some minimum acceptable variance. Again, the exponent *ex* is less predictable but the values are within a reasonable range (-0.25 to 0).

$$P_o = 1.586 + 3.312\sigma_y - 0.0084\varphi + 1.298h_{ice} + 0.039\beta \quad (25)$$

$$ex = -0.065 + 0.007\sigma_y + 0.00003\varphi + 0.047h_{ice} - 0.001\beta \quad (26)$$

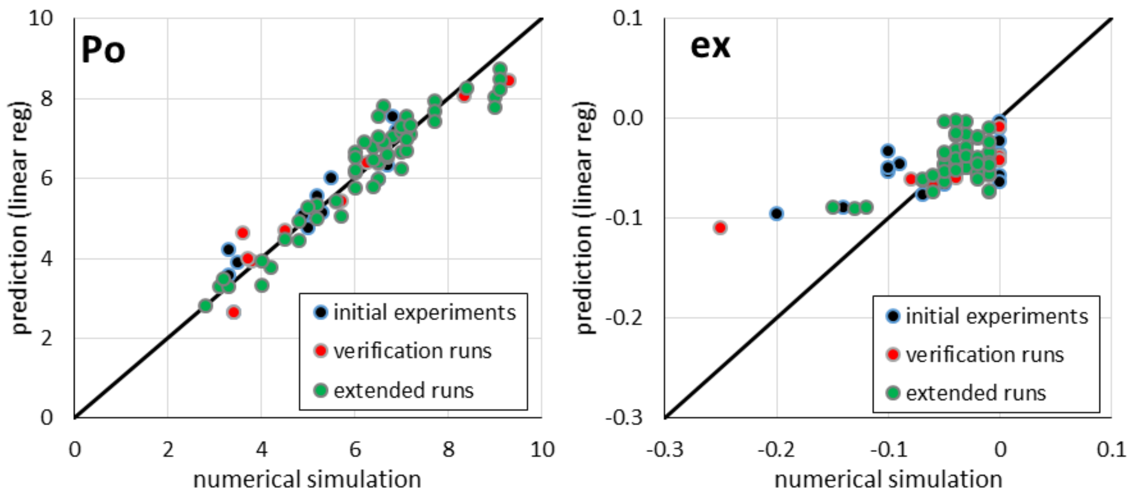

Figure 40: Linear regression predictions for numerical simulation results for P_o and *ex* (taking into account Φ)

Finally, equation *(25)* can be rearranged to find an appropriate ice yield strength σ_y for the numerical model, given an ice thickness h_{ice}, ice wedge angle Φ, frame angle β, and target nominal pressure term P_o. This is shown as equation *(27)* and offers a fairly simple method for using LS-DYNA's elasto-plastic material model as constructed proxy for ice that will produce target process-pressure area curves for a variety of interaction scenarios.

$$\sigma_y = \frac{P_o - 1.586 + 0.0084\Phi - 1.298h_{ice} - 0.039\beta}{3.312} \quad (27)$$

6. Response of Representative Bow Panels to Deformable Ice Model

The mathematical model used in the safe speed assessment presented in section 4 assumed the structure is rigid and that all effective kinetic energy in a collision is expended into ice crushing. This section describes a numerical analysis of ice-structure interaction which takes into account the compliance of the structure during the indentation process. The analysis follows procedures presented in section 5 and explores when the assumption of a rigid structure is no longer valid. This analysis suggests that the structural compliance of the non-ice strengthened Notional Destroyer plays a critical role in the ice structure interaction process. Table 13 lists a series of numerical simulations between the various representative bow structural panels and deformable ice models of various thicknesses. The ice strength term (σ_{y_ice}) for each run was determined using the linear regression equation *(25)* which has been calibrated for a target nominal P_o = 3.0 MPa.

Table 13: Numerical simulations between notional destroyer bow panels and deformable ice model

Run #	*P_{o_eff} (MPa)*	*h_{ice} (m)*	*β (°)*	*σ_{y_ice}[a] (MPa)*	*X_{cen} (m)*	*Y_{cen} (m)*	*Z_{cen} (m)*	*structure_k_file*	*ice_k_file*	*description*
D_101	5.7	0.14	11.7	1.36	-1.31	3.31	7.37	NDP1_03_rot.k	ice_140_123.k	ice140_centered_on_longl
D_102[b]	5.7	0.35	11.7	1.28	-1.31	3.31	7.37	NDP1_03_rot.k	ice_350_123.k	ice350_centered_on_longl
D_103	5.7	0.7	11.7	1.14	-1.31	3.31	7.37	NDP1_03_rot.k	ice_700_123.k	ice700_centered_on_longl
D_111	5.7	0.14	17.6	1.29	-4.01	17.22	7.37	NDP1_710_rot.k	ice_140_123.k	ice140_centered_on_longl
D_112	5.7	0.35	17.6	1.21	-4.01	17.22	7.37	NDP1_710_rot.k	ice_350_123.k	ice350_centered_on_longl
D_113	5.7	0.7	17.6	1.07	-4.01	17.22	7.37	NDP1_710_rot.k	ice_700_123.k	ice700_centered_on_longl
D_121	5.7	0.14	10.2	1.38	-6.51	31.35	7.37	NDP1_1417_rot.k	ice_140_123.k	ice140_centered_on_longl
D_122	5.7	0.35	10.2	1.30	-6.51	31.35	7.37	NDP1_1417_rot.k	ice_350_123.k	ice350_centered_on_longl
D_123	5.7	0.7	10.2	1.15	-6.51	31.35	7.37	NDP1_1417_rot.k	ice_700_123.k	ice700_centered_on_longl

[a]Determined based on metamodel, equation *(27)*
[b]Examples presented below:
Target P_{o_eff} = 5.7 MPa, *ex* = -0.1
Wedge angle φ = 123°

The ice wedges all feature a 123° opening angle. The target strength for the ice model was based on effective process pressure area-model of P_{o_eff} = 5.7, *ex* = -0.1. This corresponds with a nominal P_o value of 3MPa (also assuming a nominal 150° wedge angle and contact area reduction). Applying the metamodel developed by the ice calibration exercise outlined in section 5, the elasto-plastic ice model parameters (i.e. yield strength) are also listed in the table for each simulation run.

A snapshot of an example simulation run (D_102) is shown in Figure 41. In this example, a 35 cm thick ice edge is crushed against at the center of a longitudinal frame. Figure 42 highlights the development of applied pressure and von-Mises stress distribution of the hull structure. The pressure distributions exhibit areas of high and low pressures with a nominal contact area that grows as the simulation progresses. Hull stresses highlighted by a red fringe indicate areas of plasticity in the structure.

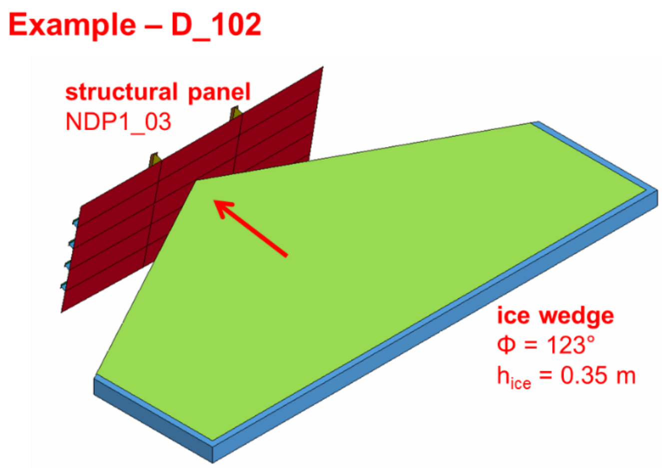

Figure 41: Ice-structure interaction simulation setup – e.g. run D_102 (35cm ice edge centered on longitudinal frame)

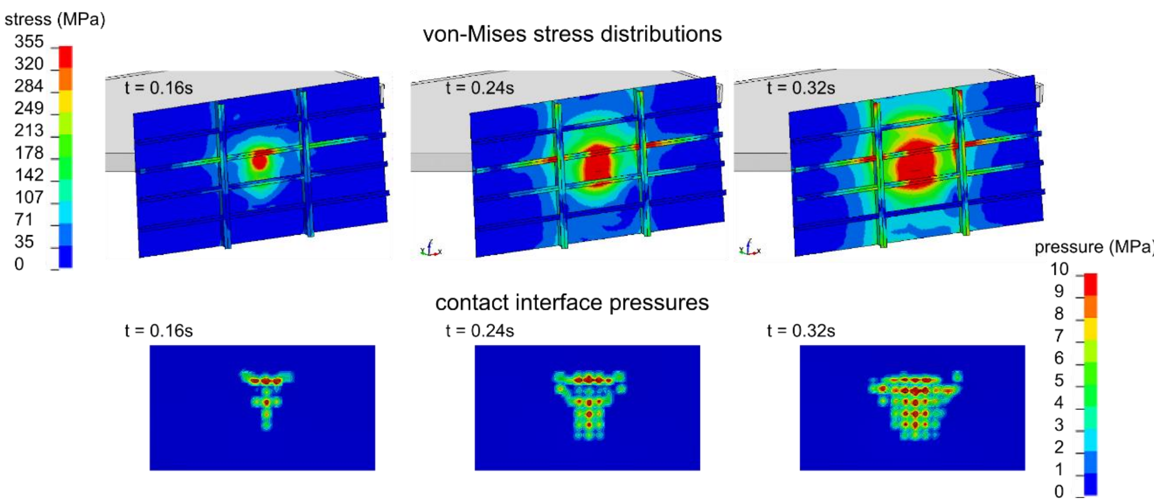

Figure 42: Ice-structure interaction simulation – e.g. run D_102 (35 cm ice edge centered on longitudinal frame)

From the simulation results, the total normal displacement can be plotted against the contact force to extract the necessary power function parameters, C_s and k_s, described in section 5. This is shown in Figure 43 for the forward-most structural panel NDP1_03. Each curve represents a different ice thickness and highlights the change in load development with increasing ice thickness. Ultimately, C_s and k_s are each represented as linear functions of ice thickness.

The structural deformation can also be extracted and compared with the ice crushing component of total normal displacement. Figure 44 shows the force versus structural deformation, a direct output of the numerical simulations, for each of the longitudinal frame load cases. Consider structural deformations less than 10 cm (a 5 cm large deformation limit will be applied in the next section). Zooming into this portion of the plot, the load deflection curves exhibit an elastic portion followed by a plastic response. Both of these can be linearized within this range. The slope of the elastic portion (green line, k_{el} = 31.71 MN/m) is the same for each of the simulations (i.e. independent of ice thickness). Also, the force level corresponding to the transition point between the elastic and plastic responses can be considered constant (for this particular panel, F_{el} = 0.22 MN). The slope of the plastic regime, however, varies a function of ice thickness (red line). This can be explained by the change in load pattern on the frame due to different ice thicknesses.

The linear equations for C_s, k_s, and k_p can be incorporated via lookup tables into DDePS for each representative structural panel. The simulation results for the other panels (NDP1_710 and NDP1_1417) are shown in Figure 44 through Figure 47. A summary of all results is provided in Table 14.

Table 14: Summary of numerical simulations - parameters for DDePS

Structural Panel	C_s	k_s	F_{el} *(MN)*	k_{el} *(MN)*	k_p *(MN/m)*
NDP1_03	$C_s = 20.2h_{ice} + 1.23$	$k_s = 0.76h_{ice} + 1.11$	0.22	31.71	$k_p = 8.01h_{ice} + 15.10$
NDP1_710	$C_s = 15.4h_{ice} + 2.81$	$k_s = 0.64h_{ice} + 1.26$	0.17	21.25	$k_p = 2.84h_{ice} + 12.25$
NDP1_1417	$C_s = 10.7h_{ice} + 2.06$	$k_s = 0.55h_{ice} + 1.14$	0.11	12.22	$k_p = 1.75h_{ice} + 6.04$

Results – Bow Shoulder Panels

The following plots show the behavior of the three bow panels in the Notional Destroyer in response to ice loads. Figure 43 and Figure 44 show the results for panel NDP1_03. The plots include the total force versus deflection curves expressed as power equations. The equations on Figure 43 are for total deflection (ice + structure), while those on Figure 44 are the just the structural component. Both these are needed for determining the vessel's capacity. Figure 45 and Figure 46 provide similar information for panel NDP1_710. Figure 47 and Figure 48 provide similar information for panel NDP1_1417.

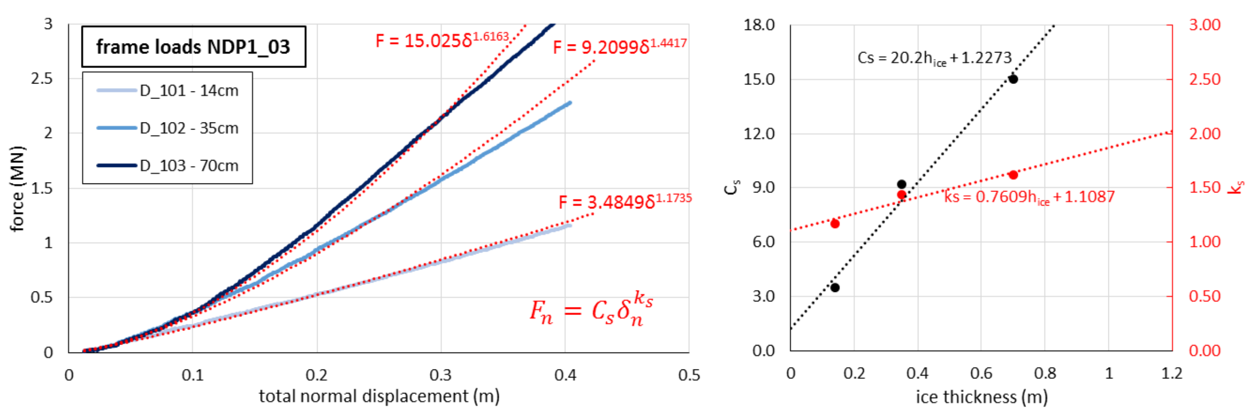

Figure 43: Numerical simulation results for NDP1_03 - force versus total displacement (left) and power function parameters (right)

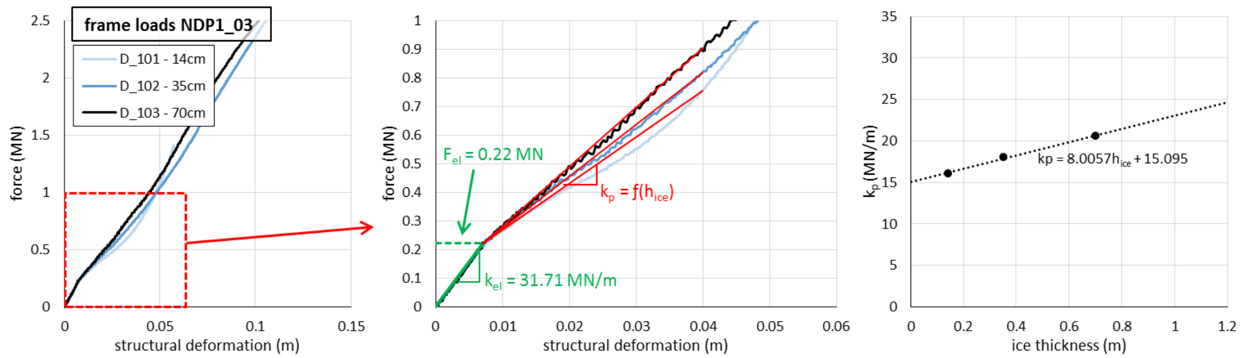

Figure 44: Numerical simulation results for NDP1_03 - force versus structural deformation (left & center) and plastic term (right)

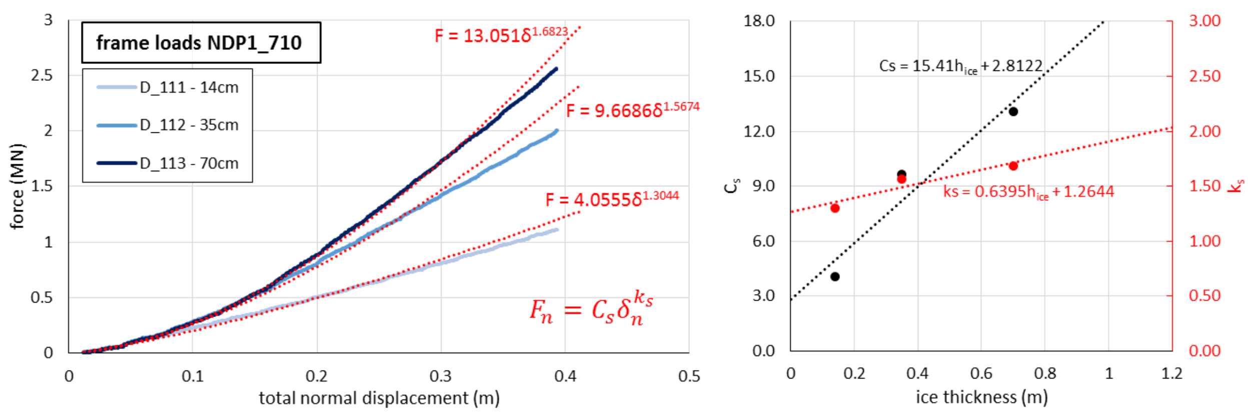

Figure 45: Numerical simulation results for NDP1_710 - force versus total displacement (left) and power function parameters (right)

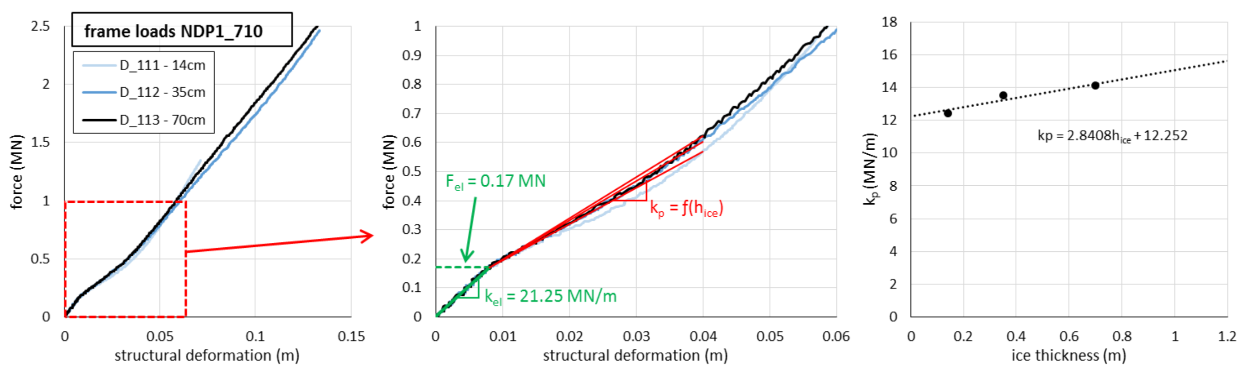

Figure 46: Numerical simulation results for NDP1_710 - force versus structural deformation (left & center) and plastic term (right)

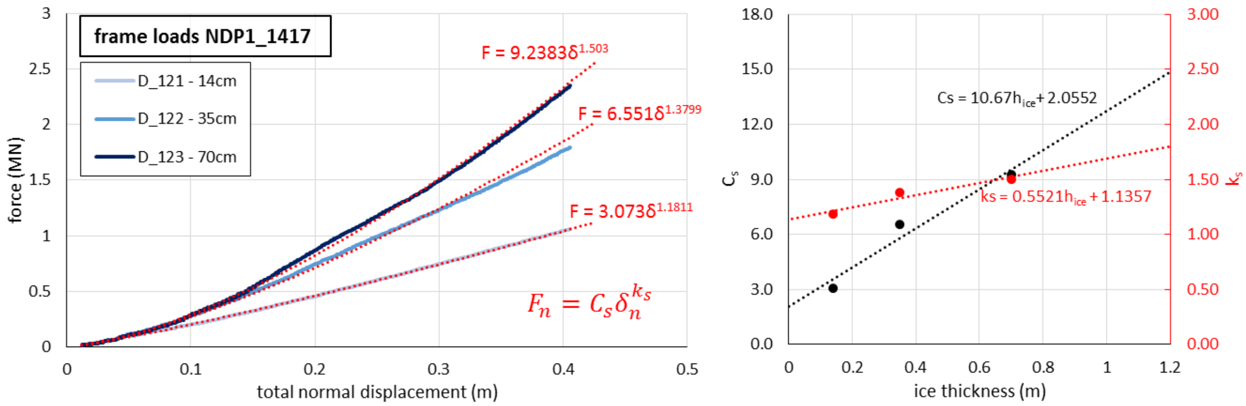

Figure 47: Numerical simulation results for NDP1_1417 - force versus total displacement (left) and power function parameters (right)

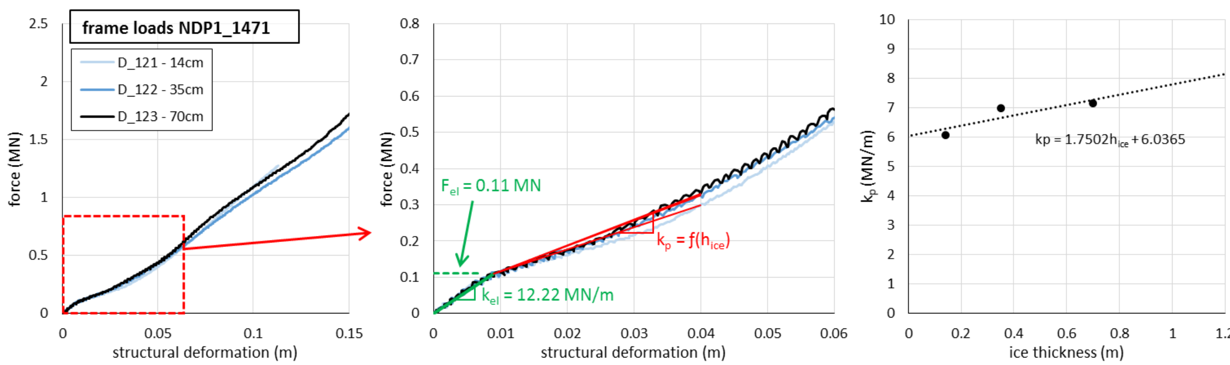

Figure 48: Numerical simulation results for NDP1_1417 - force versus structural deformation (left & center) and plastic term (right)

Reassessment of Notional Destroyer Considering Deformable Structure

This section presents a reanalysis of technical limit speeds for the notional destroyer taking into account the compliance of the structure and considering different tolerance levels for structural damage. Comparisons are also made to the results of the 'direct' analysis discussed in section 4. In this analysis, energy absorbed by the structure due to elastic and plastic deformations is considered in the kinetic energy balance along with the ice crushing energy. The mathematical model follows the procedure outlined in section 5 to resolve the ice load parameters. The parameters obtained from numerical simulations of ice-structure interaction are utilized in the model.

Figure 49 presents the technical limit speeds for 30 cm, 50 cm, and 1 m thicknesses considering three limit conditions. The top row of plots assume the structure is rigid and represent the speeds that bring the longitudinal frames to their plastic limit states (i.e. direct limit state, same as Figure 22). The middle row of plots take into account structural compliance in the ice load model but the same direct limit state is used. This highlights the effect of structural energy absorption on the indentation process. The total normal force applied to the hull structure is reduced for the same available kinetic energy which effectively results in slightly higher speeds (a 1 to 2 knot increase) to bring the structure to same plastic limit. The bottom row of plots represent the speeds that bring the structure to a 5 cm total deformation (including both elastic and plastic deformations). Limit speeds are established when the structural deformation calculated in the mathematical model exceeds the user defined value.

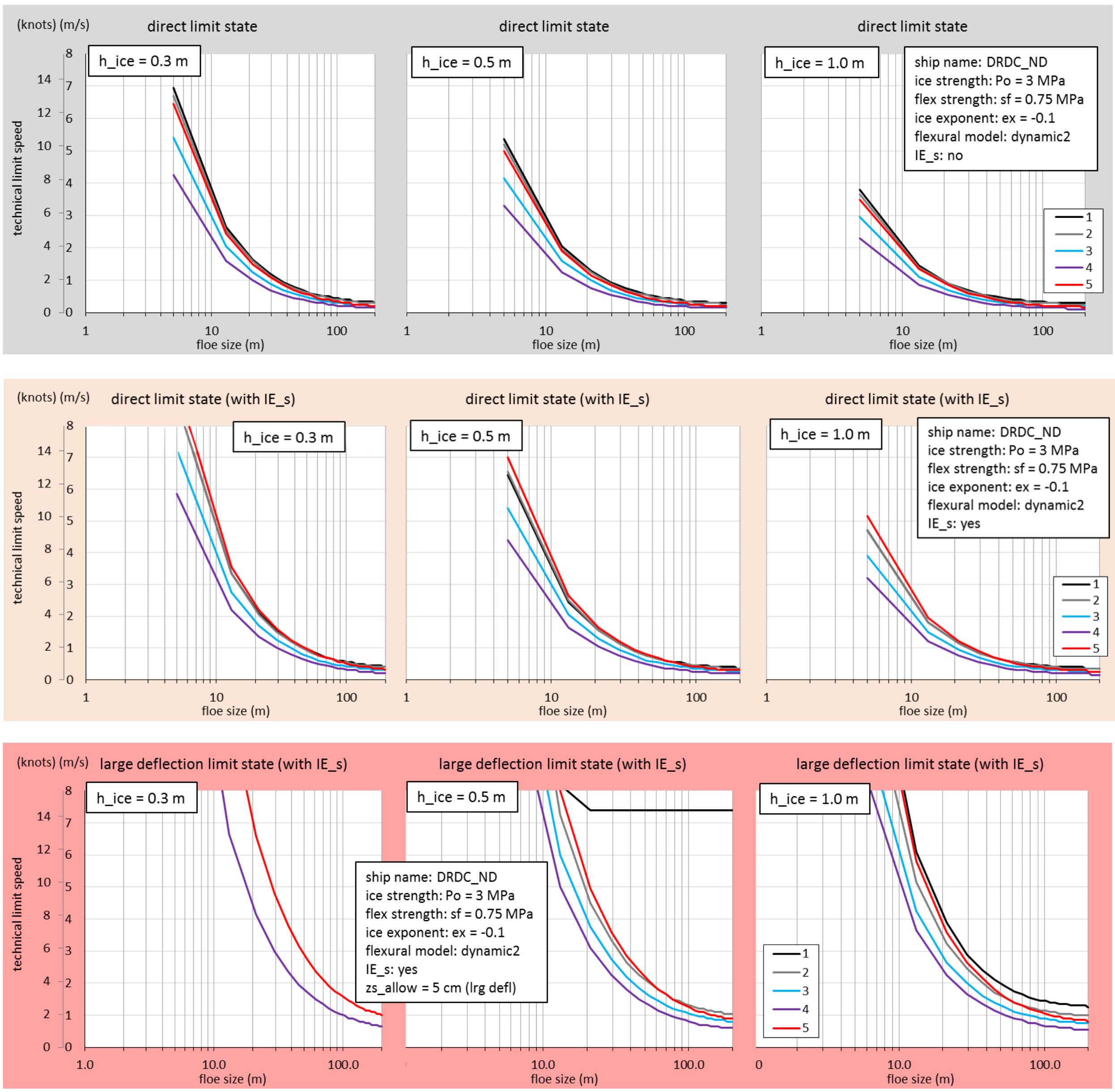

Figure 49: Technical limit speeds considering different damage tolerances

To summarize the results into a more comprehensive form, Figure 50 through Figure 52 have been produced. Rather than show either load levels or velocity limits, this plots show what ice conditions (floe size and thickness) can be safely entered at various speeds.

Figure 50 shows the safe ice operational conditions when assuming the hull has no compliance (i.e. all energy crushes ice). There is a very small range for safe operations. For example, at 6 knots, any ice larger than brash ice would exceed the capability.

Figure 51 shows a slightly improved case when the structural compliance is taken into account (the elasticity of the structure). Still, this case shows a small range of safe operations.

Figure 52 presents the technical limit speeds that bring the structure to 5cm of total deflection for any combination of floe size and thickness. The resulting plastic deformations would be visible, but would permit considerably more aggressive impacts. At 6 knots, floes up to 20m diameter (60 cm thick) could be contacted.

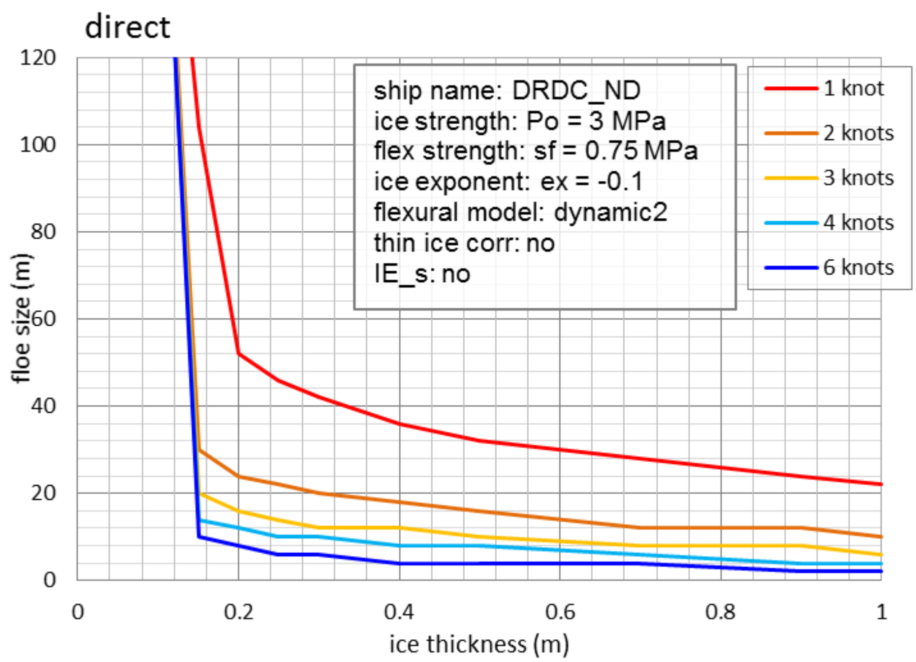

Figure 50: Summary plot of direct limit speed curves versus ice thickness and floe size (without structural compliance)

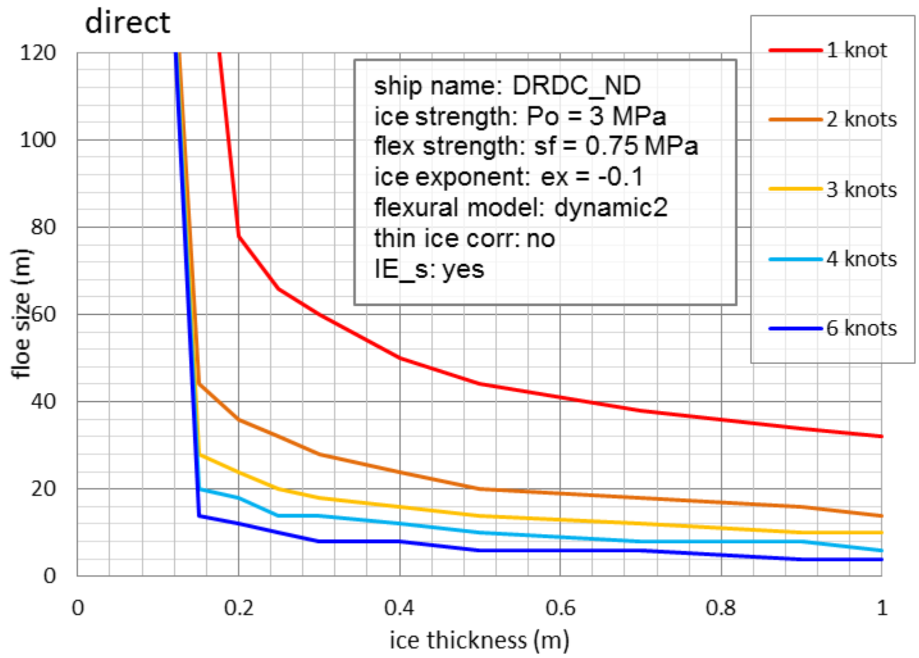

Figure 51: Summary plot of direct limit speed curves versus ice thickness and floe size (with structural compliance)

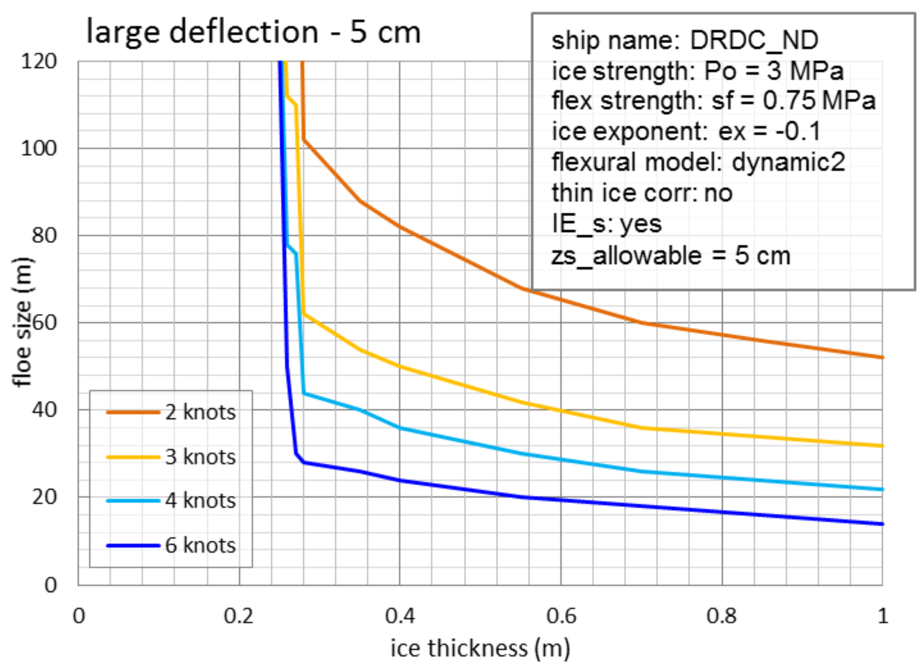

Figure 52: Summary plot of 5 cm deflection limit speed curves versus ice thickness and floe size

7. Notional Destroyer Stem Analysis

The Notional Destroyer has a sharp stem which is inclined 45.4 degrees from vertical at the waterline. The stem will experience a large number of impacts in pack ice. To examine the possibility of stem damage, an analysis similar to the panel impact safe speed assessment has been conducted.

Detailed design drawings of the stem were not available, so a design as sketched in Figure 53 and Figure 54 has been assumed. While the stem may have a cast stem bar, modelling difficulties would arise. Instead, the actual stem has been modelled as having the 10.5 mm bow plating come to the stem on a 50 mm radius. A 67 mm x 36 mm stem bar runs down the stem. The bow longitudinal frames are joined at the stem, stopping just before the radius in the shell, but attached to the stem bar. This model is believed to be sufficient to determine the general strength level of the stem in comparison to the bow panels described above.

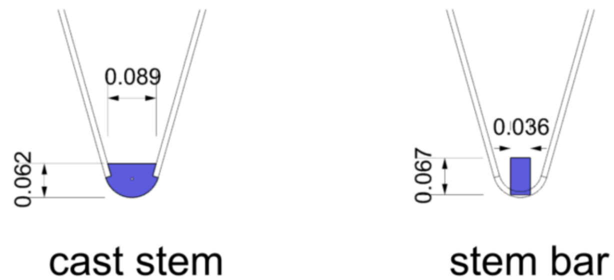

Figure 53: Stem Bar modelling

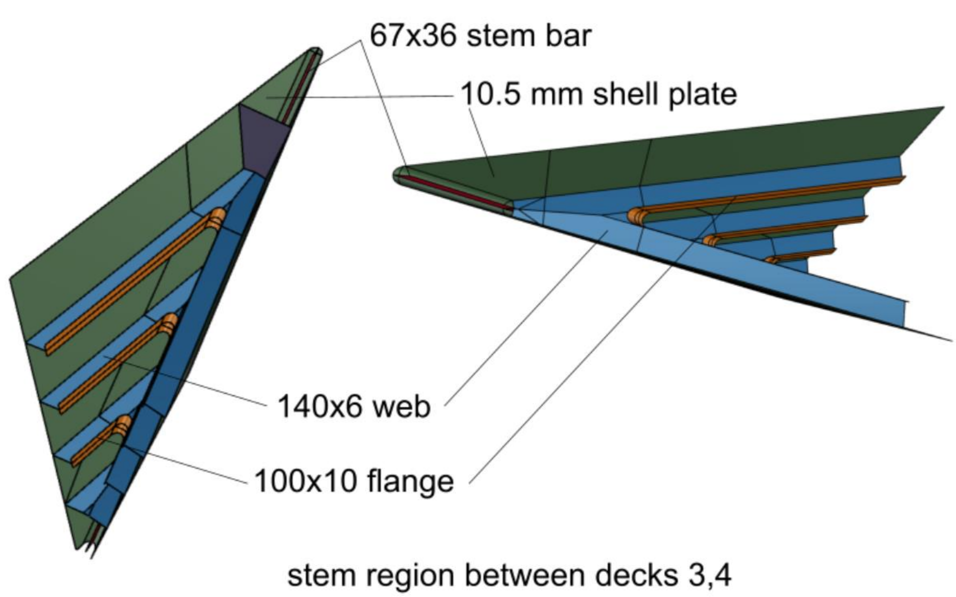

Figure 54: Stem region model

Rigid cylinder analysis

To first assess the stem, a simple rigid cylinder load case was conducted in LS-DYNA. Figure 55 shows how the stem region responds to contact with a displacement-controlled rigid cylinder. At a load of about 0.75 MN, the stem begins to collapse. The load versus time history is shown in Figure 56.

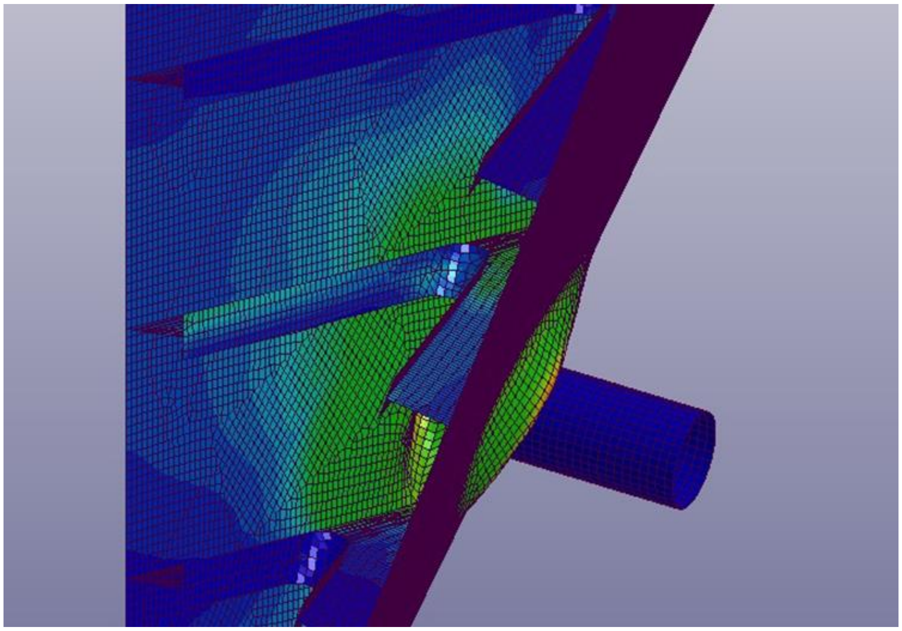

Figure 55: LS-DYNA Model Stem collapse at approximately 0.75 MN

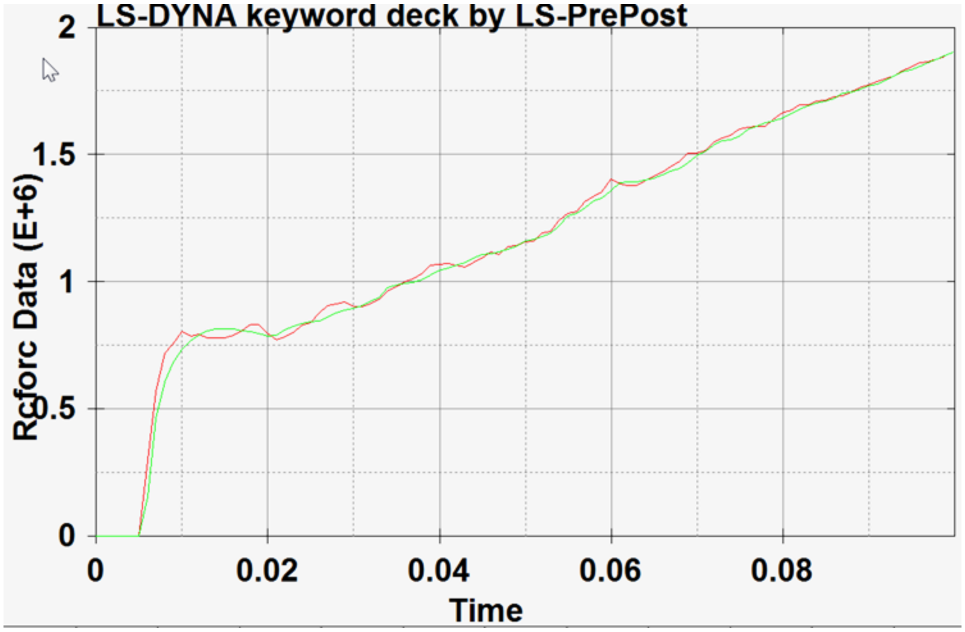

Figure 56: LS-DYNA Load versus Time showing stem collapse at approximately 0.75 MN

Ice contact analysis

The arrangement for LS-DYNA simulations of stem interaction with a deformable ice block is shown in Figure 57. The results showed that there was no plastic deformation up to 0.75 MN. This would be expected, as the ice causes a more distributed load than the rigid cylinder. Figure 58 shows the force versus normal indentation. There were slight differences in force versus total normal deformation (predominately ice crushing) when the hull was modelled as a compliant structure (elasto-plastic) versus rigid. Overall, the analysis indicated that the stem is notably stronger than the flat panels in the bow.

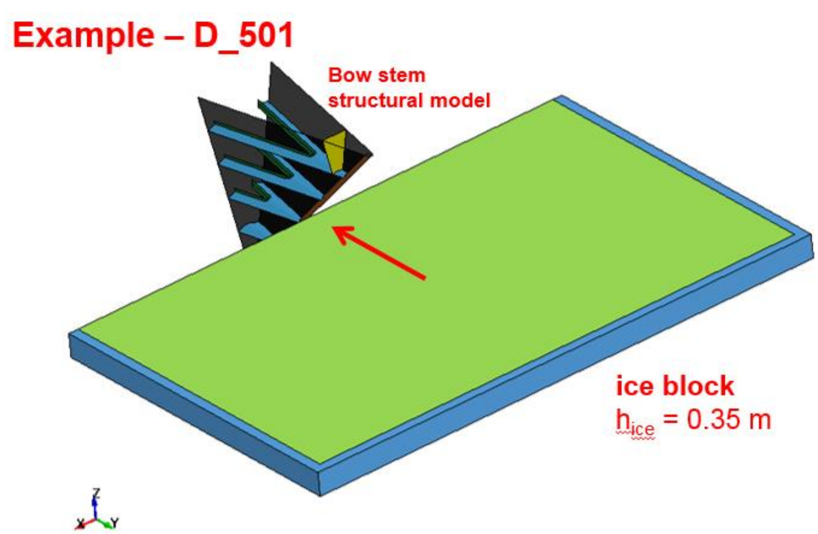

Figure 57: LS-DYNA model for ice sheet contact with the stem of the Notional Destroyer

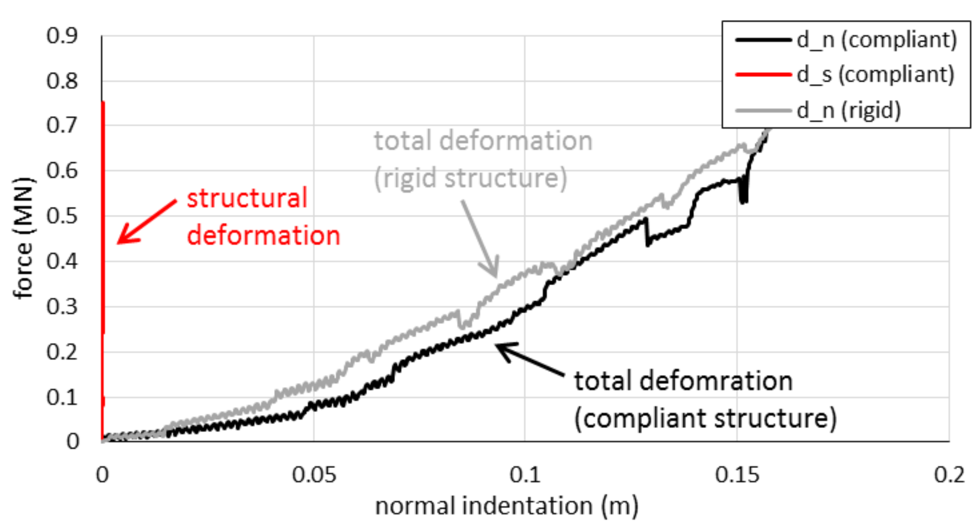

Figure 58: LS-DYNA force-indentation for ice sheet contact with the stem of the Notional Destroyer

DDePS comparison of glancing collision versus. stem collision

Figure 59 shows the Case 2a loads for 20m floes at location 4 (same as Figure 21) which is the governing condition for Notional Destroyer as presented in Section 4, with a limit state at approximately 0.1 – 0.2 MN (Figure 15). This indicates that for higher speeds the Notional destroyer has a limit of about 0.2 m of ice for 20 m diameter floes.

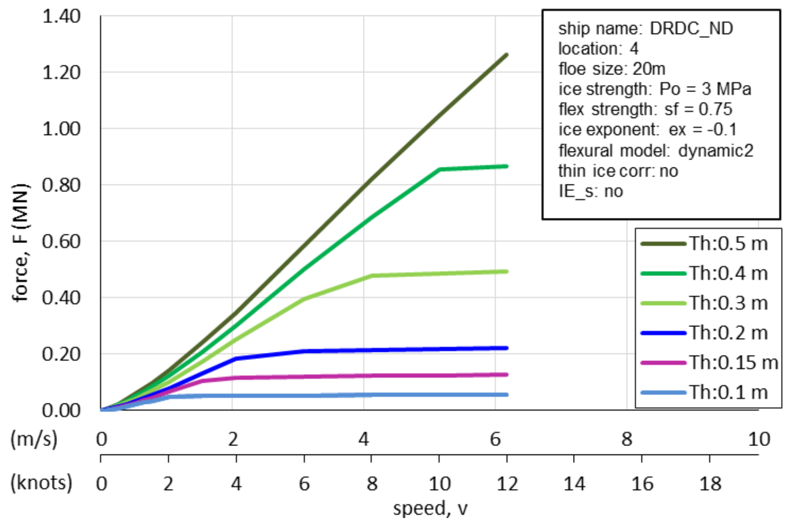

Figure 59: DDePS Case 2a Glancing Loads – 20m floes, at location 4 (same as Fig 21)

Case 1a loads for 20 m floes at stem don't exceed 0.35 MN for thicknesses up to 50cm of ice (Figure 60). The same assumptions for ice strength (P_o = 3.0 MPa, ex = -0.1, σ_y = 0.75 MPa) have been made. The ice loads on the stem in these regimes are limited by flexural failure due to the stem angle (horizontal portion). This analysis makes it clear that the stem is unlikely to be an area of concern in ice.

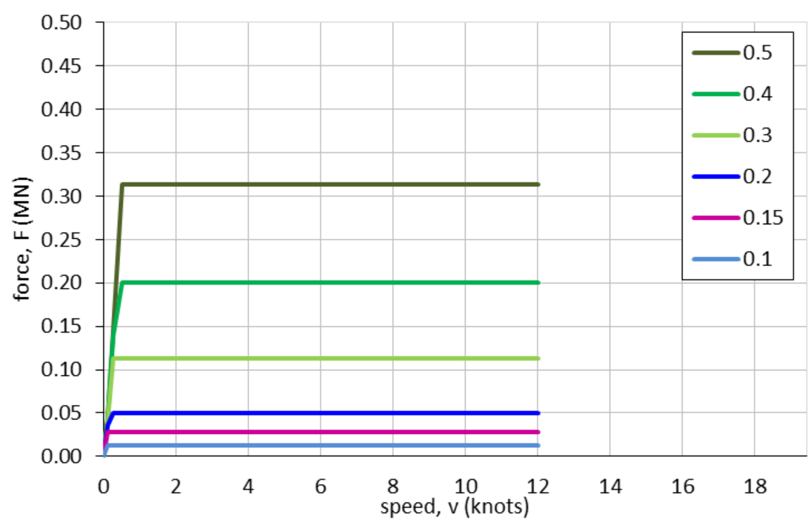

Figure 60: DDePS Case 1a Stem Loads - 20 m floes.

8. GEM Analysis

Overview of GEM

The GEM program developed at Memorial University[1] simulates the motions and interactions of ships and offshore structures with ice floes. Figure 61 illustrates the overall concept of the program. The simulations begin from a 'scene', which contains the initial state of all the objects in the simulation. A 'scene' can either be imported or created. When the user starts a simulation, the program applies the algorithms to the object motions and interactions and determines the evolving behavior of all objects in a sequence of time steps. A new set of conditions are computed for each time step. A new 'frame' is created and saved every 'n' time steps (typically every 10 time steps). A 'frame' is essentially like a 'scene' with the exception that frames are part of a time sequence and are locked after they are created. A set of frames (beginning with the starting 'scene') is the record of a simulation. A file containing a single scene (a scene file), is designated with the ".icsn" extension. A simulation file is designated with the ".ice" extension. Simulation files can be viewed in sequence like a video file or reviewed one frame at a time. All relevant motion and interaction values can also be stored in data files for post-simulation analysis. There are 31 vessel motion parameters stored for each time step and 51 collision parameters stored for every ship-ice impact.

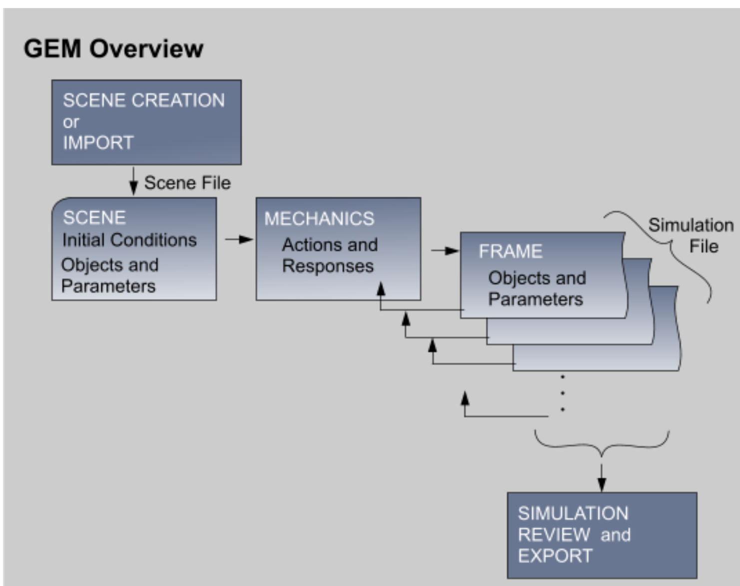

Figure 61: GEM Program General Overview

For this project, GEM has been used to model the DRDC Notional Destroyer interacting with pack ice. In this other parts of this report the focus is on single impacts. With GEM we can examine the more complex aspects of ice load that arise as a ship moves through pack ice. The collision sequence that occurs in pack ice causes the vessel to sway and yaw and this creates considerable

[1] Dr. C. Daley is the PI for the GEM development project. While GEM is formally owned by Memorial, and is proprietary, Dr. Daley has written permission to use GEM for evaluation and demonstration projects such is the one reported here.

variability. Another significant aspect is how the ice floes interact with each other, which can both raise or lower the magnitude of loads. GEM is capable of examining the statistics of load. The various results presented below are intended to illustrate the potential of GEM in both design and operations planning. Figure 62 shows a scene from GEM, with the Notional Destroyer approaching a patch of pack ice.

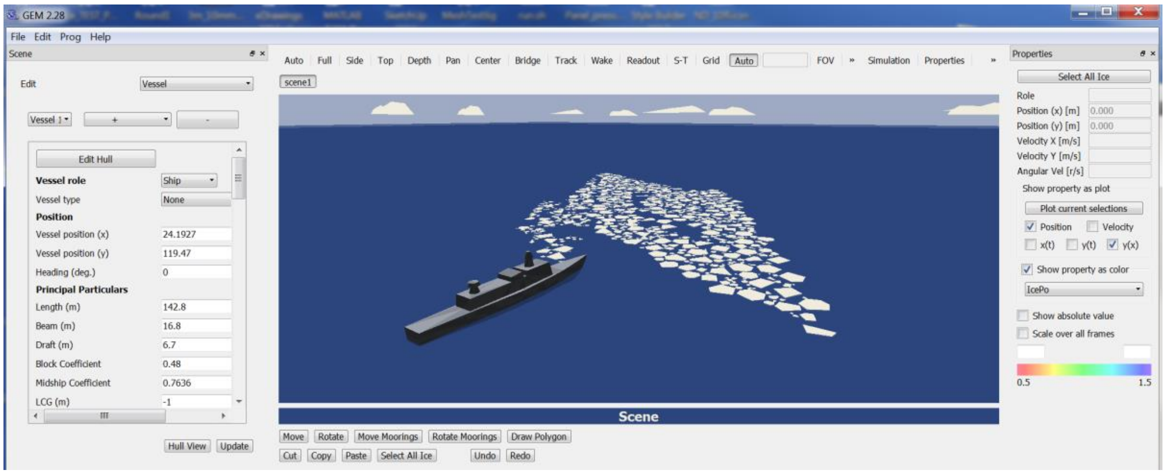

Figure 62: GEM Program with Notional Destroyer approaching pack ice

GEM Model of Notional Destroyer

The GEM representation of the Notional Destroyer is a 2D polygon of the 6.7 m waterline (Figure 63). It must be noted that a slight change in hull form was required in order to allow GEM to function. The ice collision detection algorithms in GEM require that all objects be convex. The Notional Destroyer has a slight concavity in the bow and aft-body. Figure 64 shows the slight change adopted for GEM to make the hull convex. The effect on ice load results is expected to be immeasurably minor. These coordinates are very slightly different from those used in the DDePS analysis.

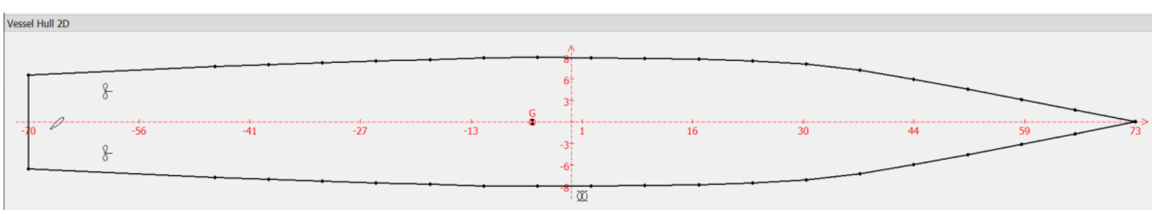

Figure 63: GEM 2D polygon of Notional Destroyer at 6.7 m draft.

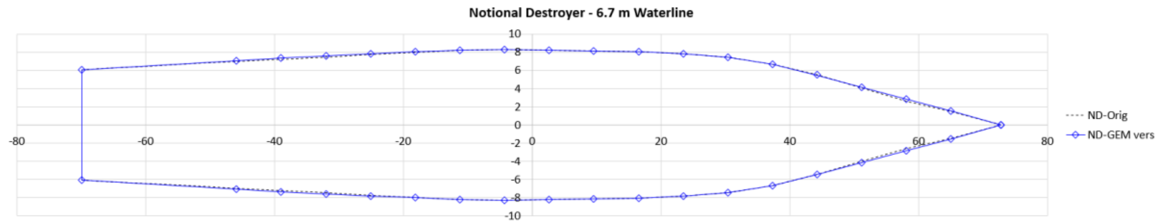

Figure 64: GEM 2D polygon of Notional Destroyer at 6.7 m draft versus Original.

Figure 65 shows a 3D rendering of the Notional Destroyer in GEM. The 3D render is done merely to provide the user with a better sense of the problem being simulated. The simulation is mainly 2D with limited 3D components. The 3D response of both ship and ice is considered in all collisions, but only 2D positions and motions are computed. Another way to describe this is to say that all collisions assume that objects are moving only in the water plane prior to the collision. Roll heave and pitch accelerations may occur during the collision, but are such motions considered to return to zero prior to the next collision. This is a reasonable assumption when vessels are in open pack ice, traveling at low to moderate speeds in calm water.

Figure 66 shows the coordinates of the Notional destroyer polygon, along with the true frame angles (beta). True frame angles indicate the true inclination of the hull from the vertical (measured in a vertical plane normal to the hull).

Figure 67 shows the vessel principal particulars (length, beam etc.) which are used to determine the vessel’s dynamic behavior. Also shown are the hydrodynamic derivatives which define the vessel’s maneuvering and performance characteristics.

Figure 68 shows the propeller and rudder parameters, which are used to model thrust and turning performance. The values presented here are estimates based on the available information. If an actual vessel were to be modeled, then this information would need to be obtained from design information, model tests and sea trials.

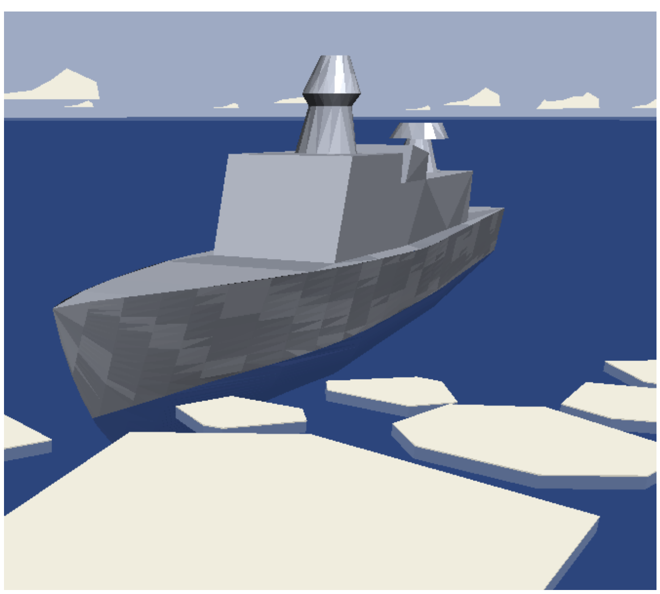

Figure 65: GEM 3D render of the Notional Destroyer

Hull X	Hull Y	Beta
72.82	0	10.95
65.065	1.5095	13.34
58.13	2.8586	16.69
51.195	4.1737	17.11
44.2599	5.4813	13.27
37.3249	6.6485	9.76
30.39	7.4454	7.94
23.455	7.8561	7.89
16.52	8.0328	8.6
9.585	8.1361	9.5
2.65	8.2093	9.53
-4.285	8.2557	7.3
-11.22	8.2052	5.21
-18.154	8.0172	4.78
-25.0933	7.8194	5.14
-32.0321	7.5934	5.12
-38.9584	7.3463	3.66
-45.8975	7.0812	5.37
-69.98	6.042	0
-69.98	-6.042	5.37
-45.8975	-7.0812	3.66
-38.9584	-7.3463	5.12
-32.0321	-7.5934	5.14
-25.0933	-7.8194	4.78
-18.154	-8.0172	5.21
-11.22	-8.2052	7.3
-4.285	-8.2557	9.53
2.65	-8.2093	9.5
9.585	-8.1361	8.6
16.52	-8.0328	7.89
23.455	-7.8561	7.94
30.39	-7.4454	9.76
37.3249	-6.6485	13.27
44.2599	-5.4813	17.11
51.195	-4.1737	16.69
58.13	-2.8586	13.34
65.065	-1.5095	10.95

Figure 66: GEM 2D polygon coordinates of the Notional Destroyer at 6.7 m draft along with frame angles

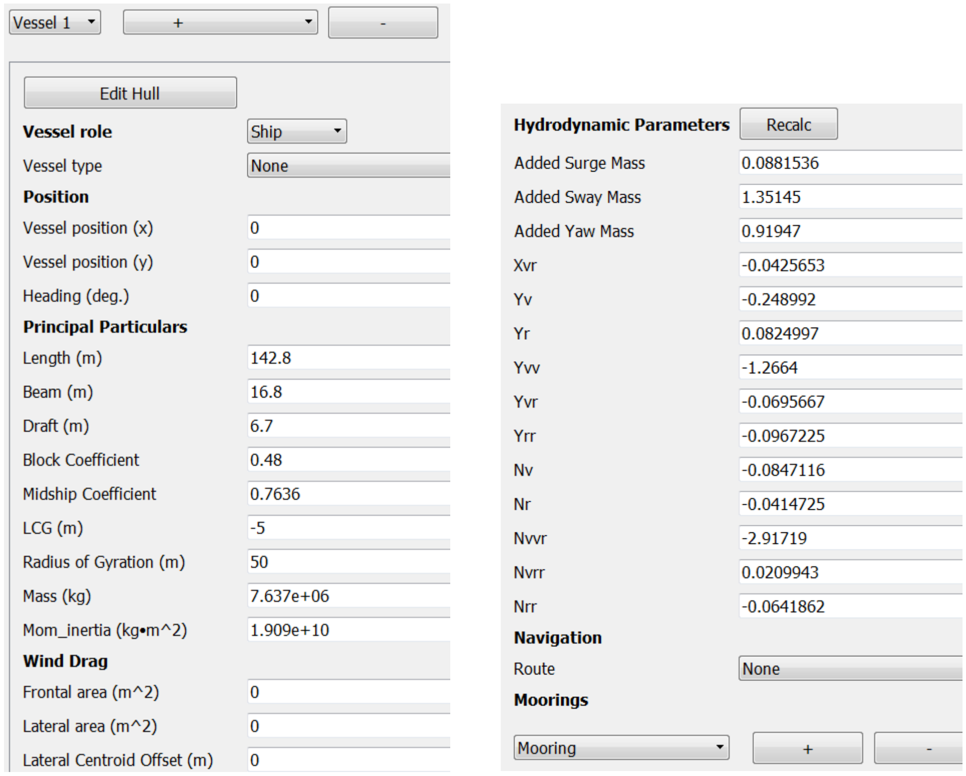

Figure 67: GEM hull data for the Notional Destroyer

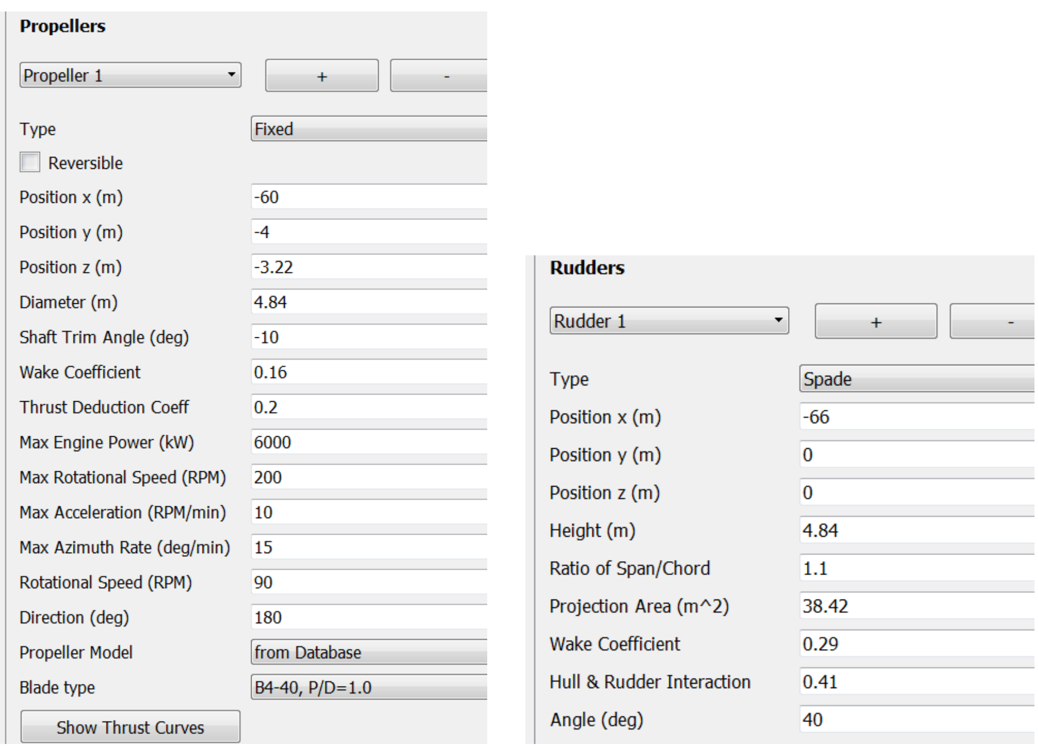

Figure 68: GEM propeller (1 of 2) and rudder data for the Notional Destroyer

GEM Open Water Simulations

Prior to conducting pack ice simulations, a simple set of open water simulations were performed to provide baseline vessel behaviors. Simple straight run simulations show the acceleration and top speed for various propeller speed values. Turning circle simulations then show the basic maneuvering characteristics of the vessel. The Notional Destroyer does not have detailed performance information, as one might obtain from model test or full scale trials. These GEM ‘trials’ are thus only intended to clarify the assumptions that the GEM simulations have made concerning the basic behavior of the Notional Destroyer.

RPM/Speed Simulations

The propeller rotational speed was varied from 0 rpm to 190 rpm. The maximum assumed propeller speed for this vessel is 200 rpm. Figure 69 shows the initial setup in GEM, where the vessel was set at the origin heading in the x direction. Figure 70 shows the ship moving along a 0 degree heading.

A set of 6 straight run tests were conducted. Each simulation began with the vessel stopped and the propellers spinning at the fixed speed. In all cases the vessel accelerated in a straight line. No wave effects were considered. Table 15 shows the time to reach maximum vessel speed at each propeller setting, as well as the time to 90% of the maximum speed. Figure 71 to Figure 76 show plots of the speed curves. Figure 77 shows a relative comparison of all propeller speeds. Figure 78 shows the linear relationship between vessel speed and propeller rotational speed.

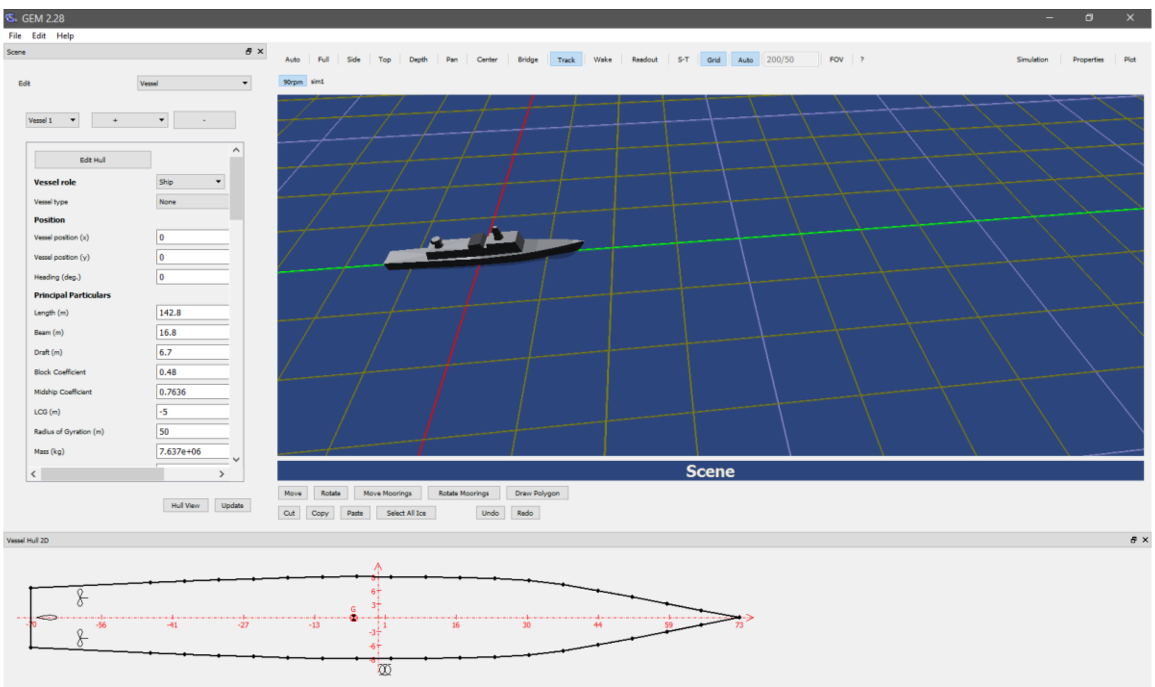

Figure 69: Initial 90 RPM GEM Setup

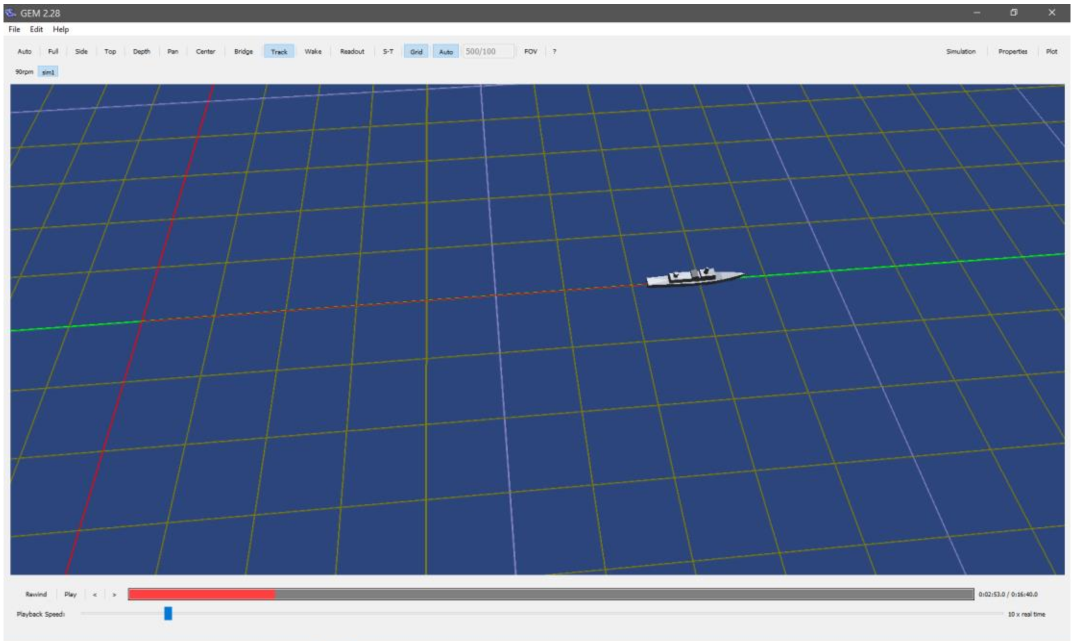

Figure 70: 90 RPM 0 degree heading in GEM showing the vessel track

Table 15: Time to Maximum Speed and 90% of Max Speed

Propeller Speed [RPM]	***max speed [m/s]***	***max speed [kn]***	***Time [s]***	***90% max speed [m/s]***	***90% max speed [kn]***	***Time [s]***
10	0.59	1.15	2647.6	0.53	1.04	806.3
50	3.4	6.57	714.1	3.0	5.91	182.9
90	6.3	12.32	423.5	5.7	11.09	105.0
100	7.1	13.75	385.4	6.4	12.37	94.4
150	10.6	20.60	244.1	9.5	18.54	61
190	13.1	25.56	171.8	11.8	23.00	45.3

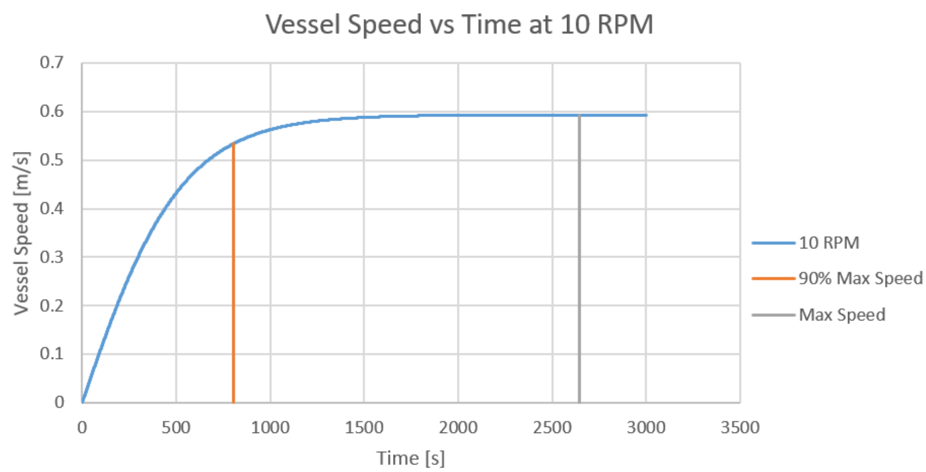

Figure 71: Vessel Speed versus Time at 10 RPM

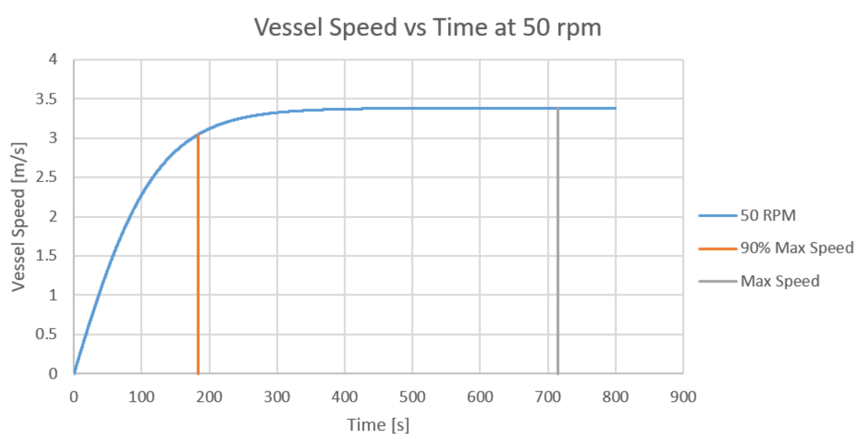

Figure 72: Vessel Speed versus Time at 50 RPM

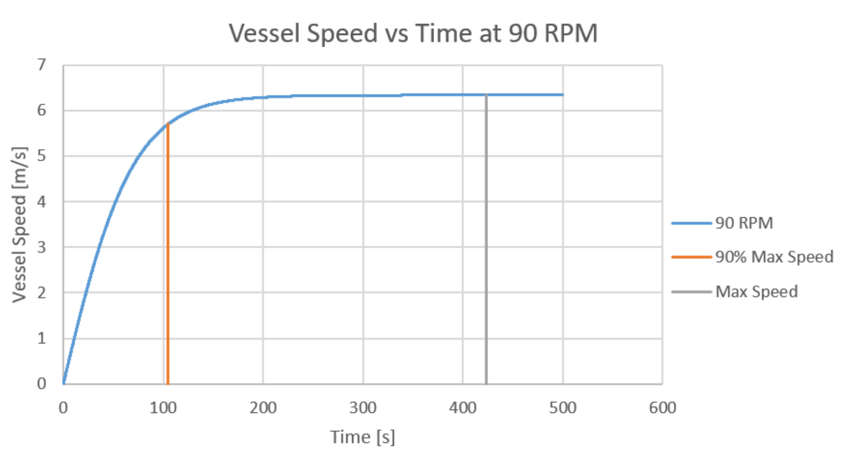

Figure 73: Vessel Speed versus Time at 90 RPM

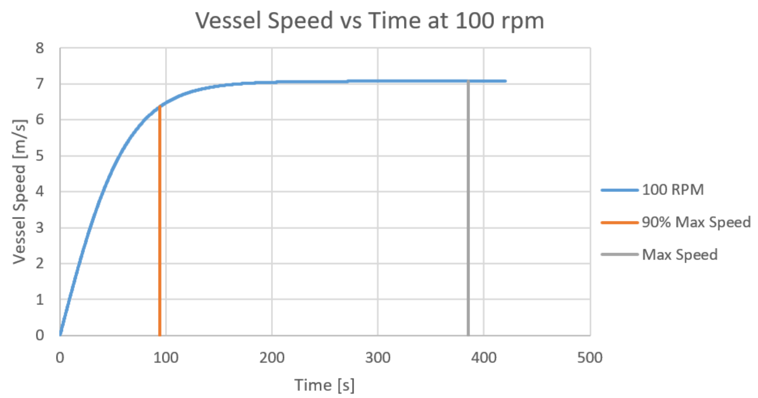

Figure 74: Vessel Speed versus Time at 100 RPM

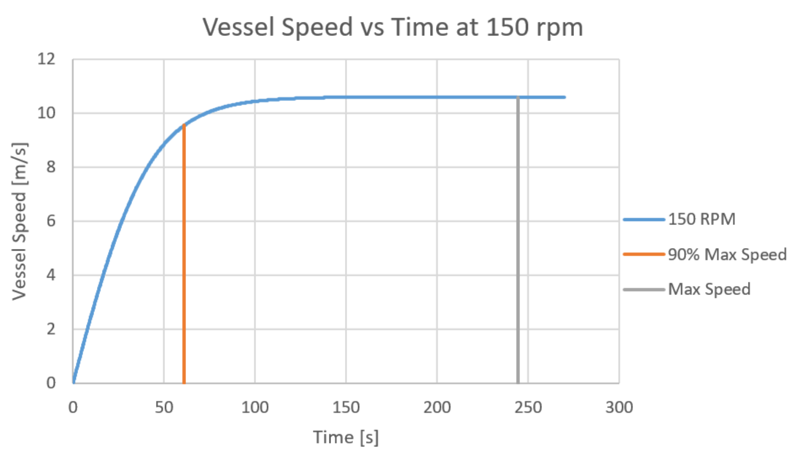

Figure 75: Vessel Speed versus Time at 150 RPM

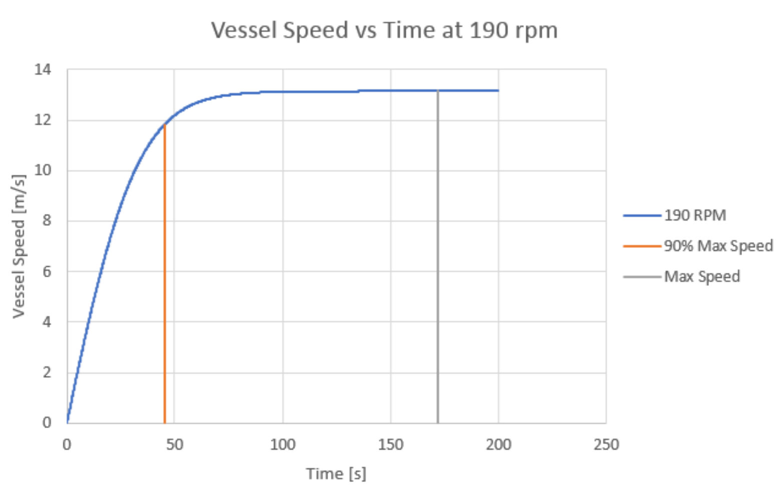

Figure 76: Vessel Speed versus Time at 190 RPM

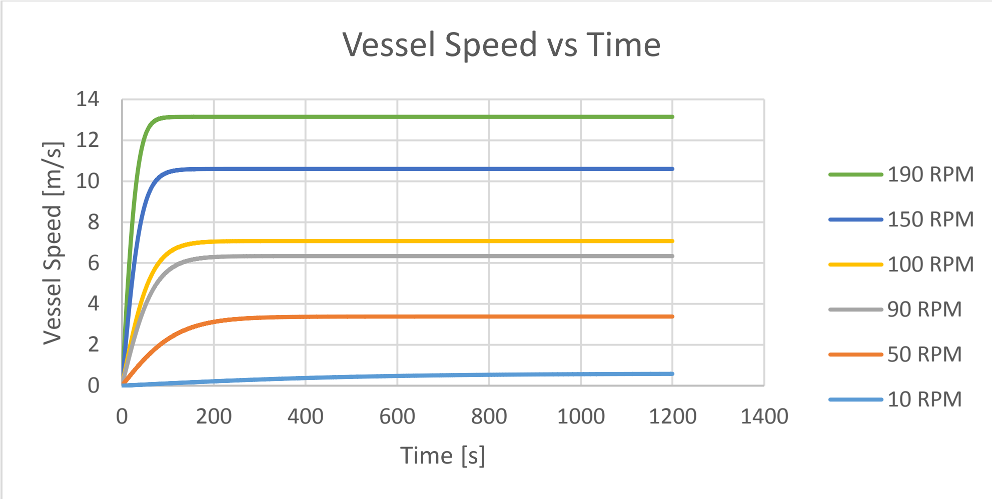

Figure 77: Vessel Speed versus Time Comparison for all Rotational Speeds

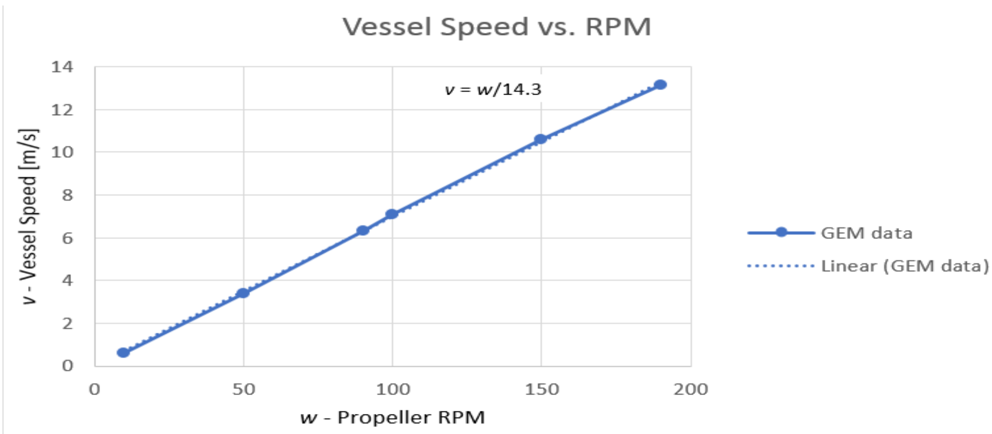

Figure 78: Linear relationship between vessel speed and propeller RPM at max speed

Turning circles

The vessel's turning characteristics were investigated by orienting the rudder at various angles from 1 to 40 degrees. All tests were conducted at 90 RPM, with an initial vessel speed of 6.3 m/s (see Table 16).

Figure 79 shows the turning circle setup for the 25 degree angle. Figure 80 shows the turning circle route. Table 16 shows the results of the GEM turning circles. Figure 81 shows the diameter versus rudder angle plot.

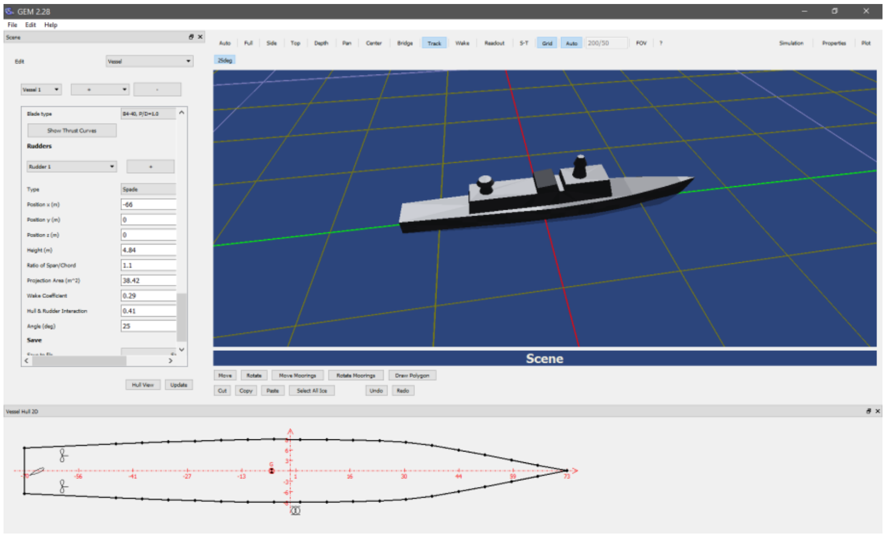

Figure 79: Turning Circle Setup at 25 degrees

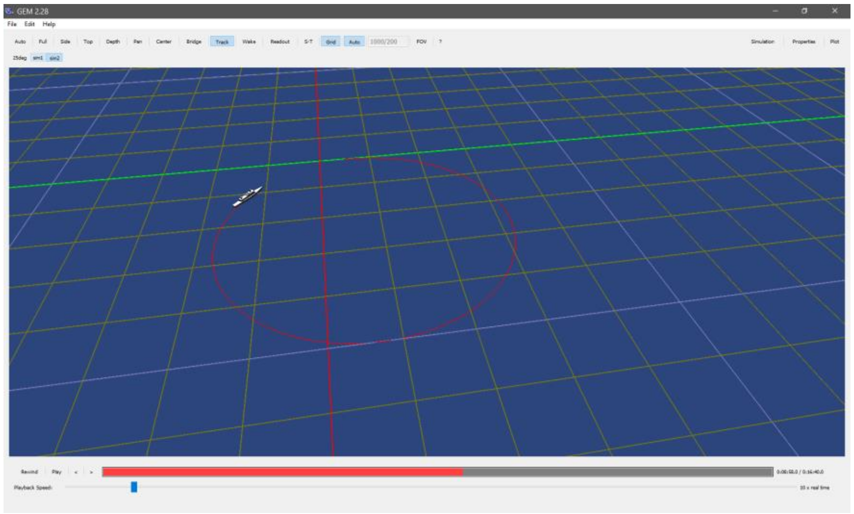

Figure 80: Turning circle track for 25 degree rudder

Table 16: Turning Circle Diameter at Various Rudder Angles

Rudder Angle [deg]	*Diameter [m]*
1	16925
5	4074
10	2406
15	1826
20	1526
25	1341
30	1216
35	1126
40	1062

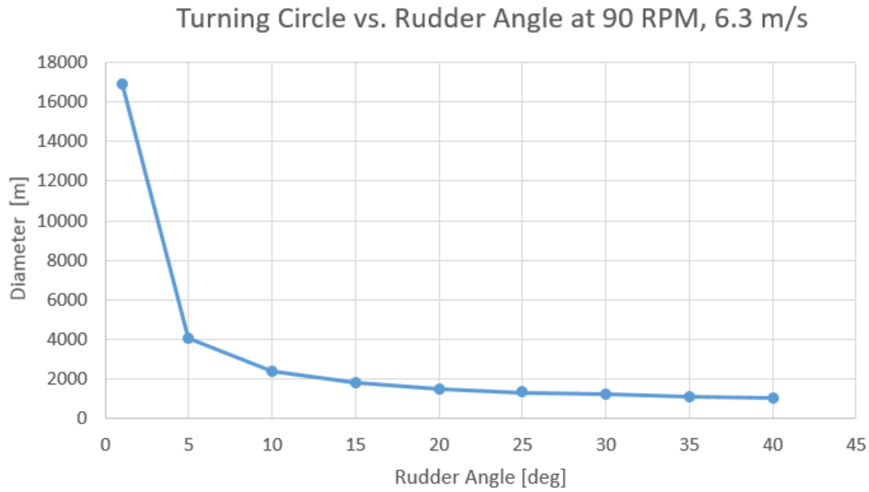

Figure 81: Turning Circle Diameter versus Rudder Angle at 90 RPM, 6.3 m/s

Single Ice Floe Collisions

The following set of results examine single ice floe collisions with the Notional Destroyer, as modelled by GEM. A set of 70 runs examine the influence of vessel speed and vessel position relative to the ice floe (i.e. glancing and head-on collisions). The vessel and ice parameters are shown in Table 17. The glancing collision setup is shown in Figure 82, with a close-up view of -1 m (Figure 83) and -7 m (Figure 84). The ice motion is shown in Figure 85. The head-on collision setup is shown in Figure 86. The forces at each speed for each ice floe size are shown in Figure 87 to Figure 90. The x-coordinate (from c.g.) impact location on the hull, hull beta and alpha angles, and ice wedge angle are shown in each plot.

Figure 92 shows how force varies with vessel position. Head-on collisions are limited by flexural failure, because the stem is significantly more inclined than frames. The stem is inclined about 45 deg. from vertical, while plating in the bow is only inclined in the 10 to 20 deg. range. Of the glancing collisions, the greatest forces are experienced with vessel position y is -5 m (i.e. the ship center line is 5 meters away from the ice floe edge).

Table 17: Initial Set of Single Floe Impact Parameters (Runs 1-70)

Vessel Speed [m/s]	***Vessel Position [m from ice edge]***	***Ice Floe Diameter [m] Thickness = 1 m***
1	0 (head-on)	10
2	-1	20
3	-3	30
5	-5	40
7	-7	50
		60
		70
		80
		90
		100

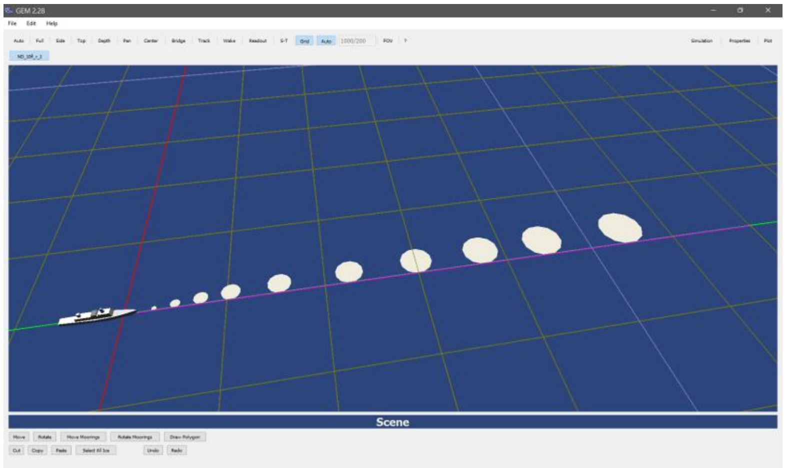

Figure 82: Glancing Collision Setup (y = -1 m)

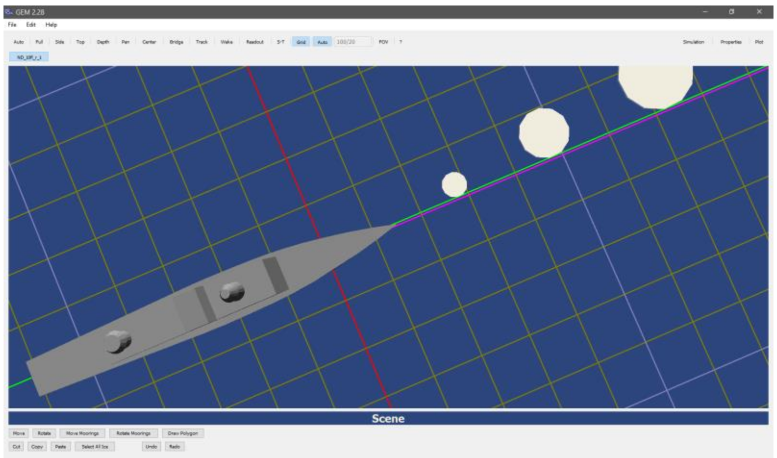

Figure 83: Glancing Collision Setup (y = -1 m)

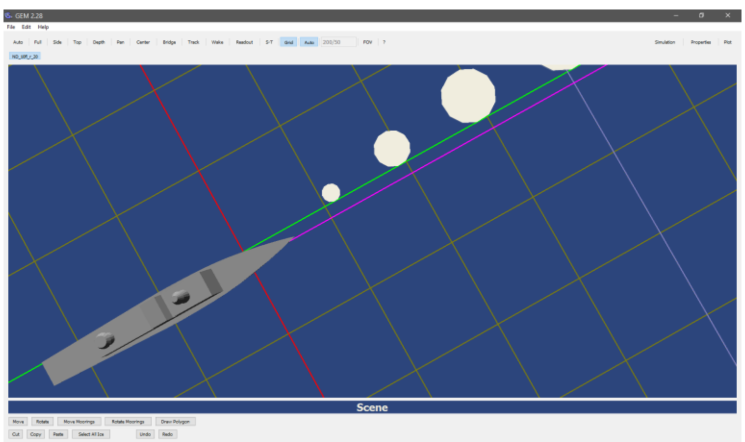

Figure 84: Glancing Collision Setup (y = -7 m)

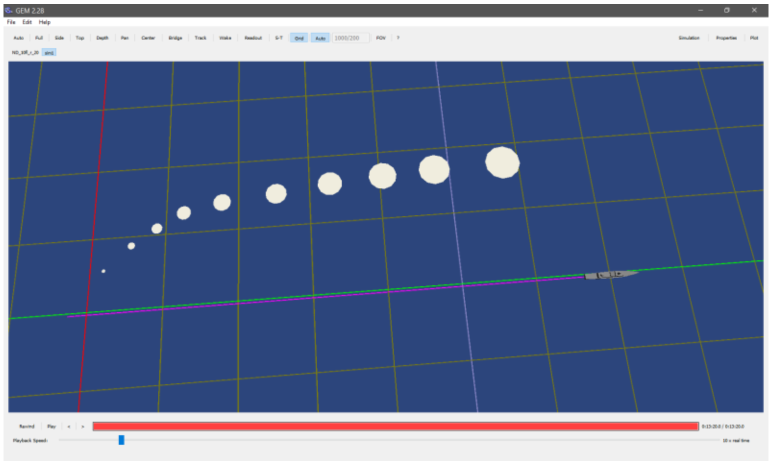

Figure 85: Glancing Collision Result (y = -7)

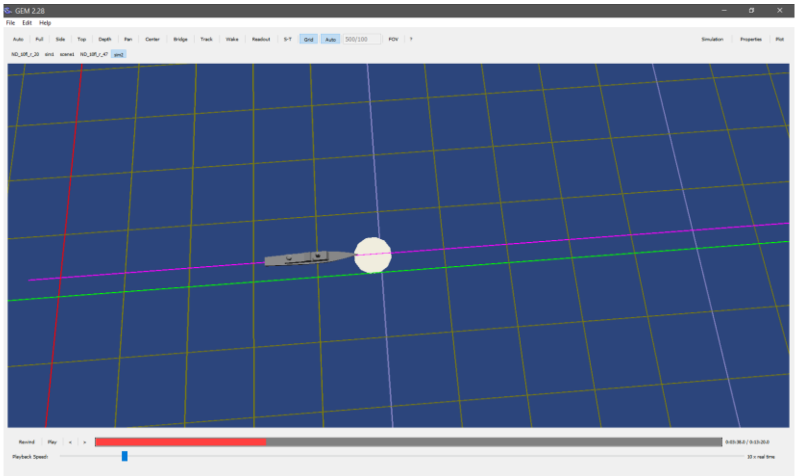

Figure 86: Head-on (y = 0) collision with 60 m floe

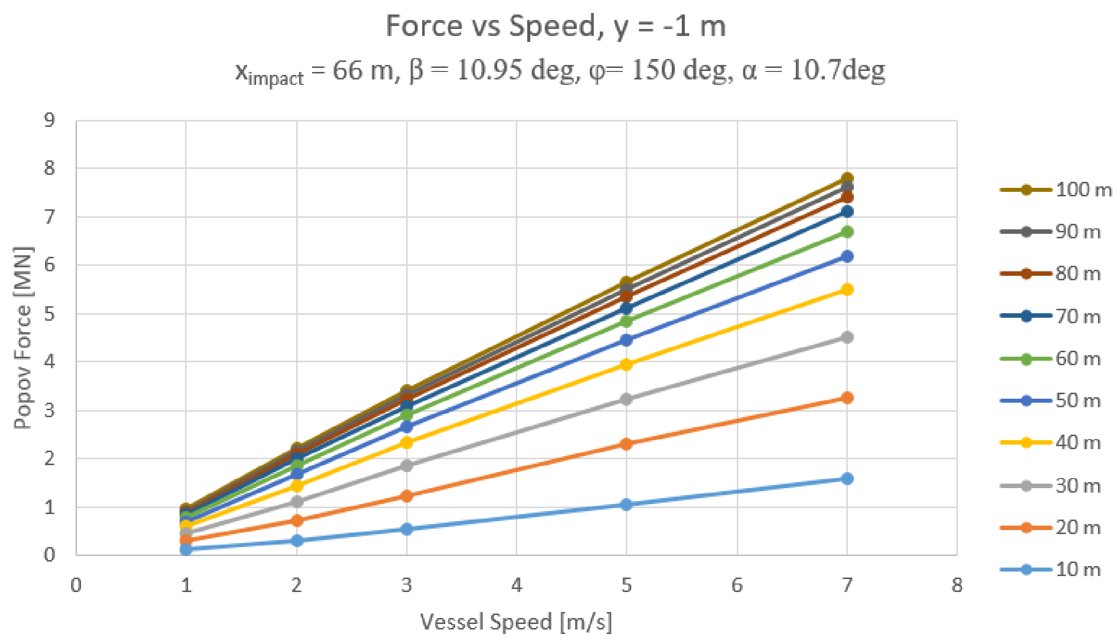

Figure 87: Glancing Force versus Vessel Speed, y = -1 m, 1m ice thickness

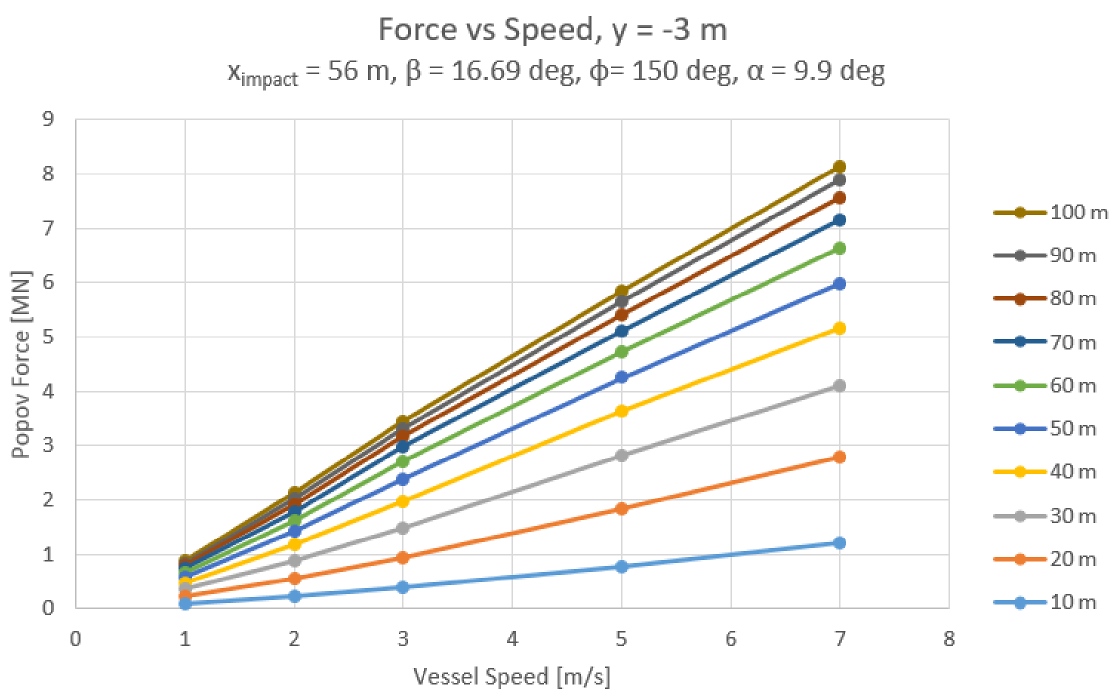

Figure 88: Glancing Force versus Vessel Speed, y = -3 m, 1 m ice thickness

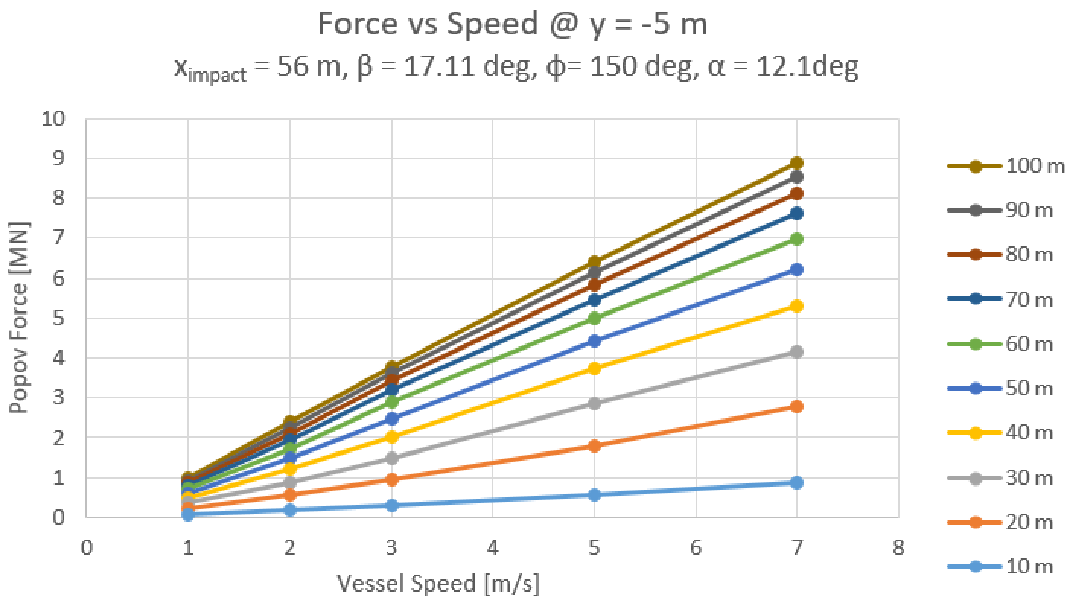

Figure 89: Glancing Force versus Vessel Speed, y = -5 m, 1 m ice thickness

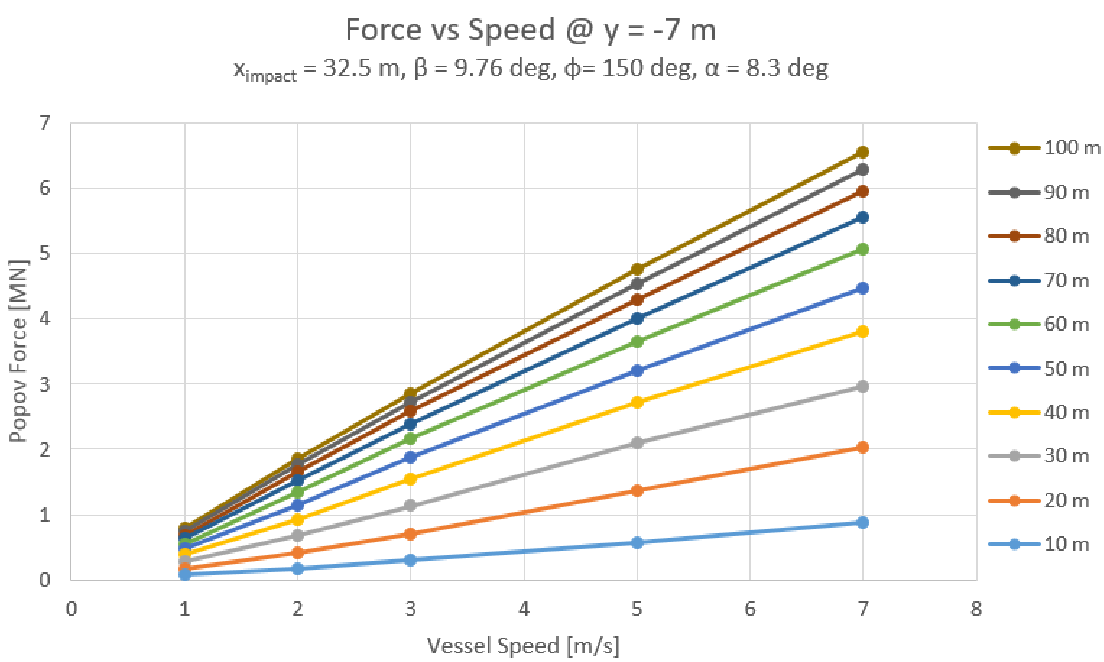

Figure 90: Glancing Force vs Vessel Speed, y = -7 m, 1 m ice thickness

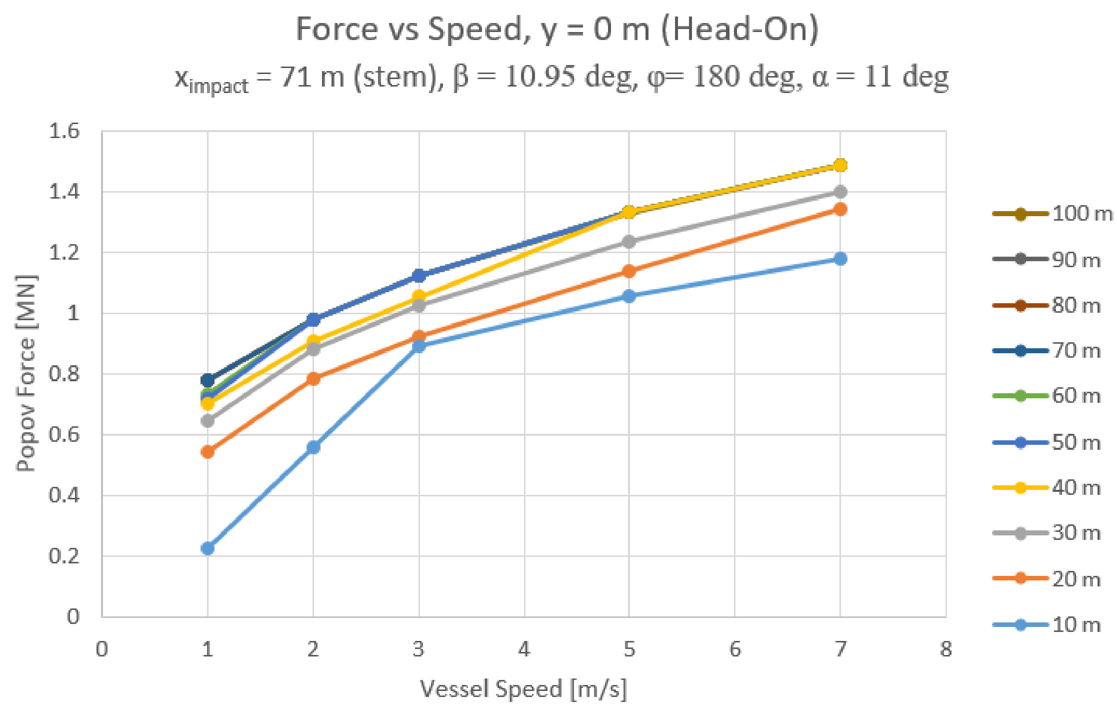

Figure 91 - Force vs Vessel Speed, y = 0 m (Head-on), 1 m ice thickness

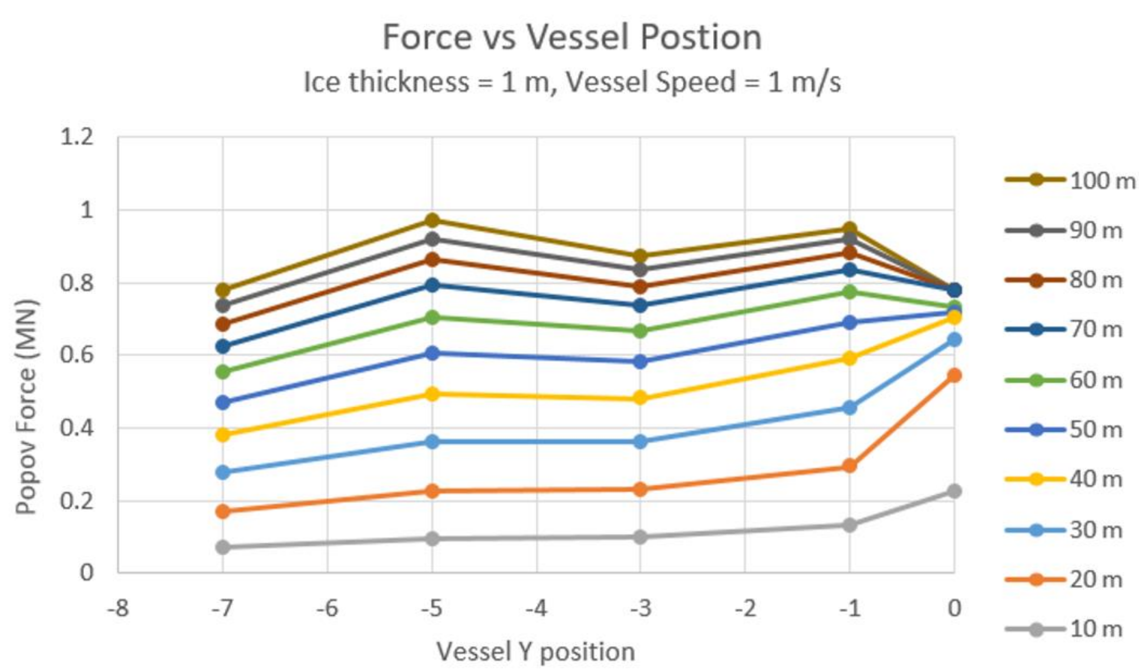

Figure 92: Force versus Vessel Position, 1 m ice thickness, 1 m/s vessel speed

Ice Thickness Variation Analysis in GEM

The effect of ice thickness on the force was investigated using only the 10 m and 20 m diameter floes, as these smaller floes are more likely to be involved in a collision with the ND vessel. The parameters for runs 71 – 124 are listed in Table 18.

Table 18: Initial Set of Parameters (Runs 71 - 124)

Vessel Speed [m/s]	*Vessel Position y [m from ice edge]*	*Ice Floe Diameter [m]*	*Ice Floe Thickness [m]*
1	0	10	0.2
3	-1	20	0.3
7	-3		0.5
	-5		1.0 [a]
	-7		

[a] for comparison

Force versus speed plots looking at the effect of ice thickness are shown in Figures 93 to 97. As expected, forces are reduced when ice thickness is smaller, though ice floe diameter also has an effect.

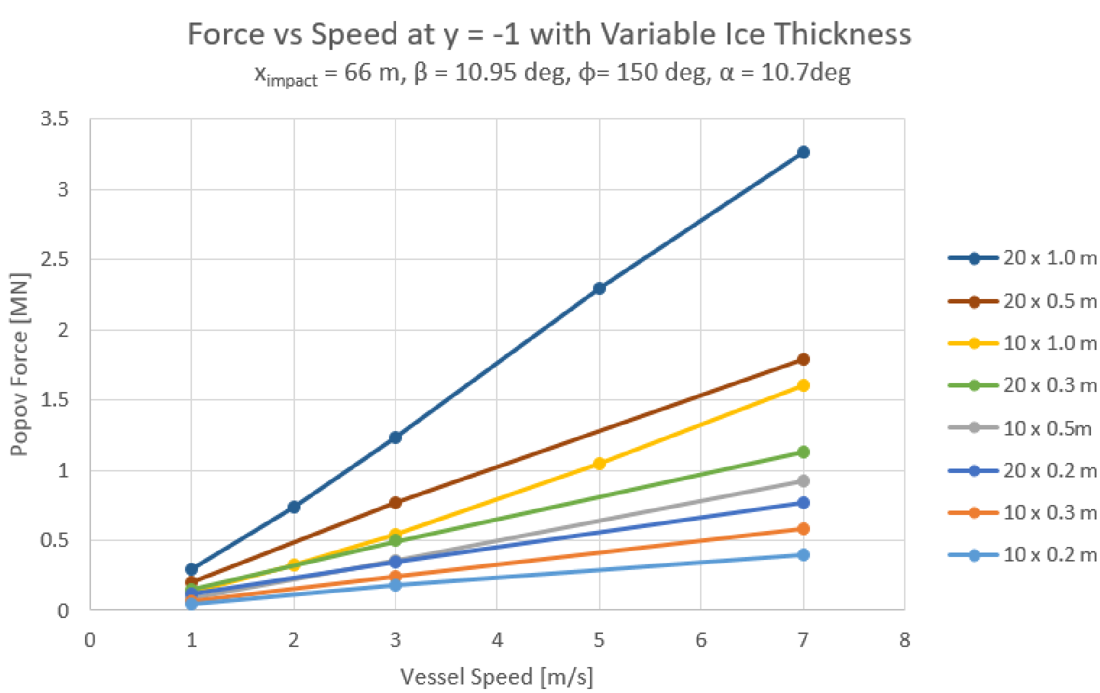

Figure 93: Glancing Force versus Vessel Speed, y = -1 m, with variable ice thickness

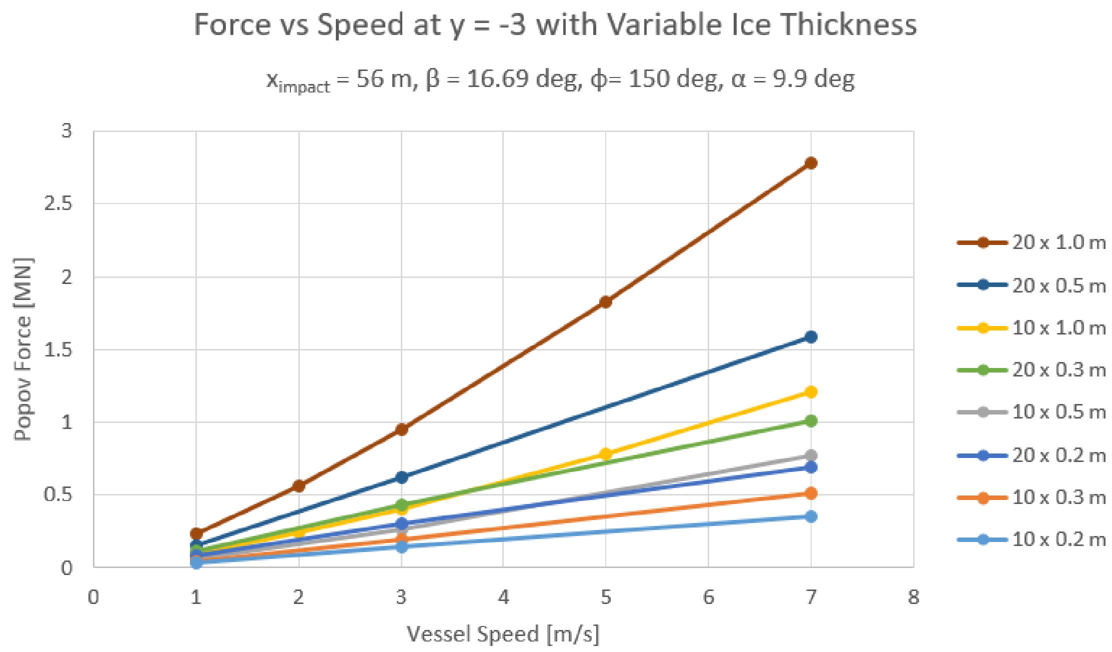

Figure 94: Glancing Force versus Vessel Speed, y = -3 m, with variable ice thickness

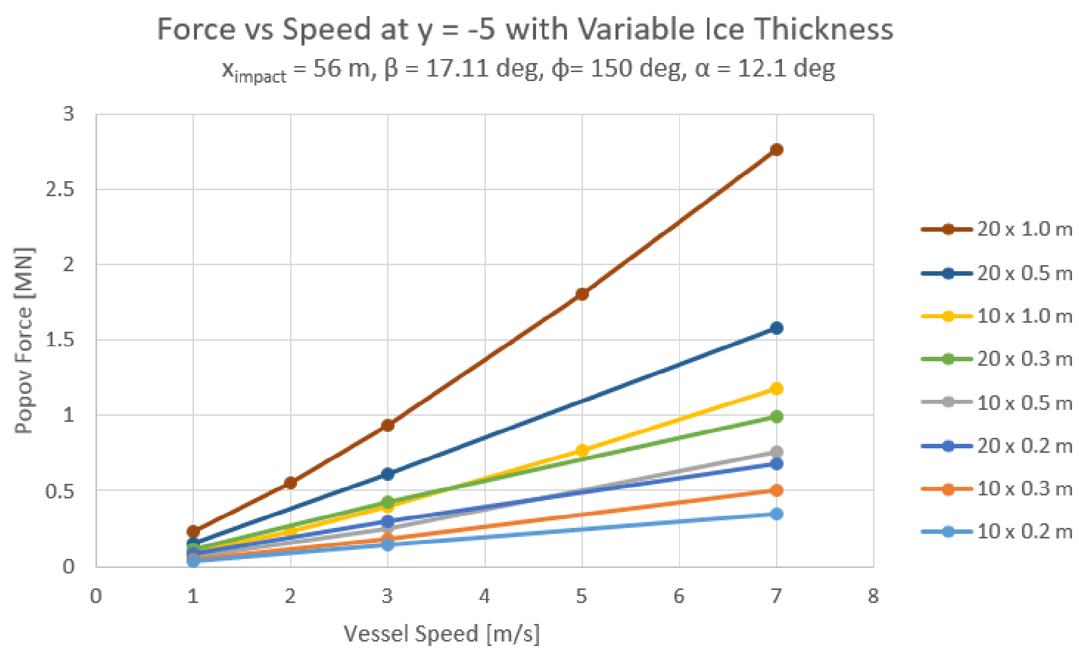

Figure 95 : Glancing Force versus Vessel Speed, y = -5 m, with variable ice thickness

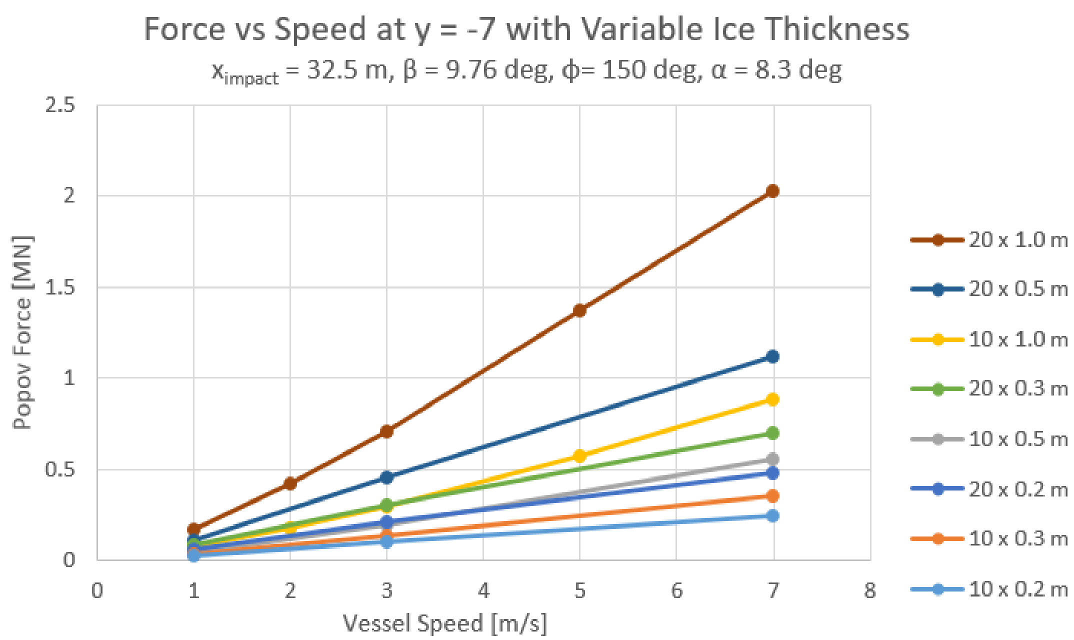

Figure 96: Glancing Force versus Vessel Speed, y = -7 m, with variable ice thickness

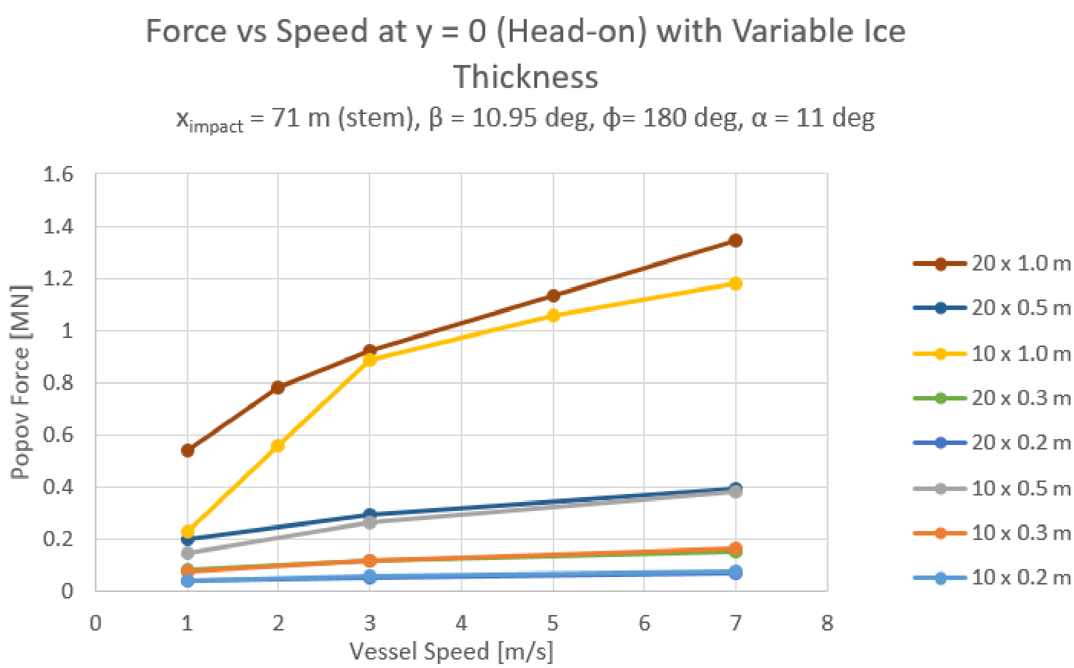

Figure 97: Force versus Vessel Speed, y = 0 m (head-on), with variable ice thickness

Ice Material Properties Variation

The effect of ice material property P_o on the force was investigated using the 10 m and 20 m diameter floes, as these smaller floes are more likely to be involved in a collision with the ND vessel. The previous runs were done using P_o = 2 MPa. The parameters for runs 125 – 178 are listed in Table 19.

Table 19: Initial Set of Parameters (Runs 125 - 178)

Vessel Speed [m/s]	*Vessel Position [m from ice edge]*	*Ice Floe Diameter [m]*	*Ice Po [MPa]*
1	0	10	0.5
3	-1	20	1.0
7	-3		2.0[a]
	-5		6.0
	-7		

[a] for comparison

Force versus Speed plots looking at the effect of ice material property P_o are shown in Figure 98 to 102. As expected, forces are reduced when ice P_o is smaller, though ice floe diameter also has an effect. For example, the force values for collisions with 20 m floes with P_o of 1 MPa ("weak" ice) were very close to force values for collisions with a 10 m floe with a P_o of 6 MPa ("strong" ice).

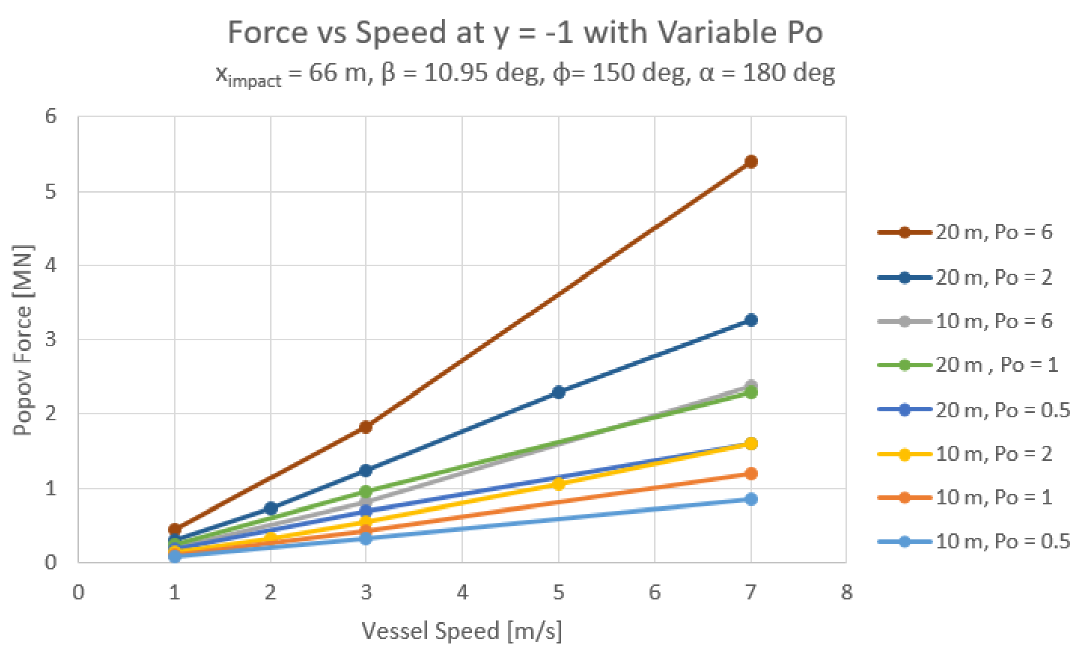

Figure 98: Glancing Force versus Vessel Speed, y = -1 m, with variable ice P_o

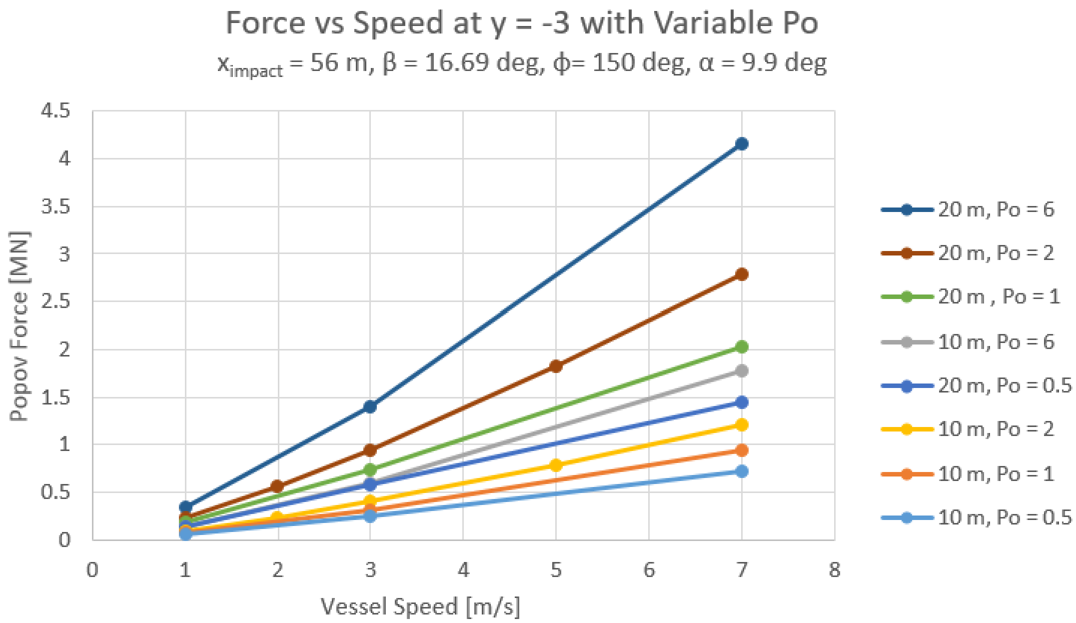

Figure 99: Glancing Force versus Vessel Speed, y = -3 m, with variable ice P_o

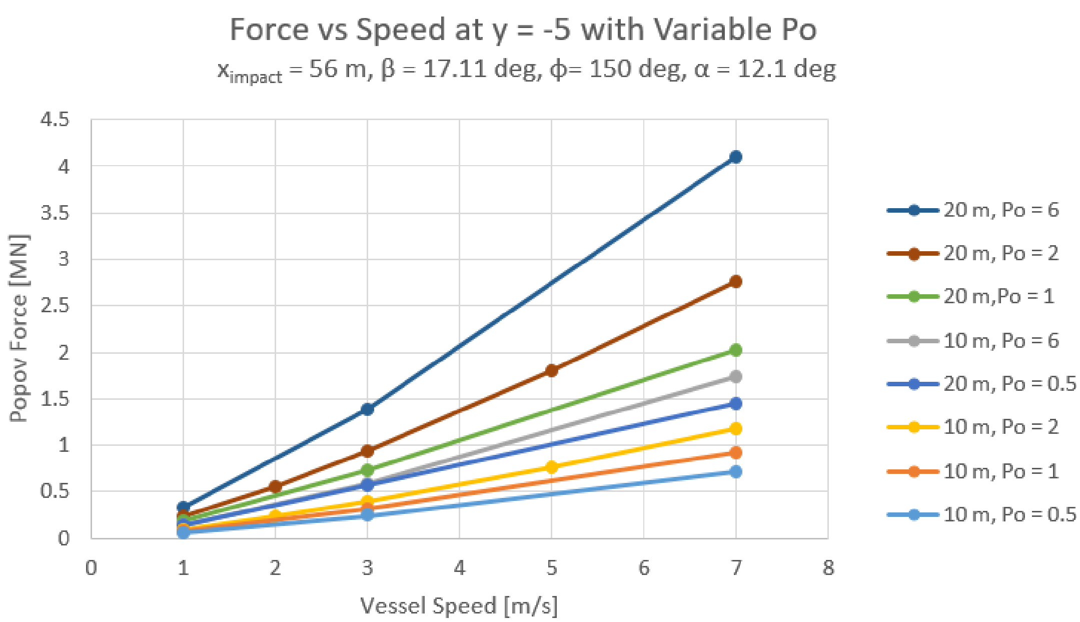

Figure 100: Glancing Force versus Vessel Speed, y = -5 m, with variable ice P_o

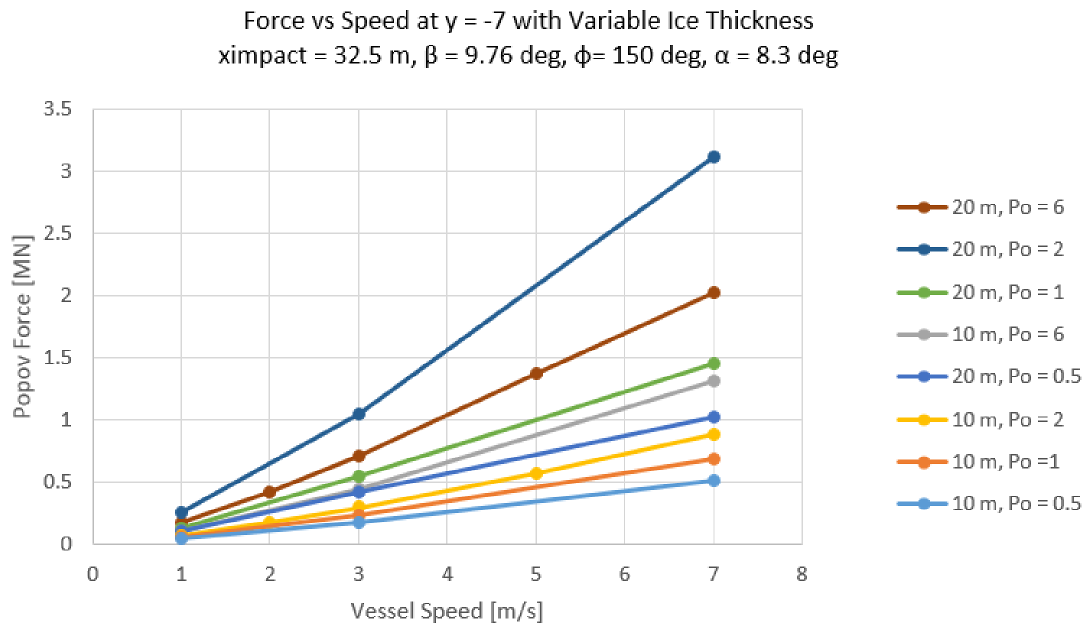

Figure 101: Glancing Force versus Vessel Speed, y = -7 m, with variable ice P_o

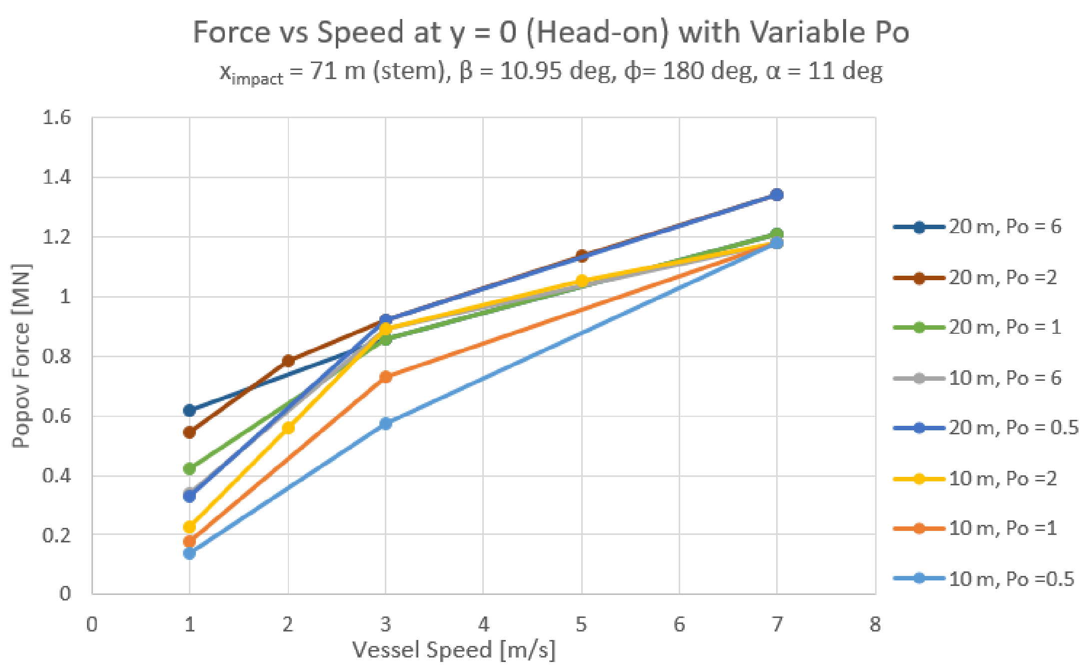

Figure 102: Force versus Vessel Speed, y = 0 m (head-on), with variable ice P_o

GEM Simple Pack Ice Scenarios and Results

The above GEM simulations demonstrate some fundamental vessel behaviors and loads. This section will explore the ice loads as they develop in pack ice. To begin, the vessel will be run along a straight path at 1 m/s, striking a set of identical floes, at locations that are increasingly aft of the stem (Figure 103).

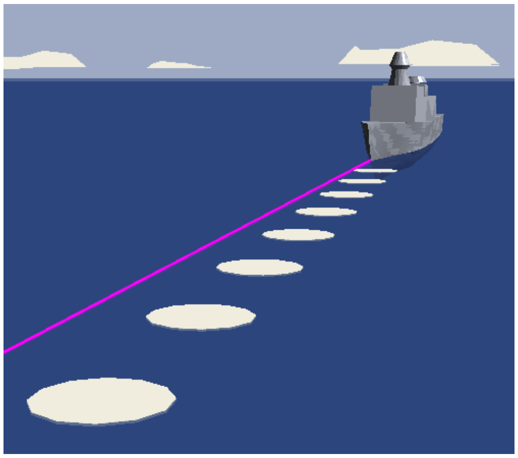

Figure 103: Impacts with 8 ice floes, 10 m diameter, 0.2 m thick, ship speed 1m/s

For these nine simple impacts, the forces are in the range of 25 to 48 kN as shown in Figure 104. (**Note** – this comparison to DDePS has used different added mass assumptions for the ice than were used in the safe speed assessment in sections 4 and 5 above, resulting is slightly different results.)

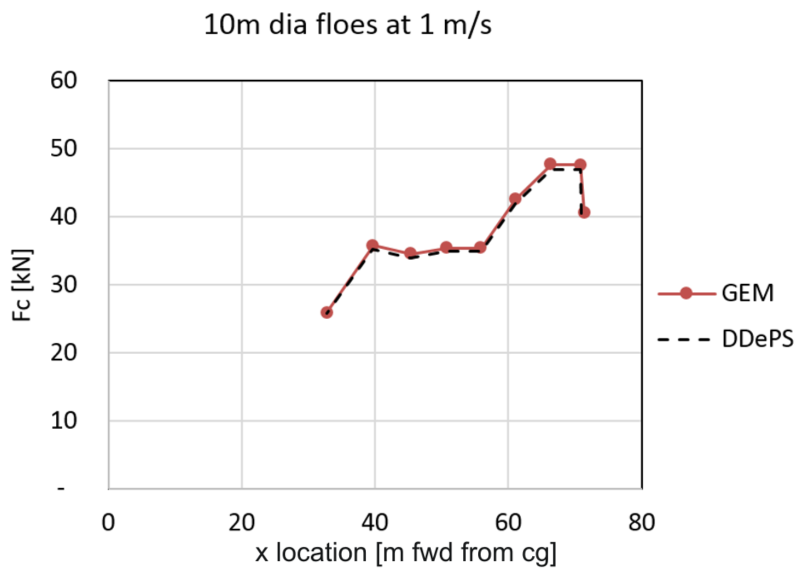

Figure 104: Force versus x location on hull for impacts with 8 ice floes, at 1m/s.

The following set of GEM runs will all involve the vessel transiting open pack ice at approximately 1 m/s. In all cases the pack ice is comprised of 1585 ice floes, each 10 m diameter 12-sided polygons, randomly placed at 50% concentration. All floes are 0.2 m thick, with P_o= 2MPa, sf= 0.3 MPa. The overall ice pack is 800 m x 300 m (Figure 105). In this case the ship is in captive mode, moving at exactly 1 m/s in a perfectly straight line. Cases with the ship in auto-pilot mode, following a straight route, or with the auto-pilot off all produced similar load data (not shown). The impact results for these three cases are all plotted in Figure 106.

To examine the effect of turning, the free runs were repeated with 5, 10 and 20-degree rudder angles. Figure 107 shows the 10-degree rudder angle run. Figure 108 shows the straight run data combined with the data from the turning cases. The results show that the turns have little effect on bow loads but do cause impact to occur on the stern, and at level that approach the size of the bow loads.

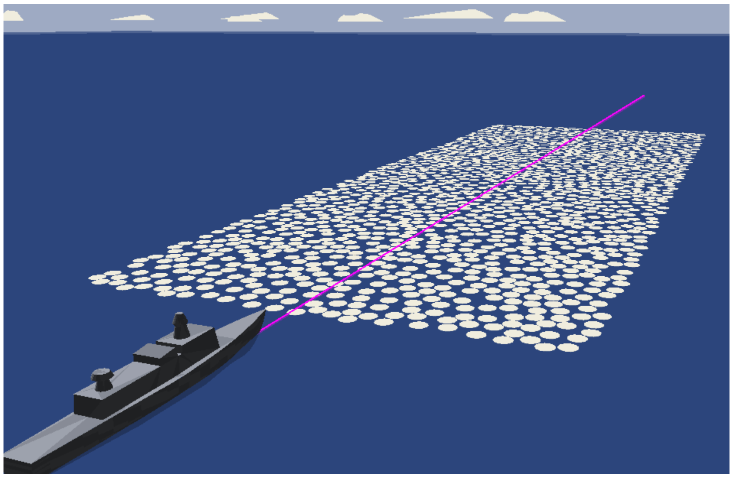

Figure 105: Pack Ice scenario

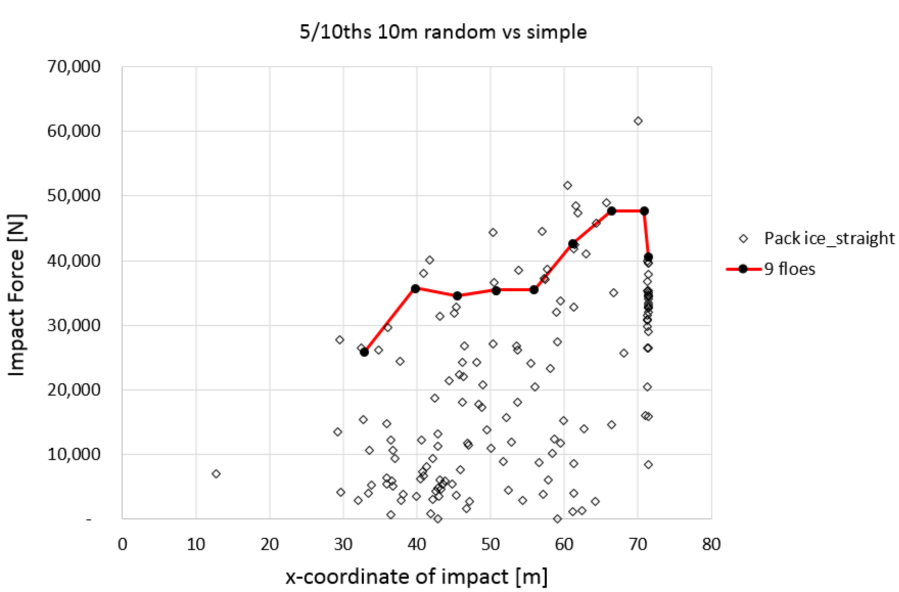

Figure 106: Force versus location on hull for impacts in pack ice, pack ice versus single impacts

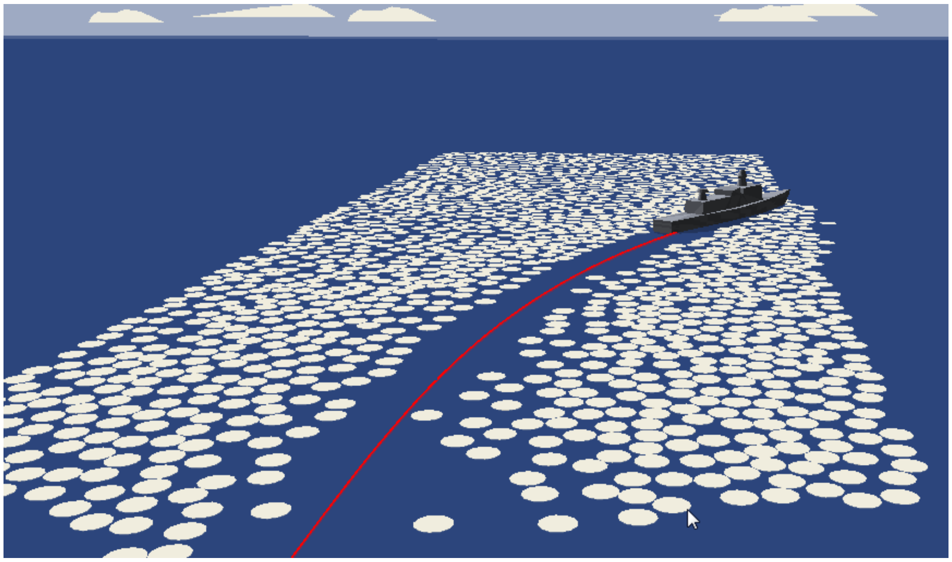

Figure 107: Pack ice for 10 degree rudder angle free run

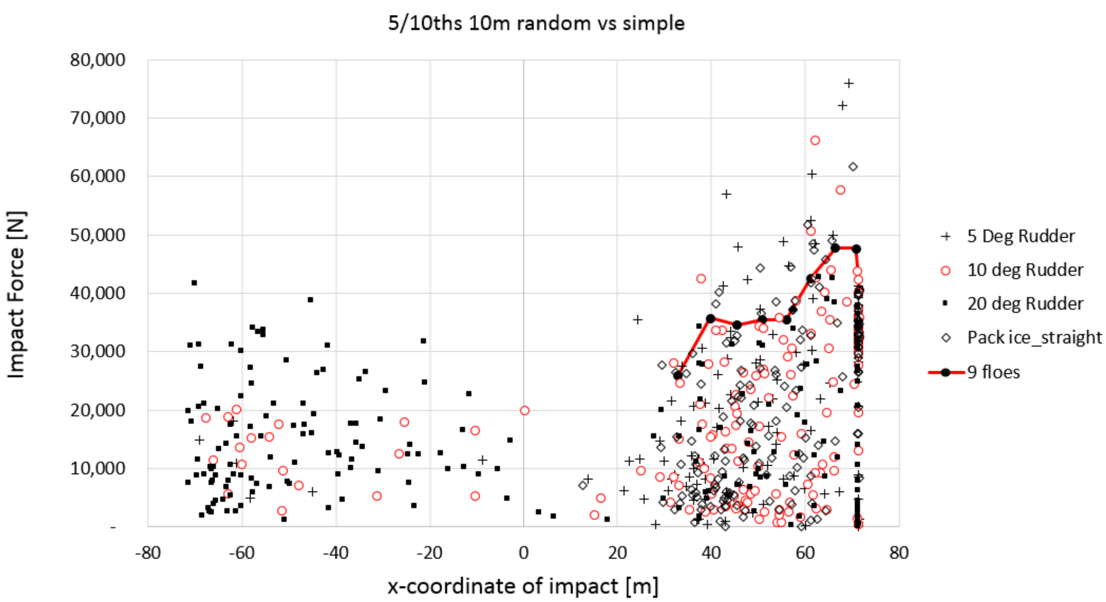

Figure 108: Force versus location on hull for impacts in pack ice including both straight and turning

GEM Variable Size Pack Ice Scenarios and Results

The next set of GEM results examines the Notional Destroyer transiting 40% coverage pack ice at approximately 6 knots. The ice covers a range of thicknesses from 0.2m to 1m, with floe sizes from 10m to 40m diameter. Both variables are uniformly distributed. This simulation will examine the situation described in the Safe-Speed evaluation above (Figure 52). The GEM simulation is shown in Figure 110. The variable ice thickness is shown in Figure 111. Ice strength was set as per Figure 109.

GEM models all the collisions that occur in the ice pack and records all the kinematic and interaction parameters. Normally GEM computes the collision force according to the standard assumption that the ship is rigid. All GEM values can be saved to a 'collision.txt' file for post processing. In this case the GEM collision data was re-computed using the information on the Notional destroyer structure in Table 14. Equations (14) through (19) are used to determine the corrected loads and response of the actual compliant bow structural panels of the Notional Destroyer. The GEM data contains the hull coordinates and kinematic information of all the impacts, and therefore one can determine exactly which panels were impacted and what their damage levels would be. Using the equations for elasto-plastic response these damage levels have been computed.

Figure 112 shows the computed total (elastic + plastic) and permanent deflections at each impact location. For the conditions modeled (Figure 109), DDePS is predicting that permanent damages would occur, especially for the thicker ice/larger floes in the range. The results agree with this expectation, with total deflections up to 24cm and permanent deflections up to 10 cm. Figure 113 attempts to show the results in terms similar to Figure 109. Figure 113 shows impact events in terms of whether they caused more or less than 5cm deflection. The red triangles and purple diamonds indicate cases of computed deflections greater than 5cm. The red triangles are impacts where the forward ship speed is above 6 knots while the purple diamonds are impacts where speed is below 6 knots. The results tend to agree with expectations, although there are some purple diamonds below the blue 6 knot limit curve. These are not expected. However, it is noted that these points all have velocities near 6 knots and are in all cases but one just below the line. This shows general agreement between GEM, which included sway and yaw, with the safe speed DDePS results, which did not.

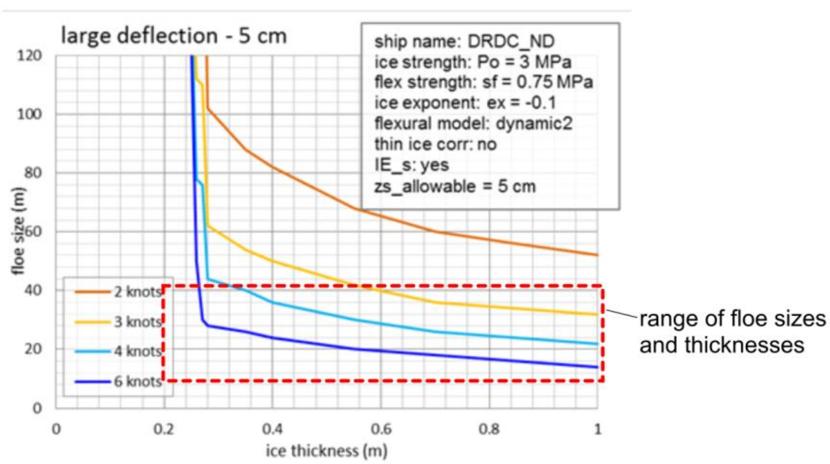

Figure 109: Range of conditions in GEM simulation (see Figure 52)

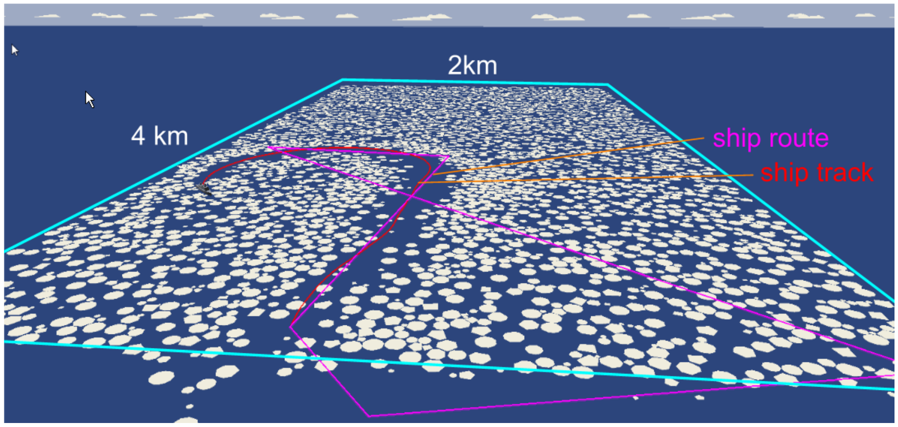

Figure 110: View of GEM 40% simulation (partly completed route)

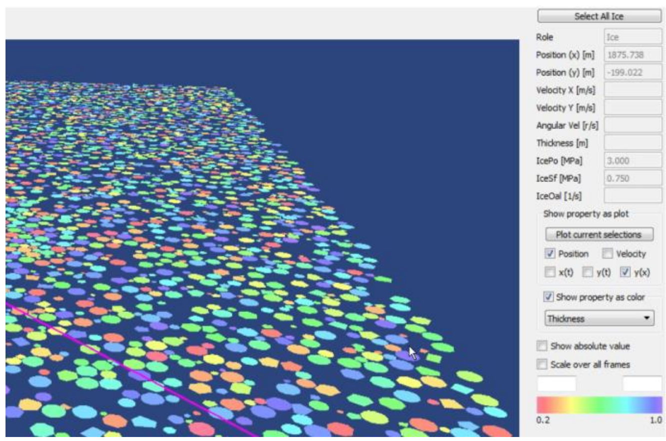

Figure 111: GEM 40% simulation showing ice thickness variations (0.2 to 1.0 m)

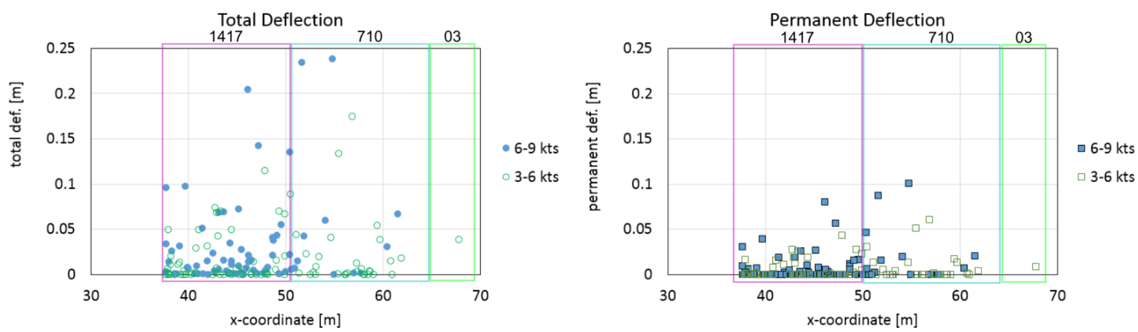

Figure 112: GEM 40% simulation results showing total and permanent structural deflections

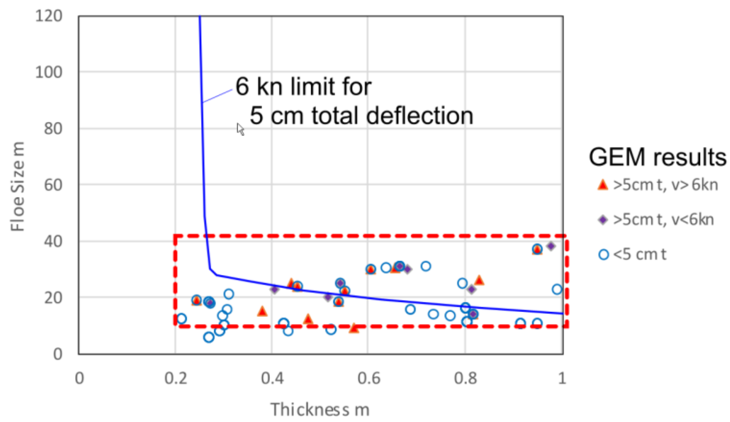

Figure 113: GEM 40% simulation results showing total structural deflections on condition plot

GEM Variable Concentration Pack Ice Scenarios and Results

In this set of simulations, GEM examines ice at concentrations from 5% to 40% coverage. To keep the general amount of ice constant, the 40% runs covered 2km, the 20% covered 4km, the 10% 8km and the 5% covered 16km. In all cases the vessel was in navigation mode, travelling at around 6 knots. The actual speed was influenced by the ice impacts and the autopilot. The number of ice floes were 581,417, 379 and 343 in the 40%, 20%, 10% and 5% cases respectively. The variation in ice floe count was due to the ice generation algorithm, as more smaller floes were needed when generating the higher concentrations. Figure 114 shows the ice concentrations for the various runs.

Figure 115 shows the effect of variable ice concentration. The main change is that there are more impact cases even though the field extent is proportional. In higher concentrations, there are fewer chances to miss the ice (no actual avoidance strategy was used). In higher concentrations, one impact can result in secondary impacts as the vessel sways and yaws. In very low concentrations, these secondary impacts are quite unlikely. Of course, humans would have the ability to steer clear of ice in very low concentrations, although that human pilotage is not simulated in GEM.

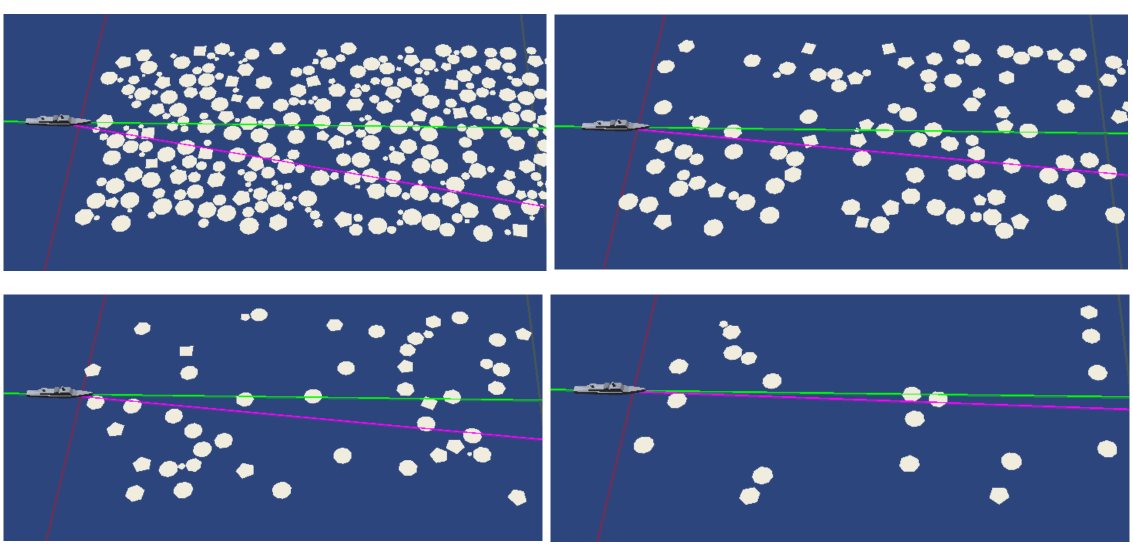

Figure 114: GEM showing 40%, 20%, 10% and 5% simulations

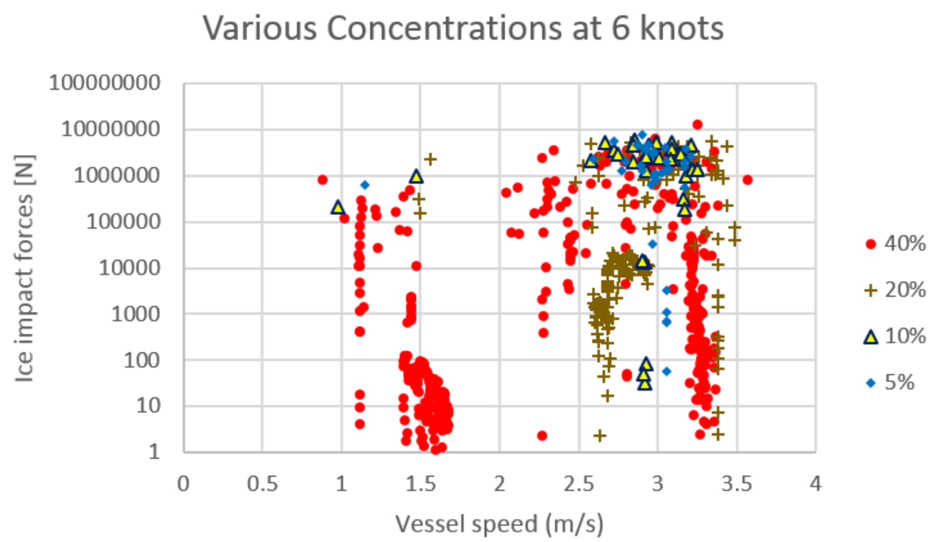

Figure 115: GEM showing 40%, 20%, 10% and 5% simulations

Discussion of GEM Results

The GEM results presented above are indicative of the kinds of analysis that GEM permits. The loads are generally comparable to the deterministic results provided by DDePS, but they allow for the examination of the effects of the navigation mechanics (turning in pack ice), the mechanics of pack ice (multi-body interactions), and the sources and character of variability of the loads. The number of variables, both input and output, is very large and presents challenges to fully explore. Statistical analysis, while possible, can be challenging to present in ways that correctly reflect the numerous interdependencies that are involved. It will take further work to find clear ways to present the data that GEM can create.

The simulation of the 40% ice cover has shown that GEM is in general agreement with the safe speed analysis presented earlier in this report. However, it is clear that GEM produces additional variability in the results due to the modeling of pack ice and vessel navigation mechanics. The DDePS safe speed assessment has produced what is termed a “technical safe speed”, in a deterministic way. The GEM results have begun to illustrate some of the additional variables and complications that need to be considered when actual safe operational limits are being set.

The GEM analysis of variable ice concentration illustrates that concentration has a significant influence on the outcomes. GEM is only modeling the actual mechanics, and not the human control of the vessel. Even so, the lower concentrations result in a significant reduction in the number of impacts, even when adjusted for ice floe count. It is likely that this is the result of reduced secondary impacts.

9. Conclusions

The aim of this project has been to extend the analysis of the capability of the Notional Destroyer in ice. New aspects have been examined. The updated bow structure design, combined with an improved analysis approach has enhanced the analysis, which indicates a slightly greater capability than was determined in the Phase 1 report. Nevertheless, it remains clear that the Notional Destroyer has only marginal ability to operate in ice. Essentially is can only operate very cautiously in very light pack ice conditions (very small floes of limited thickness). It is also clear that the operational envelope would be significantly expanded if the operator were to tolerate small permanent deformations (5 cm) of the outer hull on a very localized basis. The expanded operational envelope would allow for operation in somewhat heavier ice at low speeds. While great caution would still be required, this expanded operational envelope might be important in certain emergency situations.

An analysis of the loads and capacity of the stem of the Notional Destroyer has shown that the stem is relatively strong in comparison to the bow shoulders. There is a greater likelihood of impacts on the stem, but it appears that there is little to be concerned about.

The novel use of GEM in this analysis has demonstrated good agreement with the DDePS Safe Speed assessment approach. GEM has also indicated that maneuvering operations result in a wider range of interactions (e.g. on the midbody and stern). GEM is also capable of showing the wide distribution of ice load magnitudes that can be expected in actual operations.

The real outcomes of this report concern the technology that can be brought to bear for assessment of vessel capability. The report has demonstrated that a combination of numerical (LS-DYNA and GEM) simulation tools used in combination with analytical models (in DDePS and GEM) can permit a comprehensive assessment of a vessel's structural safety during operations in ice. This is a form of direct risk assessment, in which the complex mechanics of ice and structure are used to determine capability levels.

10. Recommendations

The complexity of the analyses presented above lead to many areas of improvement. This direct assessment technology has been steadily developing over that past decade and will continue to improve. In general terms the following recommendations are made;

- Validation of the technical methodologies applied to this study presents a perennial challenge. Most field trials of ships in ice tend to focus on ice breakers and high ice class cargo ships. A focus towards full scale validation efforts on the structural response of lighter ships in marginal pack ice regimes and thin ice mechanics would certainly help progress the state-of-the-art and raise the confidence level of these models when applied to naval ships
- The assessments presented here should be extended to the midbody and stern regions with appropriately updated scenarios
- The assessments should then be further extended to evaluate appendages (rudder, sonar etc.) which are particularly critical to naval missions but perhaps more vulnerable to ice damage in even the lightest ice conditions

- More detailed structural overload models should examine connection details, moving loads and fracture limits
- The GEM model should be updated to include the assessment of structural capacity and response levels. This could be readily done with existing approaches, and only requires software development (extensive but not especially difficult)
- A project should be started to explore how to bring this technology into practical use within the Navy. Training and bridge deck systems are needed.

11. References

ABS (2016). ABS Technical Report "ONR Ice Capability Assessment and Experimental Planning - DDePS_SafeCheck Technical Background and Safe Speed Assessment of NSWCCD Hull 3000", October 2016 American Bureau of Shipping, Report to ONR

ABS (2017). ABS Technical Report "ONR Ice Capability Assessment and Experimental Planning - Advanced Modeling and Re-assessment of NSWCCD HULL 3000" , February 2017 American Bureau of Shipping, Report to ONR

ABS. (2015). ABS Technical Report - USCG WMSL Class - Operational Capabilities and Limitations in Ice. Houston, TX, USA.

Bruneau, S. E., Colbourne, B., Dragt, R., Dillenburg, A. K., Ritter, S., Pilling, M., & Sullivan, A. (2013). Laboratory Indentation Tests Simulating Ice-Structure Interactions Using Cone-Shaped Ice Samples and Steel Plates. Port and Ocean Engineering under Arctic Conditions, POAC'13. Espoo, Finland.

Bruneau, S. E., Dillenburg, A. K., & Ritter, S. (2013). Ice Sample Production Techniques and Indentation Tests for Laboratory Experiments Simulating Ship Collisions with Ice. International Offshore and Polar Engineering Conference, ISOPE'13 (Vol. 9, pp. 1268–1271). Anchorage, AK, USA.

Daley, C. (1999). "Energy based ice collision forces". Port and Ocean Engineering under Arctic Conditions, POAC'99. Espoo, Finland.

Daley, C. (2000). IACS Unified Requirements for Polar Ships - Background Notes to Design Ice Loads.

Daley, C. (2015). Ice Impact Capability of DRDC Notional Destroyer. Prepared for Defense Research and Development Canada, Warship Performance Section. Halifax, N.S., CANADA

Daley, C., & Hermanski, G. (2009). Investigation of Plastic Limit States for Design of Ship Hull Structures - Ship Frame Research Program - A Experimental Study of Ship Frames and Grillages Subjected to Patch Loads (Ship Structure Committee Report SSC-457). Washington, DC, USA.

Daley, C., & Kendrick, A. (2011). Safe Speeds in Ice (BMT Report 6931DFR.Rev00).

Daley, C., & Kim, H. (2010). Ice Collision Forces Considering Structural Deformation. International Conference on Offshore Mechanics and Arctic Engineering, OMAE'10. Shanghai, China.

Daley, C., & Liu, J. J. (2009). DDePS for Ship Ramming Infinite / Finite Ice.

Daley, C.G., (2002), "Derivation of Plastic Framing Requirements for Polar Ships", Journal of Marine Structures, Elsevier, 15(6) pp 543-559

Dolny, J. (2017). "A Technical Methodology for Establishing Structural Limitations of Ships in Pack Ice." Master's Thesis, Memorial University of Newfoundland.

Dolny, J., Yu, H., Daley, C., & Kendrick, A. (2013). Developing a Technical Methodology for the Evaluation of Safe Operating Speeds in Various Ice Conditions. Port and Ocean Engineering under Arctic Conditions, POAC'13. Espoo, Finland.

DRDC (2015) – Notional Destroyer Particulars and Summary, PowerPoint slides provided by DRDC.

Gagnon, R. E., & Derradji-Aouat, A. (2006). First Results of Numerical Simulations of Bergy Bit Collisions with the CCGS Terry Fox Icebreaker. IAHR International Symposium on Ice, IAHR'06 (pp. 9–16). Sapporo, Japan.

IACS. (2011). IACS Unified Requirements Concerning Polar Class. London, UK: International Association of Classification Societies.

Kendrick, A., & Daley, C. (2006a). Ice Interaction Scenarios and Load Modeling Approaches (BMT Report 6007A.DFR submitted to ABS).

Kendrick, A., & Daley, C. (2006b). Ice Loads for Structural and Vibration Analysis of Large Arctic LNG Carriers – Phase II (BMT Report 6055 DR submitted to ABS).

Kendrick, A., & Daley, C. (2009). DDPS for Stern Impacts with Ice (BMT Report 6512D.FR submitted to ABS and DSME).

Liu, J. J., Daley, C., Yu, H., & Bond, J. (2012). Comparison of Analytical and Numerical Models of Glancing Ship-Ice Collisions. International Conference and Exhibition on Performance of Ships and Structures in Ice, IceTech'12. Banff, AB, Canada.

Liu, J. J., Daley, C., Yu, H., & Bond, J. (2012). Comparison of Analytical and Numerical Models of Glancing Ship-Ice Collisions. International Conference and Exhibition on Performance of Ships and Structures in Ice, IceTech'12. Banff, AB, Canada.

Lloyd's Register (2016) Notional Vessel Design Improvement, Technical Report # TR-16-07 Rev01, prepared by LRATG (Martec Limited) for DRDC Atlantic, Dartmouth, N.S., Canada

Montgomery, D. C. (2008). Design and Analysis of Experiments (7th ed.). John Wiley & Sons, Inc.

Zong, R. (2012). Finite Element Analysis of Ship-Ice Collision Using Ls-Dyna. Memorial University of Newfoundland.

Other relevant materials

Kendrick, A., & Daley, C. (2000). IACS Unified Requirements for Polar Ships - Background Notes to Derivation and Use of Formulations for Framing Design.

Manual, M., Gudimelta, P. S. R., Daley, C., & Colbourne, B. (2013). Controlled Plastic Deformation of a Grillage Using Artificial Freshwater Ice at a Large Scale. Port and Ocean Engineering under Arctic Conditions, POAC'13. Espoo, Finland.

Popov, Y. N., Faddeyev, O. V, Kheysin, D. Y., & Yakovlev, A. A. (1967). Strength of Ships Sailing In Ice (Translated), F3TC-HT-23-96-68 (Technical.). Leningrad, USSR: Sudostroyeniye Publishing House.

Rhinoceros (2010) – NURBS Modelling for Windows v 4.0, Copyright Robert McNeel and Associates.

Sazidy, M., Daley, C., & Colbourne, B. (2014). A Mathematical Model of Icebreaking for Safe Speed Assessment. International Conference and Exhibition on Performance of Ships and Structures in Ice, IceTech'14 (pp. 1–8). Banff, AB, Canada.

Sazidy, M., Daley, C., Colbourne, B., & Wang, J. (2014). Effect of Ship Speed on Level Ice Edge Breaking. International Conference on Offshore Mechanics and Arctic Engineering, OMAE'14. San Francisco, CA, USA.

APPENDIX 1: Extended Ice Calibration Runs

Extended Runs								
run	σ_y (MPa)	Φ (°)	h_{ice} (m)	β (°)	computed		predicted (linear regression)	
					P_o (MPa)	ex	Po (MPa)	ex
A_301	1.5	90	0.35	0.001	7	-0.01	6.3	0.0
A_302	1.5	90	0.35	10	7	-0.03	6.6	0.0
A_303	1.5	90	0.35	20	6.8	-0.05	7.0	-0.1
A_304	1.5	90	0.35	40	6.6	-0.13	7.8	-0.1
A_305	1.5	90	0.7	0.001	7.1	-0.02	6.7	0.0
A_306	1.5	90	0.7	10	7.2	-0.03	7.1	0.0
A_307	1.5	90	0.7	20	7.1	-0.05	7.5	0.0
A_308	1.5	90	0.7	40	8.4	-0.06	8.3	-0.1
A_309	1.5	90	1.05	0.001	7	-0.03	7.2	0.0
A_310	1.5	90	1.05	10	7.1	-0.04	7.6	0.0
A_311	1.5	90	1.05	20	7.7	-0.03	7.9	0.0
A_312	1.5	90	1.05	40	9.1	-0.02	8.7	-0.1
A_313	1.5	120	0.35	0.001	6.5	-0.01	6.0	0.0
A_314	1.5	120	0.35	10	6.5	-0.03	6.4	0.0
A_315	1.5	120	0.35	20	6.4	-0.07	6.8	-0.1
A_316	1.5	120	0.35	40	6.5	-0.15	7.6	-0.1
A_317	1.5	120	0.7	0.001	6.4	-0.02	6.5	0.0
A_318	1.5	120	0.7	10	6.6	-0.04	6.8	0.0
A_319	1.5	120	0.7	20	7.1	-0.05	7.2	0.0
A_320	1.5	120	0.7	40	9	-0.01	8.0	-0.1
A_321	1.5	120	1.05	0.001	6.6	-0.04	6.9	0.0
A_322	1.5	120	1.05	10	7	-0.03	7.3	0.0
A_323	1.5	120	1.05	20	7.7	-0.03	7.7	0.0
A_324	1.5	120	1.05	40	9.1	-0.02	8.5	-0.1
A_325	1.5	150	0.35	0.001	6	-0.01	5.8	0.0
A_326	1.5	150	0.35	10	6	-0.04	6.1	0.0
A_327	1.5	150	0.35	20	6.7	-0.07	6.5	-0.1
A_328	1.5	150	0.35	40	7.2	-0.12	7.3	-0.1
A_329	1.5	150	0.7	0.001	6	-0.02	6.2	0.0
A_330	1.5	150	0.7	10	6.7	-0.04	6.6	0.0
A_331	1.5	150	0.7	20	7.1	-0.04	7.0	0.0
A_332	1.5	150	0.7	40	9	-0.01	7.8	-0.1
A_333	1.5	150	1.05	0.001	6	-0.04	6.7	0.0
A_334	1.5	150	1.05	10	6.5	-0.04	7.1	0.0
A_335	1.5	150	1.05	20	7.7	-0.03	7.4	0.0
A_336	1.5	150	1.05	40	9.1	-0.01	8.2	-0.1

Extended Runs (con't)								
run	σ_y (MPa)	Φ (°)	h_{ice} (m)	β (°)	computed		predicted (linear regression)	
					P_o (MPa)	ex	Po (MPa)	ex
A_337	0.5	90	0.35	10	4	-0.01	3.3	-0.1
A_338	0.5	90	0.7	10	4.2	-0.04	3.8	0.0
A_339	1	90	0.35	10	5.2	-0.05	5.0	-0.1
A_340	1	90	0.7	10	5.6	-0.05	5.4	0.0
A_341	0.5	150	0.35	10	2.8	-0.02	2.8	-0.1
A_342	0.5	150	0.7	10	3.1	-0.03	3.3	0.0
A_343	1	150	0.35	10	4.5	-0.04	4.5	-0.1
A_344	1	150	0.7	10	4.8	-0.05	4.9	0.0
A_345	1.3	90	0.35	5	6.4	-0.01	5.8	0.0
A_346	1	90	0.7	0.001	5.7	-0.01	5.1	0.0
A_347	0.7	90	0.7	10	4.8	-0.02	4.5	0.0
A_348	0.7	120	0.35	15	4	-0.02	3.9	-0.1
A_349	1.5	120	1.05	0.001	6.2	-0.05	6.9	0.0
A_350	0.7	150	0.35	5	3.3	-0.01	3.3	0.0
A_351	1.2	150	0.35	15	5.2	-0.06	5.3	-0.1
A_352	1.1	150	0.7	10	5	-0.05	5.3	0.0
A_353	0.5	150	0.7	15	3.2	-0.02	3.5	0.0
A_354	1.4	150	1.05	5	6	-0.01	6.5	0.0

APPENDIX 2: Effective Collision Energy

This appendix provides the technical derivations for the effective kinetic energy that is needed to solve a ship-ice collision. These are the effective velocity and mass terms for the ship and ice that are used in DDePS as well as in GEM. This approach was first developed by Popov et al. (1967). The approach is valid for collisions with certain parameters, specifically where the collision is of relatively short duration (so that changes in orientation or gravitational potential energy can be ignored) but long enough so that the primary dynamics can be treated as rigid body accelerations, and local effects can be treated as quasi-static. Collisions which involve extensive sliding contact would not be modeled appropriately. Extremely sudden impacts (e.g weapons effects or shock loading from very rapid changes in contact area) would also not be correctly modelled. Fortunately, ship ice collisions are in the middle range, where like billiard ball collisions, the rigid body mechanics, coupled with a contact process can accurately model the problem.

Popov Terms for Ship

A collision taking place at a point (see Figure 116), will result in a normal force F_n. The point of contact will accelerate, and a component of the acceleration will be along the normal vector, with a magnitude $\ddot{\zeta}$. The collision can be modeled as if the point were a single mass (a 1 degree of freedom system) with an equivalent mass M_e of;

$$M_e = F_n / \ddot{\zeta} \qquad (28)$$

The equivalent mass is a function of the inertial properties (mass, radii of gyration, hull angles and moment arms) of the ship. The equivalent mass is linearly proportional to the mass (displacement) of the vessel, and can be expressed by the following equation.

$$M_{e_{ship}} = \frac{M_{ship}}{C_o} = \frac{1}{\frac{l^2}{M_{sx}} + \frac{m^2}{M_{sy}} + \frac{n^2}{M_{sz}} + \frac{\lambda^2}{I_{sx}} + \frac{\mu^2}{I_{sy}} + \frac{\nu^2}{I_{sz}}} \qquad (29)$$

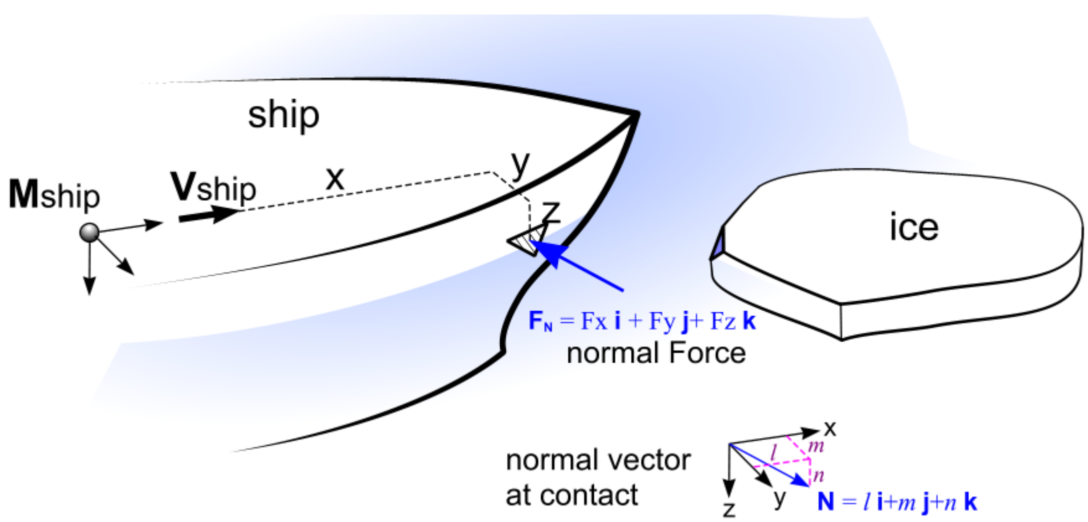

Figure 116: Collision point geometry

The inertial properties of the vessel are as follows;

Hull angles at point P:

α : waterline angle

β : frame angle

β' : normal frame angle

γ : sheer angle

The various angles are related as follows:

$$\tan(\beta) = \tan(\alpha)\tan(\gamma) \qquad (30)$$

$$\tan(\beta') = \tan(\beta)\cos(\alpha) \qquad (31)$$

Based on these angles, the direction cosines l, m, and n are:

$$l = \sin(\alpha)\cos(\beta') \qquad (32)$$

$$m = \cos(\alpha)\cos(\beta') \qquad (33)$$

$$n = \sin(\beta') \qquad (34)$$

and the moment arms are;

$$\lambda = ny - mz \quad \text{(roll moment arm)} \qquad (35)$$

$$\mu = lz - nx \quad \text{(pitch moment arm)} \qquad (36)$$

$$\eta = mx - ly \quad \text{(yaw moment arm)} \qquad (37)$$

The added mass terms for the ship are represented by the following geometric relationships (from Popov);

$$AM_x = 0 \quad \text{(added mass factor in surge)} \qquad (38)$$

$$AM_y = 2\,T/B \quad \text{(added mass factor in sway)} \qquad (39)$$

$$AM_z = 2/3\,(B\,{C_{wp}}^2)/(T(C_B(1 + C_{wp}))) \quad \text{(added mass factor in heave)} \qquad (40)$$

$$AM_{roll} = 0.25 \quad \text{(added mass factor in roll)} \qquad (41)$$

$$AM_{pit} = B(T/(3 - 2C_{wp})(3 - C_{wp})) \quad \text{(added mass factor in pitch)} \qquad (42)$$

$$AM_{yaw} = 0.3 + 0.05\,L/B \quad \text{(added mass factor in yaw)} \qquad (43)$$

The mass radii of gyration (squared) are;

$$rx^2 = C_{wp}B^2/(11.4\,C_m) + H^2/12 \quad \text{(roll)} \qquad (44)$$

$$ry^2 = 0.07\,C_{wp}L^2 \quad \text{(pitch)} \qquad (45)$$

$$rz^2 = L^2/16 \quad \text{(yaw)} \qquad (46)$$

The six force (moment) actions on the six degrees of freedom of the vessel's center of gravity are;

$$F_x = F_n l \quad \text{(force in surge)} \tag{47}$$

$$F_y = F_n m \quad \text{(force in sway)} \tag{48}$$

$$F_z = F_n n \quad \text{(force in heave)} \tag{49}$$

$$M_{rol} = F_n \lambda \quad \text{(moment in roll)} \tag{50}$$

$$M_{pit} = F_n \mu \quad \text{(moment in pitch)} \tag{51}$$

$$M_{yaw} = F_n \eta \quad \text{(moment in yaw)} \tag{52}$$

There are six accelerations at the center of gravity which are:

$$a_x = F_n l/(M(1 + AM_x)) \quad \text{(acceleration in surge)} \tag{53}$$

$$a_y = F_n m/(M(1 + AM_y)) \quad \text{(acceleration in sway)} \tag{54}$$

$$a_z = F_n n/(M(1 + AM_z)) \quad \text{(acceleration in yaw)} \tag{55}$$

$$a_{rol} = F_n \lambda/(M\, rx^2(1 + AM_{roll})) \quad \text{(acceleration in roll)} \tag{56}$$

$$a_{pit} = F_n \mu/(M\, ry^2(1 + AM_{pit})) \quad \text{(acceleration in pitch)} \tag{57}$$

$$a_{yaw} = F_n \eta/(M\, rz^2(1 + AM_{yaw})) \quad \text{(acceleration in yaw)} \tag{58}$$

Each of these accelerations contributes to the acceleration of the point of ice contact. The total acceleration at the point of contact can be expressed as;

$$\ddot{\zeta} = F_n\, C_o/M_{ship} \tag{59}$$

where;

$$C_o = \frac{l^2}{1+AM_x} + \frac{m^2}{1+AM_y} + \frac{n^2}{1+AM_z} + \frac{\lambda^2}{rx^2(1+AM_{roll})} + \frac{\mu^2}{ry^2(1+AM_{pit})} + \frac{\eta^2}{rz^2(1+AM_{yaw})} \tag{60}$$

The collision applies an impulse I_e to the vessel at the point of contact. The changes in velocity at the center of gravity are;

$$dV_x = I_e l/\big(M(1 + AM_x)\big) \quad \text{(velocity change in surge)} \tag{61}$$

$$dV_y = I_e m/\Big(M\big(1 + AM_y\big)\Big) \quad \text{(velocity change in sway)} \tag{62}$$

$$dV_z = I_e n/\big(M(1 + AM_z)\big) \quad \text{(velocity change in yaw)} \tag{63}$$

$$dV_{rol} = I_e \lambda/\big(M \cdot rx^2(1 + AM_{roll})\big) \quad \text{(velocity change in roll)} \tag{64}$$

$$dV_{pit} = I_e \mu/\Big(M \cdot ry^2\big(1 + AM_{pit}\big)\Big) \quad \text{(velocity change in pitch)} \tag{65}$$

$$dV_{yaw} = I_e \eta/\Big(M \cdot rz^2\big(1 + AM_{yaw}\big)\Big) \quad \text{(velocity change in yaw)} \tag{66}$$

Popov Terms for Ice

In the Popov model, the ice floe is regarded as another body, comparable to the ship with similar dimensional definitions. If the ice is essentially infinite, it does not accelerate and isn't included in the effective mass. If the ice is finite, it is included. The ice requires its own coordinate system, aligned with its own principal axes. The normal vector must be re-evaluated in the ice coordinate system. In this way, both the ship and ice will have effective masses and velocities along a common normal vector. The ice floe equivalent mass can be expressed as:

$$M_{e_{ice}} = \frac{1}{\frac{l^2}{M_{ix}} + \frac{m^2}{M_{iy}} + \frac{n^2}{M_{iz}} + \frac{\lambda^2}{I_{ix}} + \frac{\mu^2}{I_{iy}} + \frac{\nu^2}{I_{iz}}} \quad (67)$$

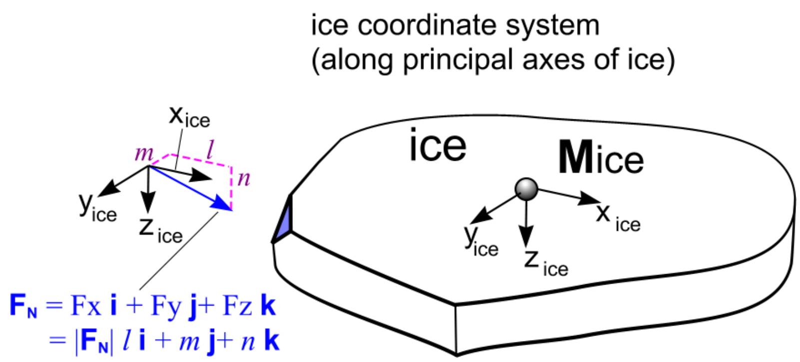

Figure 117: Ice collision point geometry

For the ice block the direction cosines l, m, and n are:

$$l_{ice} = -\cos(\beta') \quad (68)$$

$$m_{ice} = 0 \quad (69)$$

$$n_{ice} = -\sin(\beta') \quad (70)$$

and the moment arms are;

$$\lambda_{ice} = n_{ice} y_{ice} - m_{ice} z_{ice} \quad \text{(roll moment arm)} \quad (71)$$

$$\mu_{ice} = l_{ice} z_{ice} - n_{ice} x_{ice} \quad \text{(pitch moment arm)} \quad (72)$$

$$\eta_{ice} = m_{ice} x_{ice} - l_{ice} y_{ice} \quad \text{(yaw moment arm)} \quad (73)$$

The added mass terms for the ice are assumed as follows;

$$AM_{x_{ice}} = 0.05 \quad \text{(added mass factor in surge)} \quad (74)$$

$$AM_{y_{ice}} = 0.05 \quad \text{(added mass factor in sway)} \quad (75)$$

$$AM_{z_{ice}} = 1.0 \qquad \text{(added mass factor in heave)} \qquad (76)$$

$$AM_{roll_{ice}} = 1.0 \qquad \text{(added mass factor in roll)} \qquad (77)$$

$$AM_{pit_{ice}} = 1.0 \qquad \text{(added mass factor in pitch)} \qquad (78)$$

$$AM_{yaw_{ice}} = 0.05 \qquad \text{(added mass factor in yaw)} \qquad (79)$$

The mass radii of gyration (squared) are;

$$rx_{ice}^2 = L^2/12 \qquad \text{(roll)} \qquad (80)$$

$$ry_{ice}^2 = L^2/12 \qquad \text{(pitch)} \qquad (81)$$

$$rz_{ice}^2 = L^2/9 \qquad \text{(yaw)} \qquad (82)$$

The six force (moment) actions on the six degrees of freedom of the vessel's center of gravity are;

$$F_{x_{ice}} = F_n l_{ice} \qquad \text{(force in surge)} \qquad (83)$$

$$F_{y_{ice}} = F_n m_{ice} \qquad \text{(force in sway)} \qquad (84)$$

$$F_{z_{ice}} = F_n n_{ice} \qquad \text{(force in heave)} \qquad (85)$$

$$M_{rol_{ice}} = F_n \lambda_{ice} \qquad \text{(moment in roll)} \qquad (86)$$

$$M_{pit_{ice}} = F_n \mu_{ice} \qquad \text{(moment in pitch)} \qquad (87)$$

$$M_{yaw_{ice}} = F_n \eta_{ice} \qquad \text{(moment in yaw)} \qquad (88)$$

There are six accelerations at the center of gravity are:

$$a_{x_{ice}} = F_n l/(M(1 + AM_x)) \qquad \text{(acceleration in surge)} \qquad (89)$$

$$a_{y_{ice}} = F_n m/(M_{ice}(1 + AM_y)) \qquad \text{(acceleration in sway)} \qquad (90)$$

$$a_{z_{ice}} = F_n n/(M_{ice}(1 + AM_z)) \qquad \text{(acceleration in yaw)} \qquad (91)$$

$$a_{rol_{ice}} = F_n \lambda_{ice}/(M_{ice}\, rx_{ice}^2(1 + AM_{roll_{ice}})) \qquad \text{(acceleration in roll)} \qquad (92)$$

$$a_{pit_{ice}} = F_n \mu_{ice}/(M_{ice}\, ry_{ice}^2(1 + AM_{pit_{ice}})) \qquad \text{(acceleration in pitch)} \qquad (93)$$

$$a_{yaw_{ice}} = F_n \eta_{ice}/(M_{ice}\, rz_{ice}^2(1 + AM_{yaw_{ice}})) \qquad \text{(acceleration in yaw)} \qquad (94)$$

Each of these accelerations contributes to the acceleration of the point of ice contact. The total acceleration at the point of contact can be expressed as;

$$\ddot{\zeta}_{ice} = F_n\, C_{o_{ice}}/M_{ice} \qquad (95)$$

where;

$$C_{o\ ice} = \frac{l_{ice}^2}{1+AM_x} + \frac{m_{ice}^2}{1+AM_y} + \frac{n_{ice}^2}{1+AM_z} + \frac{\lambda_{ice}^2}{rx^2(1+AM_{roll})} + \frac{\mu_{ice}^2}{ry^2(1+AM_{pit})} + \frac{\eta_{ice}^2}{rz^2(1+AM_{yaw})} \quad (96)$$

The ship and ice equivalent masses are;

$$M_{e_{ship}} = \frac{M_{ship}}{C_o} \qquad M_{e_{ice}} = \frac{M_{ice}}{C_{o\ ice}}$$

The combined single equivalent mass for the impact is;

$$M_{\mathrm{e}} = \frac{1}{\frac{1}{M_{e_{ship}}} + \frac{1}{M_{e_{ice}}}}$$

For the simplest case, where the ship is moving in x only and the ice is stopped, the effective normal speed is;

$$V_e = V_{ship}\ l$$

For arbitrary initial velocities of the ship and ice, normal overlap velocity is determined by taking all geometry and kinematics into account. The impact can thus be viewed as a single degree of freedom collision (see Figure 118)

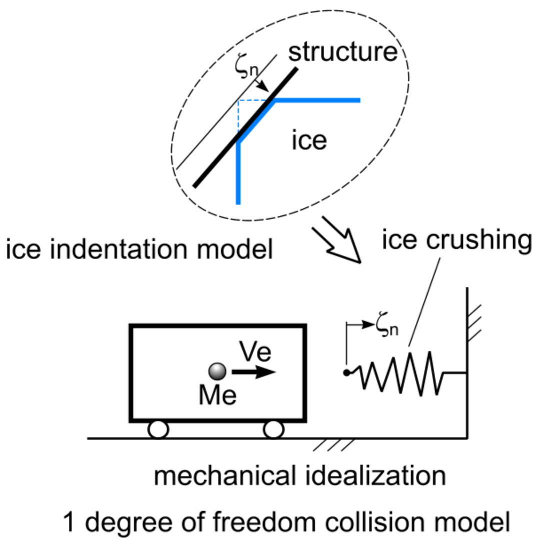

Figure 118: Ice collision point geometry